PWA FR-3299
8 AUGUST 1969

SUPPRESSION OF COMBUSTION OSCILLATIONS WITH MECHANICAL DAMPING DEVICES INTERIM REPORT

Prepared Under
Contract NAS8-21310
For
George C. Marshall Space Flight Center
National Aeronautics And Space Administration
Huntsville, Alabama

Pratt & Whitney Aircraft
DIVISION OF UNITED AIRCRAFT CORPORATION
FLORIDA RESEARCH AND DEVELOPMENT CENTER
BOX 2691, WEST PALM BEACH, FLORIDA 33402

PWA FR-3299
8 AUGUST 1969

SUPPRESSION OF COMBUSTION OSCILLATIONS WITH MECHANICAL DAMPING DEVICES INTERIM REPORT

Written by: G. D. Garrison
Assistant Project Engineer

A. C. Schnell
Senior Experimental Engineer

C. D. Baldwin
Senior Experimental Engineer

P. R. Russell
Senior Experimental Engineer

Approved by: G. D. Garrison
G. D. Garrison
Program Manager

Pratt & Whitney Aircraft DIVISION OF UNITED AIRCRAFT CORPORATION
FLORIDA RESEARCH AND DEVELOPMENT CENTER
BOX 2691, WEST PALM BEACH, FLORIDA 33402

FOREWORD

This report describes the work performed during the period 27 June 1968 to 16 June 1969 under Contract NAS8-21310 for the NASA Marshall Space Flight Center. The NASA Technical Monitor was Mr. C.R. Bailey, and Dr. Uno Ingard of the Massachusetts Institute of Technology served as technical consultant. Special acknowledgement is given to C.R. Bailey for suggesting the possible correlation between acoustic resistance and aperture flow coefficients, and to Senior Experimental Engineer J.A. Lipsit of Pratt & Whitney Aircraft for his help in the development of the electronic system for the pressure-phase impedance measuring apparatus used on this program.

CONTENTS

SECTION		PAGE
	ILLUSTRATIONS	vii
	NOMENCLATURE	x
I	OBJECTIVE OF PROGRAM	I-1
	A. Task I - High Frequency Analysis	I-1
	B. Task II - Chamber Simulator Fabrication	I-1
	C. Task III - Simulator Experiments	I-1
II	SUMMARY OF ACCOMPLISHMENTS	II-1
III	TASK I - HIGH FREQUENCY ANALYSIS	III-1
	A. Experiments	III-3
	B. Analysis of Data	III-5
IV	TASK II - CHAMBER SIMULATOR FABRICATION	IV-1
	A. Apparatus	IV-1
	B. Preliminary Experiments	IV-2
	C. Analysis of Data	IV-7
	D. Conclusions and Recommendations	IV-10
V	TASK III - SIMULATOR EXPERIMENTS	V-1
	A. Flow-Through Experiments	V-2
	B. Flow-Past Experiments	V-7
VI	REFERENCES	VI-1
	APPENDIX A - Application of Theory	A-1
	APPENDIX B - Pressure-Phase Impedance Measuring Technique	B-1
	APPENDIX C - Flow Coefficient Experiments	C-1
	APPENDIX D - Acoustic Data	D-1
	APPENDIX E - Distribution List	E-1

ILLUSTRATIONS

FIGURE		PAGE
III-1	Nonlinear Resistance Data.	III-2
III-2	High Frequency Data Comparison	III-3
III-3	High Frequency Data for a Particular Resonator Assembly	III-4
III-4	Comparison of Pressure-Phase Data With ASTM Impedance Tube Data and Anemometer Data.	III-6
III-5	Resistance Data for Low Open Area Liner Samples. . .	III-7
III-6	Resistance Data for High Open Area Liner Samples . .	III-7
III-7	Proportionality Coefficient for Resonators of Various Open Area Ratios	III-8
III-8	Effect of Sample Thickness on Acoustic Resistance Proportionality Coefficient	III-8
III-9	Results of Spectrum Analysis for 5.4 and 8% Open Area Samples	III-10
III-10	Effects of Pressure Oscillations at First Harmonic on Resistance at Fundamental Frequency. . .	III-10
III-11	Comparison of Flow and Resistance Coefficients . . .	III-12
III-12	Effect of Facing Flow Coefficient on Acoustic Resistance.	III-14
III-13	Correlation of Resistance Data In the Transition and Nonlinear Acoustic Regimes.	III-15
III-14	Comparison of Nonlinear Correction Factors From High Frequency Experiments With Results From Impedance Tube Experiments.	III-17
III-15	Comparisons of Experimental Nonlinear Resistance Correction Factors With Theory of Sirignano	III-19
III-16	Comparison of Inertance Data With Present Theory . .	III-21
III-17	Error in Theoretical Effective Length Term	III-22
III-18	Comparison of Inertance Data With Improved Theory. .	III-22
IV-1	Static Tangential Chamber.	IV-2
IV-2	Modified Chamber Simulator	IV-3
IV-3	First Tangential Pressure Profile.	IV-4
IV-4	Instrumented Chamber Simulator	IV-6
IV-5	Illustration of Resonator Cavity And Instrumentation.	IV-7

ILLUSTRATIONS (Continued)

FIGURE		PAGE
IV-6	Comparison of Resistance Coefficient for Normal and Tangential Incidence.	IV-9
IV-7	Comparison of Effective Length Data With Theory.	IV-10
V-1	Sketch of Test Section - Impedance Measuring Device Used With Flow-Through Apertures.	V-2
V-2	Comparison of Data from the ASTM and the Pressure-Phase Experiments for Flow-Through Tests. .	V-3
V-3	Correlation of Data for Constant Frequency Experiments with the Ratio of the Net Flow-Through Velocity to the Peak Orifice Velocity for No Net Flow.	V-5
V-4	Summary of Experiments Showing the Effects of Flow-Through the Apertures on the Absorption Coefficient	V-6
V-5	Effects of Flow-Through Apertures on Effective Length	V-7
V-6	Flow-Past Apparatus.	V-8
V-7	Correlation of Acoustic Resistance Data with Velocity of the Flow Past the Apertures	V-9
V-8	Correlation of Acoustic Resistance Data with Mach Number of Flow Past the Apertures.	V-10
V-9	Effects of Velocity Past Apertures on Effective Aperture Length.	V-11
V-10	Comparison of Reactance Data with Theory for Sample with 0.05-in. Diameter Apertures.	V-12
V-11	Comparison of Reactance Data with Theory for Sample with 0.1-in. Diameter Apertures	V-12
V-12	Simultaneous Flow Apparatus.	V-13
A-1	Correlation of the Orifice Particle Velocity at Resonance with the Total Sound Pressure	A-3
A-2	Comparison of Experimental Results with the New and Old Design Theories.	A-9
B-1	High Frequency and High-Sound Pressure-Phase Angle Impedance Tube	B-2
B-2	Resonator Test Section	B-2
B-3	Schematic of Pressure-Phase Impedance Measuring Apparatus.	B-3

ILLUSTRATIONS (Continued)

FIGURE		PAGE
B-4	Helmholtz Resonator in Impedance Tube.	B-3
B-5	Estimated Resistance Error as a Function of Phase Angle	B-9
B-6	Estimated Reactance Error as a Function of Phase Angle	B-9
B-7	Estimated Error in Incident Sound Pressure as a Function of Impedance	B-11
B-8	Block Diagram of One Channel of Model 1034 Dual-Channel Synchronous Filter.	B-13
B-9	Block Diagram of Type 1036 Synchronous Connector . .	B-14
C-1	Apparatus for Measuring Resonator Facing Flow Coefficient	C-1

NOMENCLATURE

SYMBOL	DESCRIPTION
A	Maximum Pressure Amplitude
A_c	Cross Sectional Area of Cavity
A_2	Area of Apertures
c	Sonic Velocity
C_f	Flow Coefficient Defined as $C_d \cdot C_v$
C_D	Discharge Coefficient
C_c	Coefficient of Contraction
d	Aperture Diameter
f	Frequency
g	Gravitational Constant
I_i	Incident Intensity
I_t	Transmitted Intensity
k	Wave Length constant = ω/c
K	Resistance Coefficient = $R/\rho u$
K_1	Resistance Coefficient = $RC_f/\rho u$
K_2	Resistance Coefficient = $RC_f^2/\rho u$
L	Backing Distance
M	Mach Number
M_p	Mach Number of Flow Past Apertures
M_T	Mach Number of Net Flow Through Apertures
ℓ_{eff}	Effective Aperture Length
P_1	Total Pressure in Front of Sample
P_2	Total Pressure in Resonator Cavity
P_i	Incident Pressure
p	Static Pressure
R	Acoustic Resistance
R_f	Time Independent Resistance
r_w	Chamber Radius
t	Sample Thickness
u	Peak Particle Velocity
u_m	Mean Particle Velocity

NOMENCLATURE (Continued)

SYMBOL	DESCRIPTION
V_p	Velocity of Flow Past Apertures
V_c	Cavity Volume
V_T	Velocity of Net Flow Through Apertures
w	Mass Flowrate
X	Acoustic Reactance
χ	Specific Acoustic Reactance = $\chi/\sigma\rho c$
Y	Expansion Coefficient Accounting for Compressible Flow Effects
Z	Specific Acoustic Impedance
Z_p	Specific Acoustic Impedance of an Orifice
α	Absorption Coefficient
β	Diameter Ratio
θ	Specific Acoustic Resistance = $R/\sigma\rho c$
θ_V	Specific Acoustic Resistance with Flow
θ_1	Resistance at Fundamental Frequency with Increased Sound Level at First Harmonic
$\Delta_n \ell/d$	Nonlinear Correction Term
ϵ	Nonlinear Correction Factor = $(\Delta_n \ell/d) + 1$
ϵ_C	Nonlinear Corrector Factor Corrected for C_f
ϵ_E	Experimental Nonlinear Correction Factor
μ	Dynamic Viscosity
ν	Kinematic Viscosity
ϕ	Phase Angle
ρ	Density
σ	Open Area Ratio
σ_1	Function for High Open Area Ratios = $\sigma/1-\sigma^2$
ω	Angular Frequency
γ	Ratio of Specific Heats

NOMENCLATURE (Continued)

SYMBOL	DESCRIPTION
λ	Flow Through Coefficient Defined as $R/\rho V_T$
τ_1	Coefficient Defined As $RC_f^2/\rho V_T$
τ_2	Coefficient Defined As $RC_f^3/\rho V_T$
ξ	Angular Position

General Subscripts

o	Denotes Conditions at Resonance
NF	Denotes No Net Flow
1	Upstream of Sample
2	Downstream of Sample
E	Experimental
T	Theoretical
V	With Net Flow

Superscript

-	Denotes Time Varying Quantity

SECTION I
OBJECTIVE OF PROGRAM

The objectives of the work performed during the first year of effort under Contract NAS8-21310 were (1) to improve the present acoustic liner design theory in the high frequency and high sound pressure regime, and (2) to develop and demonstrate, using a cold-flow acoustic device, the techniques required for the measurement of absorbing liner acoustical characteristics during hot firings of rocket chambers. To meet these objectives, three tasks were defined, as described below.

A. TASK I - HIGH FREQUENCY ANALYSIS

Conduct experimental investigations using an existing standing wave impedance measuring device at frequencies up to 8000 Hz and at sound pressure levels to approximately 160 decibels (db)* and use the data, obtained by the pressure ratio-phase angle method, to provide the basis for a new or an improved absorbing liner design theory. In addition, obtain sufficient data at frequencies lower than 2000 Hz for comparison with standard ASTM impedance tube data.

B. TASK II - CHAMBER SIMULATOR FABRICATION

Fabricate a cylindrical cold-flow test apparatus for the purpose of obtaining resonator impedance data in a simulated rocket thrust chamber. The chamber to be equipped with a high-intensity sound generator capable of exciting a tangential mode of instability. The capability for gas flow through and past the resonators to be provided. Sound pressure level capability to be at least 160 db with frequencies to approximately 2000 Hz.

C. TASK III - SIMULATOR EXPERIMENTS

Conduct tests to determine any differences in the performance of resonator arrays between standing wave impedance tube data and tangential wave data obtained during tests of the apparatus fabricated under Task II. It was expected that this series of testing would develop the techniques and give a preliminary definition of the limitations of absorber impedance measurement during thrust chamber firings.

*In this report, all pressures expressed in db are based on a reference pressure of 0.0002 microbar.

SECTION II
SUMMARY OF ACCOMPLISHMENTS

Under Task I, 23 resonator assemblies (samples) were used in an existing high-frequency impedance measuring device to supply data for analysis. More than 300 data points were obtained at sound pressures up to 176 db. Analysis of the resistance data revealed the existence of significant sample-to-sample differences that were found to be caused by minute nonuniformities in the aperture edges. Excellent correlation of resistance data was obtained using a time independent flow coefficient as a measure of the edge effects. An equation expressing the functional relationship between resistance, particle velocity, density, and flow coefficient was formulated from an analogy with time-independent flow. The agreement of reactance data with experiment was found to be good, but some improvement through the use of a simple expression for the effective aperture length was noted. Comparisons of nonlinear correction factors computed from the high-frequency data were made with those obtained using ASTM probe-type impedance tubes by correlating the correction factors with sound pressure level. Agreement was found to be only fair with a considerable amount of scatter in the factors computed from the new data. The scatter was attritubed to both aperture edge effects and to the extremely wide range of geometric variables and conditions over which the experiments were conducted. No attempts to improve the correlation between the new factors and SPL were made because the correct proportionality between resistance and particle velocity is not expressed by the equation from which the correction factor is defined.

Under Task II, a static (no flow) chamber simulator was used to provide preliminary acoustic data on which the design of flow-type apparatus could be based. From the results of the preliminary experiments, it was shown that with a partitioned liner, the effects of incidence angle were negligible; therefore, either normal or tangential standing wave impedance measuring devices could be employed for the simulator flow experiments. The existing high-frequency impedance tube was modified for testing with flow through the apertures, and a new tube was designed for the experiments with flow past the apertures.

Simulator experiments (Task III) with flow past or with flow through the apertures showed that the empirical theory derived from probe-type impedance tubes predicted effects of flow on resistance to be significantly greater than that measured using the pressure-phase impedance measuring techniques. Reasons for the observed differences are believed to be caused by limitations and inaccuracies inherent to the probe-type impedance device when used with net flows. New empirical correlations, based on the simulator data, were formulated for use in liner design analyses.

From the results of the work reported herein, it is recommended that the following equations be used in the analytical design of absorbing liners; an example of one way in which the equations may be applied is presented in Appendix A.

Acoustic resistance with no net flow in the nonlinear regime characterized by particle velocities $\geqq$ 60 ft/sec:

$$R = 0.37\,\rho u (C_f)^{-2} \tag{II-1}$$

or

$$\theta = 0.37\, u/C_f^2\, c\sigma_1 \tag{II-2}$$

For velocities less than 60 ft/sec

$$R = (8\omega\rho\mu)^{1/2}\,(1 + t/d) \tag{II-3}$$

is a reasonable approximation; however, some uncertainty still exists as to how aperture edge effects should be considered at lower particle velocities. It is therefore recommended that further analysis be conducted in an attempt to improve the theory for use in the transition and linear regimes.

The acoustic reactance of a partitioned cavity of backing depth smaller than quarter wave length can be computed for a conventional resonator array with cavity cross-sectional area approximately equal to facing surface area from

$$\chi = \frac{\ell_{eff}\omega}{c\sigma} - \frac{c}{L\omega} \tag{II-4}$$

where

$$\ell_{eff} = t + d. \tag{II-5}$$

For situations with flow through or past the apertures the following should be used:*

Flow through the apertures:

$$\theta = \frac{M_T}{C_f^3 \sigma_1} \quad \text{where } M_T \geqq 0.5\ M_{NF} \tag{II-6}$$

If the net flow through the apertures is less than 0.5 M_{NF}, then equation (II-2) should be used. The reactance for any flow-through velocity is computed from equations (II-4) and (II-5).

Flow past the apertures:

$$\theta = \theta_{NF}\ (1 + 1.9\ M_p) \tag{II-7}$$

where θ_{NF} is the resistance calculated from equation (II-2), i.e., for no zero net flow. The equation

$$\ell_{eff_v} = (t + d)(1 - 1.65\ M_p) \tag{II-8}$$

should be used to calculate the effective length and then used in equation (II-4) to compute the reactance with flow past the apertures.

It is recommended that further experiments be conducted to better define the effect of higher, i.e., greater than a Mach number of 0.26, gas flow past on the acoustic characteristic of a resonator. The experiments should be conducted with media of different density to determine if the flow effects are dependent upon velocity or Mach number and with samples of various thickness, open area ratio, backing cavity depth, and aperture diameter.

The extrapolation of the liner design theory, based on the results of cold-flow experiments to hot-firing conditions, introduces significant uncertainties, primarily because the magnitude of pressure oscillations, particle velocities, and gas flow can only be approached in cold-flow simulations. In the past, it has been necessary to assume that the

*From the results of previous experiments (Reference 2), it was found that, for liners subjected to simulataneous flow through and past the apertures, the acoustic resistance should be computed as if only flow through were present.

results from the cold-flow experiments would be applicable to hot-firing situations principally because no reliable experimental techniques for making similar measurements during firings were known. Efforts under the present program have shown the pressure-phase impedance measuring technique to be an extremely precise experimental tool that can be readily adapted to hot-firing experiments. It is, therefore, recommended that such experiments be conducted for the purpose of verifying and improving, if necessary, the above design theory. Finally, it is also suggested that attempts be undertaken to improve the absorbing liner design theory for unpartitioned liners.

SECTION III
TASK I - HIGH FREQUENCY ANALYSIS

The absorption coefficient used in the analytical design of acoustic liners is computed from

$$\alpha = \frac{4\theta}{(\theta+1)^2 + \chi^2} \qquad \text{(III-1)}$$

where θ is the specific acoustic resistance and χ is the specific acoustic reactance of the resonator arrays. At frequencies near resonance where most liners are designed to operate, the resistance is much greater than the reactance ($\theta >> \chi$); thus, the resistance is the controlling factor in predicting the absorption of the liner.

For sound intensities of less than 100 db, where viscous drag caused by the oscillatory flow of gas through the apertures is the principal mechanism for energy loss, the resistance can be determined with sufficient accuracy using existing theory. But as the intensity is increased, extreme turbulence and circulatory flow patterns develop in the apertures, causing the resistance to become a nonlinear function of sound pressure. The resistance in this nonlinear regime cannot be predicted from theoretical considerations; therefore, designers must rely on experimental data for use in their analyses.

As first suggested by Ingard (Reference 1), the data are usually correlated in the form of an "end correction" factor, $\Delta_n \ell$, which must be added to the viscous resistance in the following manner:

$$\theta = \frac{(8\mu\rho\omega)^{1/2}}{\rho c \sigma} (1 + t/d + \Delta_n \ell/d) \qquad \text{(III-2)}$$

Until recently, the generation of high intensity sound in a controlled experiment was difficult; thus, only limited amounts of correction factor data for arrays of resonators were available. In 1967, as part of the final year of effort under Contract NAS8-11038, a conventional ASTM impedance tube with a high intensity electropneumatic sound generator was used to measure the resistance of three different resonator arrays (σ = 3, 5, and 10%) over a frequency range of 400 to 2000 Hz. Correction factors, computed from the data using equation (III-2), were correlated with sound pressure, as shown in figure III-1.

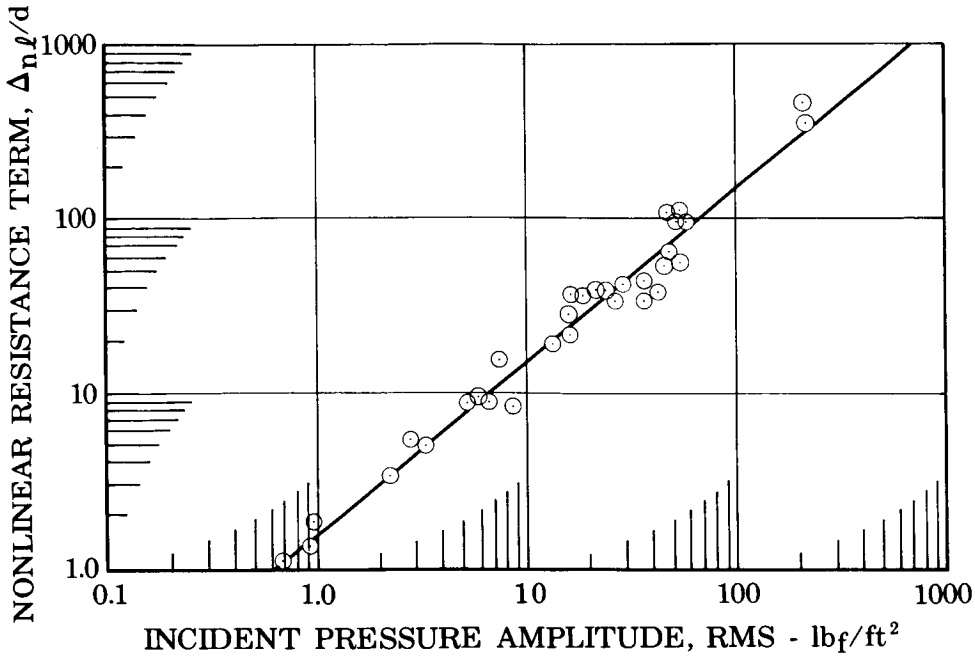

Figure III-1. Nonlinear Resistance Data FD 19156

Although the ASTM impedance tube is a useful apparatus for measuring absorption coefficients, it does have an inherent limitation, i.e., precise, high-frequency (above 2000 Hz) impedence data are difficult to obtain, especially with sound levels above 140 db. In an attempt to overcome this limitation, a pressure-phase impedance measuring device was fabricated and a series of preliminary experiments were conducted in which the absorption coefficients of several resonator arrays were measured at frequencies from 1000 to 8000 Hz (Reference 2). Comparison of results with absorption coefficients computed using the correction factors of figure III-1 showed that the coefficients could be accurately predicted up to a frequency slightly greater than that of resonance, but, at higher frequencies, the measured absorption coefficients were significantly lower than the computed values. (See figure III-2.) From these results, it was concluded that the use of the correction factor data in the acoustical regime characterized by high sound pressures and high frequencies was not valid, and it was recommended that the analysis of high-frequency impedance characteristics be continued as part of the present program.

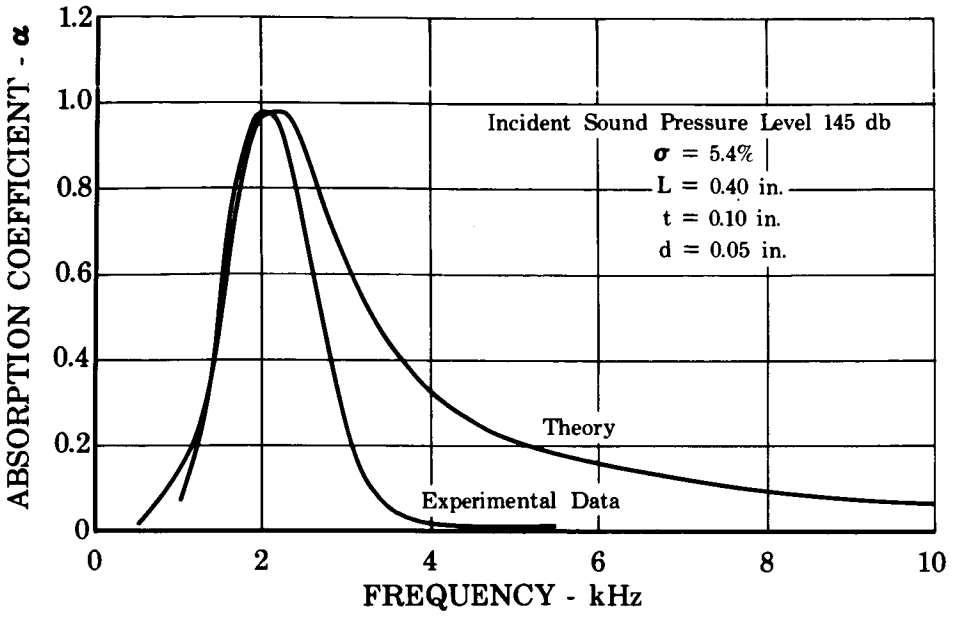

Figure III-2. High Frequency Data Comparison FD 31427A

A. EXPERIMENTS

To determine the relationship between the resonator configuration and its acoustical characteristics, each of the 23 resonator assemblies described in table III-1 was installed in the impedance apparatus described in Appendix B and tested over a range of frequencies and sound pressure levels. Over 300 data points were obtained, each consisting of a measurement of the cavity sound pressure and the phase angle for a set frequency and total sound pressure, i.e., the sound pressure in front of the resonator face. The range of frequencies and sound pressures was 700 to 5800 Hz and 140 to 176 db, respectively. The data from a series of experiments with one resonator at a constant sound level of 160 db are illustrated in figure III-3 to show how the cavity phase angle and sound pressure vary with frequency.

Table III-1. Resonator Configurations Used in Impedance Experiments

Resonator Sample No.	Open Area Ratio, %	Sample Thickness, in.	Cavity Backing Depth, in.	Aperture Diameter, in.
1	1.50	0.10	0.50	0.047
2	3.00	0.10	0.50	0.056
3	3.95	0.09	0.50	0.052
4	5.40	0.10	0.50	0.052
5	5.65	0.09	0.50	0.047
6	6.90	0.10	0.50	0.052
7	8.00	0.10	0.50	0.056
8	8.85	0.10	0.50	0.047
9	10.80	0.10	0.50	0.052
10	13.00	0.10	0.50	0.052
11	5.40	0.05	0.50	0.052
12	5.40	0.15	0.50	0.052
13	5.40	0.20	0.50	0.052
14	5.40	0.25	0.50	0.052
15	13.00	0.10	0.15	0.052
16	10.80	0.10	0.20	0.052
17	10.80	0.10	0.15	0.052
18	5.40	0.10	0.50	0.037
19	5.40	0.10	0.50	0.094
20	5.40	0.10	0.40	0.052
21	5.40	0.10	0.60	0.052
22	8.0	0.10	0.40	0.056
23	8.0	0.10	0.60	0.056

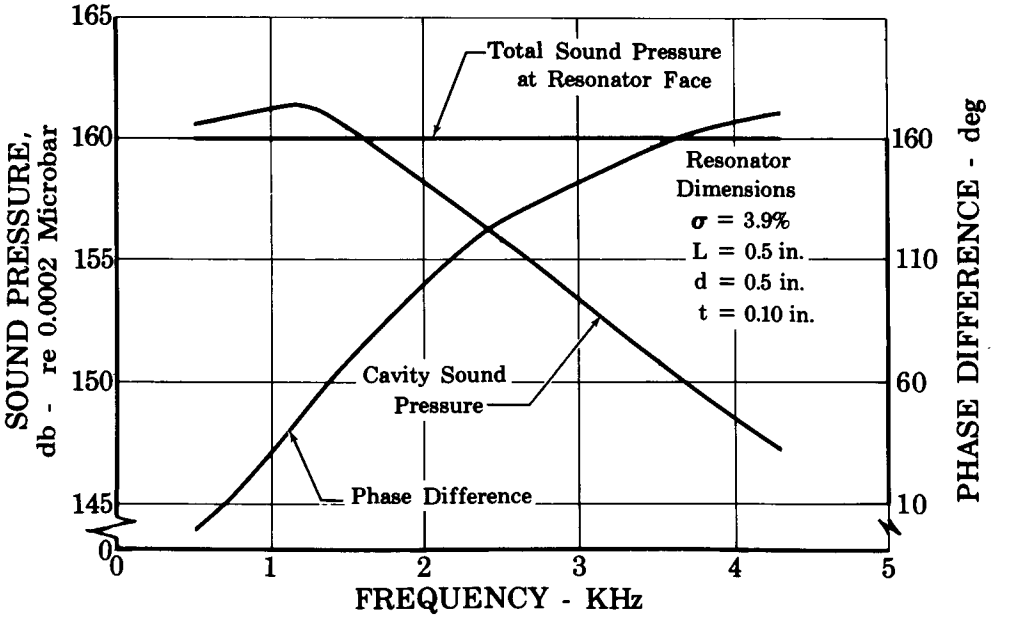

Figure III-3. High Frequency Data for a Particular Resonator Assembly FD 31349A

B. ANALYSIS OF DATA

The equations derived in Appendix B were programmed for a digital computer and were used to determine the components of impedance, absorption coefficients, incident sound pressures, and orifice velocities from the pressure-phase data; results are included in Appendix D. The computations were made for every data point, however, not all of the data were used in the following analysis. An error analysis of this experiment (see Appendix B) showed that significant errors can be introduced at certain phase angles and, if the total resonator impedance fell below 0.5, therefore, such data were excluded.

1. Acoustic Resistance Data

Originally, two approaches were to be taken in the analysis of the acoustic resistance data: nonlinear correction terms were to be computed and correlations similar to that of figure III-1 were to be attempted. The other approach was to be based on observations published by Ingard and Ising (Reference 3). A discussion of results from the latter approach is presented first.

In their work, Ingard and Ising used a hot-wire annemometer to measure the oscillatory flow velocity, u, in a single orifice mounted at the end of a tube. A piston driven at a frequency of 150 Hz was used to generate sound pressures up to 162 db. Using their data, the researchers showed that when the orifice velocity was greater than approximately 30 ft/sec, the driving sound pressure was approximately equal to ρu^2. In addition, in the nonlinear regime, when the resistance was significantly greater than the orifice reactance, they found that,

$$R \simeq \rho u$$

and confirmed that the relation was frequency-independent, at least up to a frequency at which the orifice reactance equals the resistance. (Note, however, that even though the function $R = \rho u$ is independent of frequency per se, the resistance will vary with frequency because the particle velocity for a particular resonator varies with frequency.) Such a simple expression for the acoustic resistance would be extremely useful for acoustic liner design purposes; therefore, attempts to

develop a similar function from the high-frequency resonator data were begun.

The resonator array with an open area ratio of 1.5% was most like the single orifice used by Ingard and Ising that had a σ of 0.5%; thus, the data from that array were compared with their annemometer data. Also included in the comparison were the earlier ASTM impedance tube data of Bies and Wilson (Reference 4) and Ingard's data of 1953 (Reference 1). As shown in figure III-4, excellent agreement among all of the data samples was found.

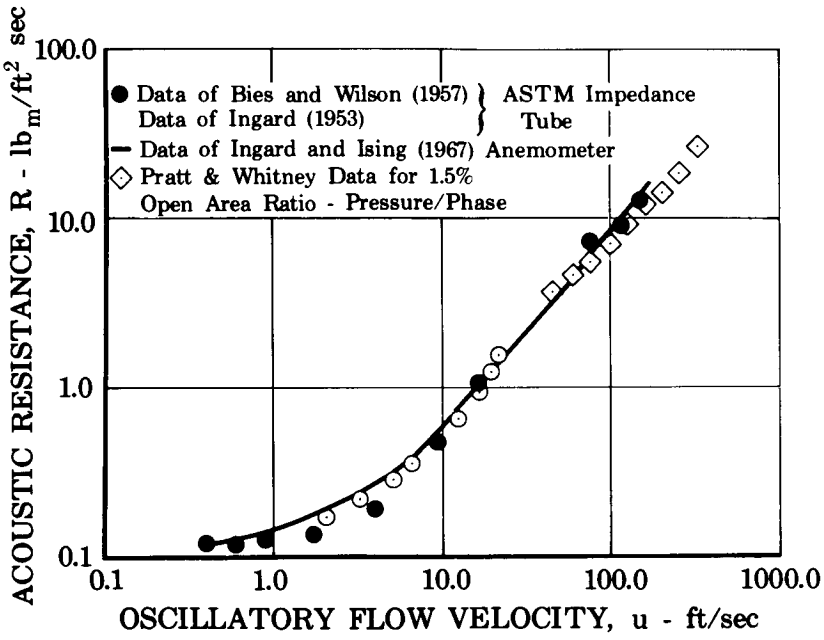

Figure III-4. Comparison of Pressure-Phase Data With ASTM Impedance Tube Data and Anemometer Data FD 33034

Shown in figures III-5 and III-6 are the results of similar comparisons of the resistance data obtained from resonators with open area ratios greater than 1.5%. The resistance for each particular facing sample was found to be directly proportional to the orifice particle velocity, but in every case the resistance fell lower than the line representing the function $R = \rho u$. In addition, significant sample-to-sample differences in the data from each resonator were evident.

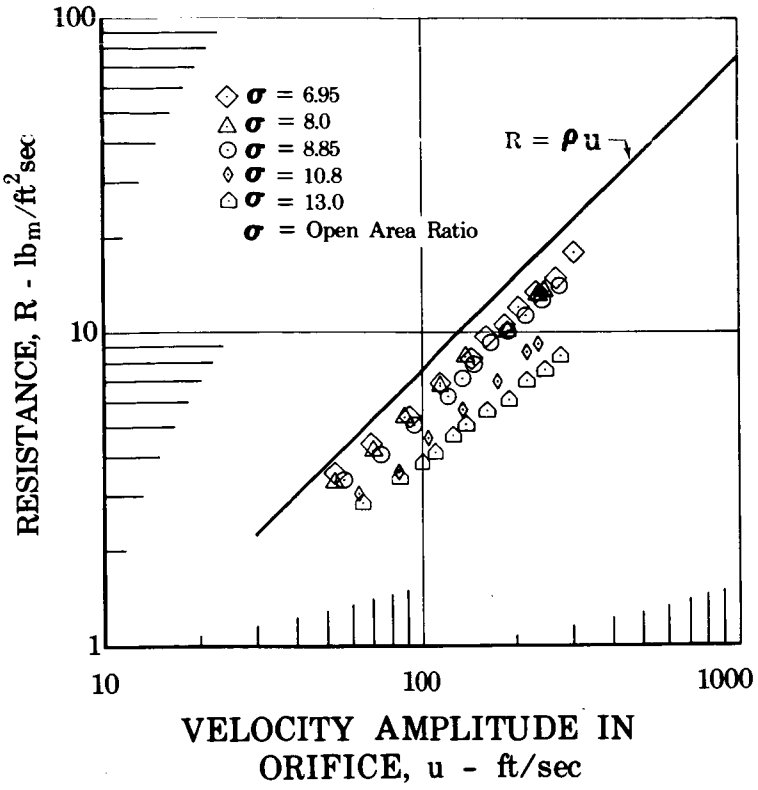

Figure III-5. Resistance Data for Low Open Area Liner Samples FD 27990A

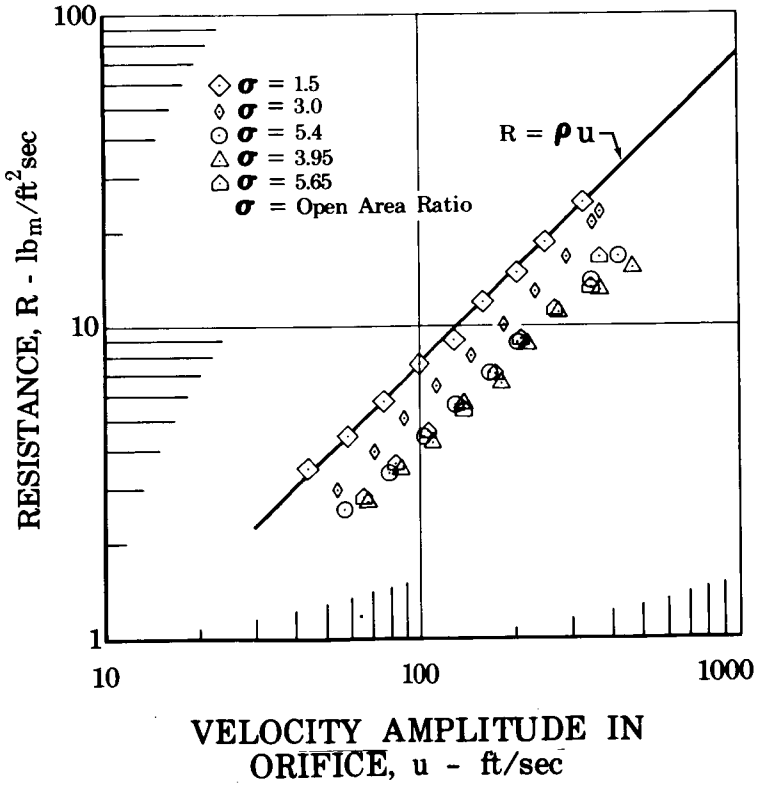

Figure III-6. Resistance Data for High Open Area Liner Samples FD 29159A

As an aid in further investigation of the sample-to-sample differences in resistance, a coefficient of proportionality, K, defined as the ratio of resistance to the product of particle velocity and density, i.e., $K = R/\rho u$, was computed for each data point. Correlation of the proportionality coefficient with open area ratio and facing thickness was attempted, as shown in figures III-7 and III-8, but no creditable functional relationship between K and either geometric variable could be established.

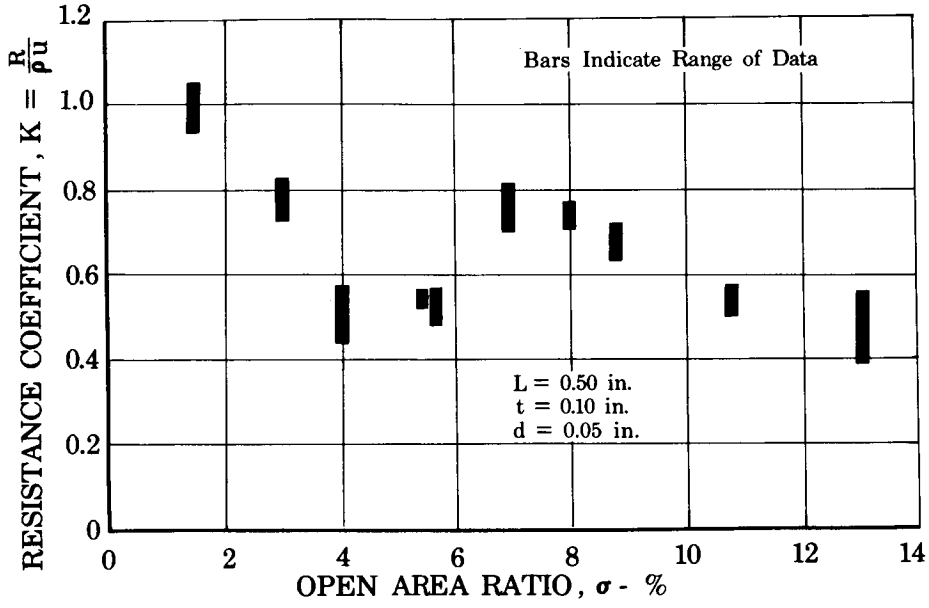

Figure III-7. Proportionality Coefficient for Resonators of Various Open Area Ratios FD 29162

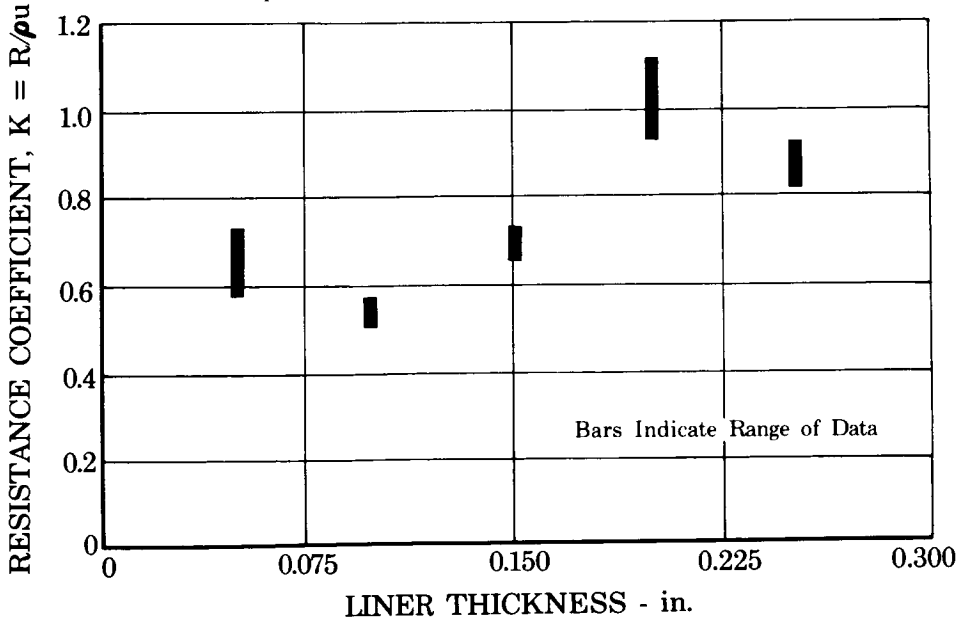

Figure III-8. Effect of Sample Thickness on Acoustic Resistance Proportionality Coefficient FD 29157

a. Spectrum Analyses

A possible cause of the variation in the resistance data was considered to be the harmonics of the fundamental frequency that might be present in the impedance apparatus and resonator cavity. Even though all harmonics are electronically filtered before the sound pressures were recorded, it was not known what effect superimposed harmonics might have on the orifice velocity. If the effect were to increase the velocity without changing the resistance, the value of K could be significantly affected. To investigate this possibility, additional high-frequency experiments were conducted. For the experiments, two of the sound sources were connected to a separate oscillator and amplifier so that sound waves at two different frequencies could be introduced. First, spectrum analyses were made with the 5.4 and 8.0% open area ratio samples installed in the impedance tube. As shown in figure III-9, sound pressures with frequencies corresponding to the first four harmonics were detected with both resonator assemblies. In neither case were pressures at frequencies lower than that of the fundamental found in the impedance tube or resonator cavity.

The fundamental frequency was next introduced at a level of 135 db using two drivers, and the resulting basepoint sound level was measured at the first harmonic. Then through the use of two additional drivers, the sound pressure at the first harmonic was increased in 5-db increments until it exceeded the 135 db level at the fundamental by 15 db. The ratio of the resistance at the fundamental frequency to the basepoint resistance at the same frequency is shown in figure III-10 as a function of the harmonic sound level. The results show that the resistance at the fundamental frequency is not affected until the sound level at the first harmonic exceeds that at the fundamental by 10 db or more. The results of the above spectrum analysis showed that the amplitude of all natural harmonics were lower than that of the fundamental; therefore, the effect of harmonics were eliminated as a possible cause of the sample-to-sample differences in the resistance data.

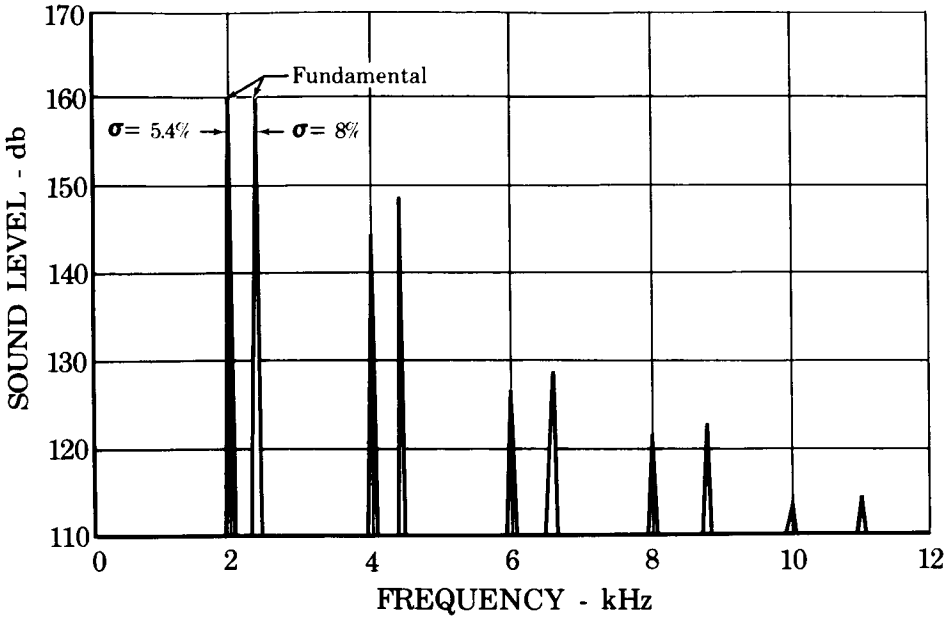

Figure III-9. Results of Spectrum Analysis for 5.4 and 8% Open Area Samples FD 29158

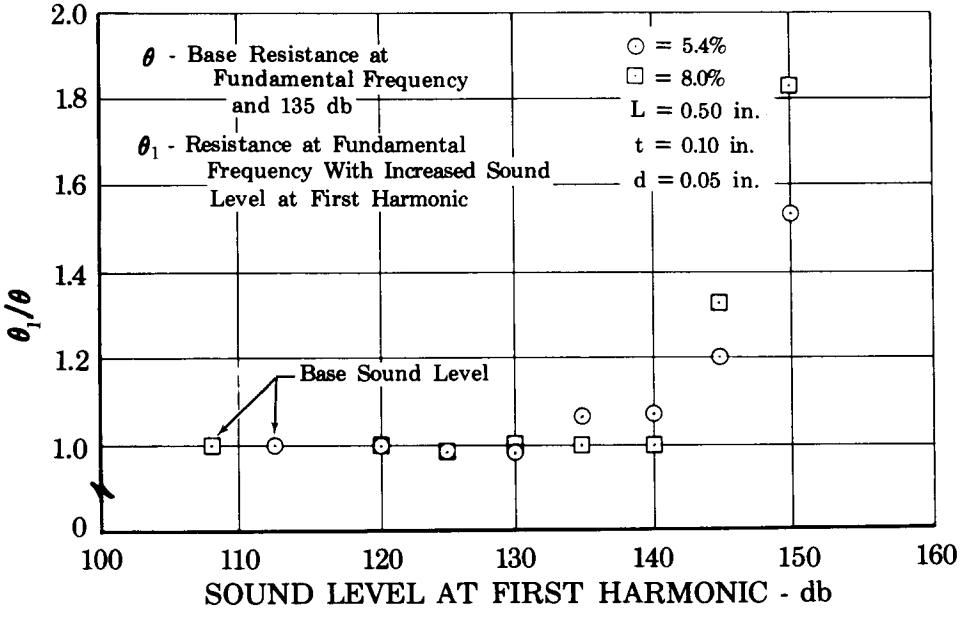

Figure III-10. Effects of Pressure Oscillations at First Harmonic on Resistance at Fundamental Frequency FD 29160

b. Flow Coefficient Effects

It has long been known that the acoustic impedance of resonators operating in the nonlinear regime is strongly affected by the circulatory flow patterns that develop in the vicinity of the orifice. In 1950,

Ingard and Labate (Reference 5), using stroboscopic illumination of smoke particles, investigated the acoustical streaming around resonator orifices. Circulatory flow patterns were analyzed as a function of the oscillatory particle velocity through the orifice and the various types of circulation were classified into the four following regions:

Region 1. A low sound region with stationary circulation; the flow is directed out from the orifice along the axis

Region 2. A region of stationary circulation in which the direction of flow along the axis is toward the orifice, i.e., the reverse of that in Region 1

Region 3. A medium sound intensity region where pulsatory effects are superimposed on circulation of the kind in Region 2

Region 4. A high sound intensity region in which pulsatory effects are predominant, resulting in the formation of jets and vortex rings: the jet consists of a strong airflow through the orifice, signified by a sudden burst of air; this burst appears symmetrically on both sides of the orifice and is made up of pulses contributed by each cycle of the sound wave.

In all of the experiments reported herein, the sound levels were high enough to cause the type of circulation patterns of Regions 3 and 4, i.e., regions of extreme turbulence characterized by pulsatory jets. Highly turbulent time-independent flow through orifices is known to be significantly affected by slight (or even minute) changes in the orifice edge shape, e.g., a square-edged orifice has a higher resistance to flow than an orifice of identical diameter but with a slightly rounded leading edge.

With time-independent flow, a measure of edge effects is obtained through the use of a flow coefficient in the equations relating flow-rate to pressure differential, (ΔP), i.e.,

$$w = A_2 C_f Y_1 \sqrt{\frac{2g\rho\Delta P}{1 - (\beta)^4}} \qquad \text{(III-3)}$$

where C_f is a single flow coefficient consisting of the product of the contraction coefficient and the discharge coefficient. This flow coefficient was experimentally determined with time-independent flow* for

*Refer to Appendix C for a description of flow coefficient experiments.

several resonator facing samples of identical open area ratio and aperture diameter for which the acoustic resistance had been previously measured.

Correlation of the inverse of the flow coefficient with the acoustic resistance coefficient, shown in figure III-11, revealed similar trends in both sets of data and indicated that further analysis was warranted.

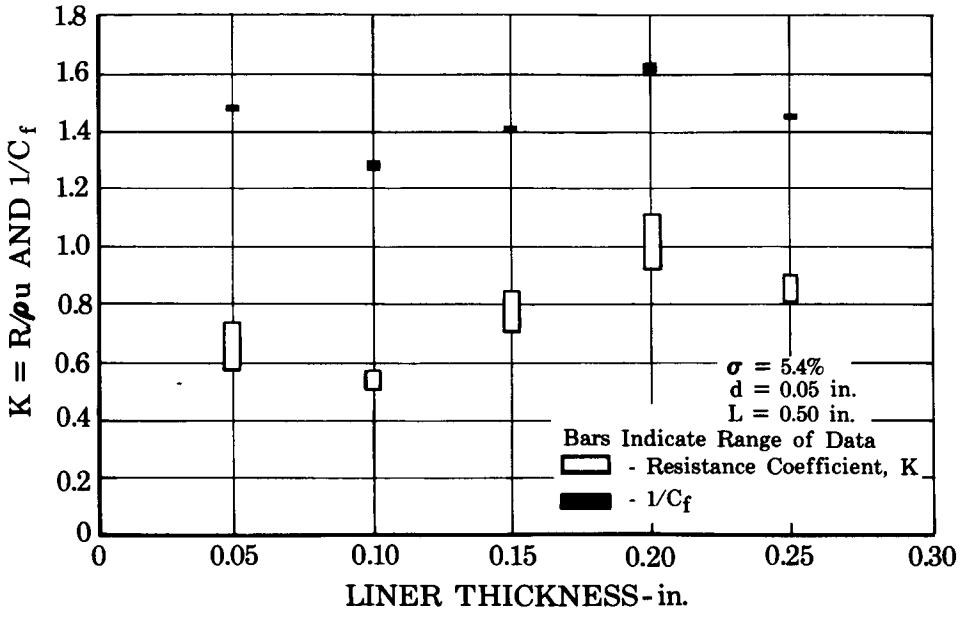

Figure III-11. Comparison of Flow and Resistance Coefficients FD 29161

Flow coefficients of the remaining facing samples were measured, and, in an attempt to determine the functional relationship between the two coefficients, the following flow-acoustic analogy was investigated.

The definition of the acoustic impedance of an orifice

$$Z_p = R + iX = \frac{\overline{P}_1 - \overline{P}_2}{u} \qquad \text{(III-4)}$$

may, for the nonlinear regime where $R \gg X$, be written as simply

$$R \simeq \frac{\overline{P}_1 - \overline{P}_2}{u} \qquad \text{(III-5)}$$

For time-independent flow through an orifice, the analogous flow resistance parameter is defined as

$$R_f = \frac{P_1 - P_2}{u_m} \tag{III-6}$$

where $P_1 - P_2$ is the pressure differential and u_m is the mean velocity in the orifice. The orifice equation for imcompressible flow and neglible approach factor

$$u_m = C_f \sqrt{2g\ (P_1 - P_2)/\rho} \tag{III-7}$$

may be rewritten as

$$\frac{P_1 - P_2}{u_m} = \frac{\rho u_m}{2g\ (C_f)^2} \tag{III-8}$$

Using equations (III-6) and (III-8), the following proportionality is established.

$$R_f \propto \frac{\rho u_m}{(C_f)^2} \tag{III-9}$$

The similarity in the acoustic and flow resistance parameters and the known dependence of the flow resistance upon the flow coefficient, C_f, suggests that if the flow coefficient is to be correlated with acoustic resistance data, the most suitable functional relationship should be of the form,

$$R = R\left(\rho,\ u,\ C_f^{-2}\right) \tag{III-10}$$

Correlation of the resistance data with the flow coefficient using the data from all facing samples was attempted. A mean value of the proportionality coefficient, K, was determined from the resistance data of each sample, and, in addition, two new proportionality coefficients defined as

$$K_1 = \frac{R}{\rho u} C_f \tag{III-11}$$

and

$$K_2 = \frac{R}{\rho u} (C_f)^2 \qquad \text{(III-12)}$$

were computed. It is worthy of note that K_2 is written in the same terms as those of equation (III-10). The results are shown in figure III-12.

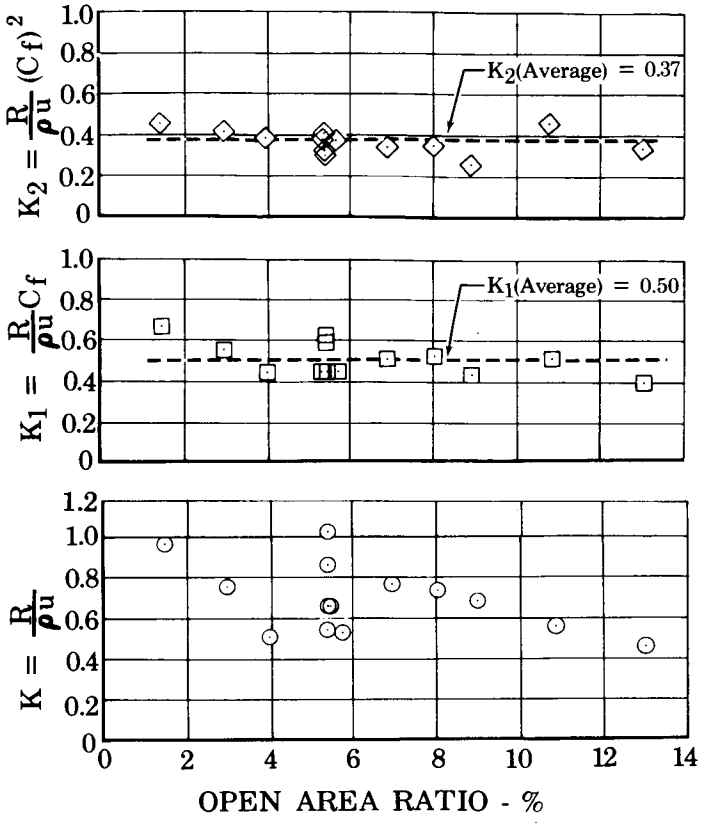

Figure III-12. Effect of Facing Flow Coefficient on Acoustic Resistance FD 29171

It is evident that the sample-to-sample differences in the K_1 and K_2 values are significantly less than the original K values; the differences in K_2 appear to be somewhat less than those of K_1, which is substantiated by comparing the deviations in the K_1 and K_2 values, as follows

Coefficient	Average Value	Average Deviation, %	Maximum Deviation, %
K_1	0.50	13.4	34
K_2	0.37	12.5	32

From the results, it is concluded that the most precise representation

of the acoustic resistance data in the nonlinear regime is

$$R = 0.37\ \rho u C_f^{-2} \qquad \text{(III-13)}$$

It is interesting to note that a sharp-edged orifice like that used by Ingard and Ising (Reference 3) is known to have a flow coefficient of approximately 0.61. If that value is used in equation (III-13)

$$R = \frac{0.37}{(0.61)^2}\ \rho u = 1.0\ \rho u \qquad \text{(III-14)}$$

further corroboration of the validity of equation (III-13) is obtained.

Equation (III-13) is only valid for use in the nonlinear regime, thus the particle velocity at which the transition from the linear to the nonlinear regime occurs must be known. To define the velocity additional data were taken using six resonator assemblies over a range of velocities from 5 to 400 ft/sec. As shown in figure III-13 the data were correlated in the form RC_f^2 as a function of particle velocity. From these results the particle velocity that separates the nonlinear regime from the transition and linear regimes was arbitrarily chosen to be 60 ft/sec.

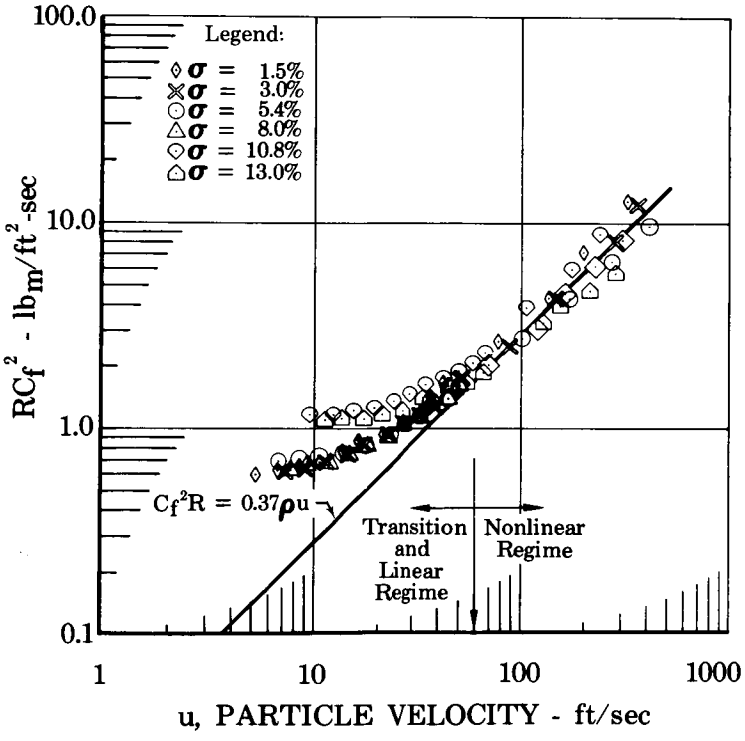

Figure III-13. Correlation of Resistance Data In the Transition and Nonlinear Acoustic Regimes FD 31421

c. Nonlinear Correction Factors

A second approach in the analysis of the resistance data involved the nonlinear correction factors commonly used for design purposes. The factors were computed from the data using equation (III-2), i.e.,

$$\Delta_n \ell/d = \frac{\theta \rho c \sigma}{(8\mu\rho\omega)^{1/2}} - 1 - t/d \qquad \text{(III-15)}$$

where θ is the experimental specific acoustic resistance. Results are shown in figure III-14; also shown are lines representing correction factors from the ASTM impedance tube experiments (Reference 2) and the original correlations of Ingard (Reference 1) and Blackman (Reference 6). Agreement between the impedance tube correction factors and those from the pressure phase experiments is as good as can be expected in view of the amount of scatter in the new data. The scatter can be attributed to both aperture edge effects and to the extremely wide range of geometric variables and conditions over which the experiments were conducted. No attempts to improve the correlation between the new factors and SPL were made due to the fact that a simple relation between incident SPL and $\Delta_n \ell/d$ is only valid for $f \leq f_o$ because the correct proportionality between resistance and particle velocity at frequencies greater than resonance is not expressed by the equation from which the correction factor is "defined" (equation III-2).

For example, assume equation (III-2) and the $\Delta_n \ell/d$ function of Reference 2, $\Delta_n \ell/d = 1.6\ P_i$, where P_i is the incident sound pressure in lb/ft^2, are used to compute the resistance for a resonator operating with constant incident pressure but variable frequency. At frequencies up to and including that of resonance, θ will be correct within the limits of experimental error. At resonance, the particle velocity is a maximum; thus, the velocity will be less at all other frequencies. Because $R \propto u$, the resistance at all other frequencies must also be less than the value at resonance. The dependence of resistance upon frequency in equation (III-2) is

$$\theta \propto f^{1/2}$$

which correctly accounts for the decrease in resistance with particle velocity below resonance, but which produces an increasing error as frequency is increased above resonance. The situation can be corrected by rewriting equation (III-2) so that the correct functional relationship between resistance and all frequencies is established. To do so, however, only leads to an unnecessary complication, because the true variable affecting resistance is velocity not frequency.

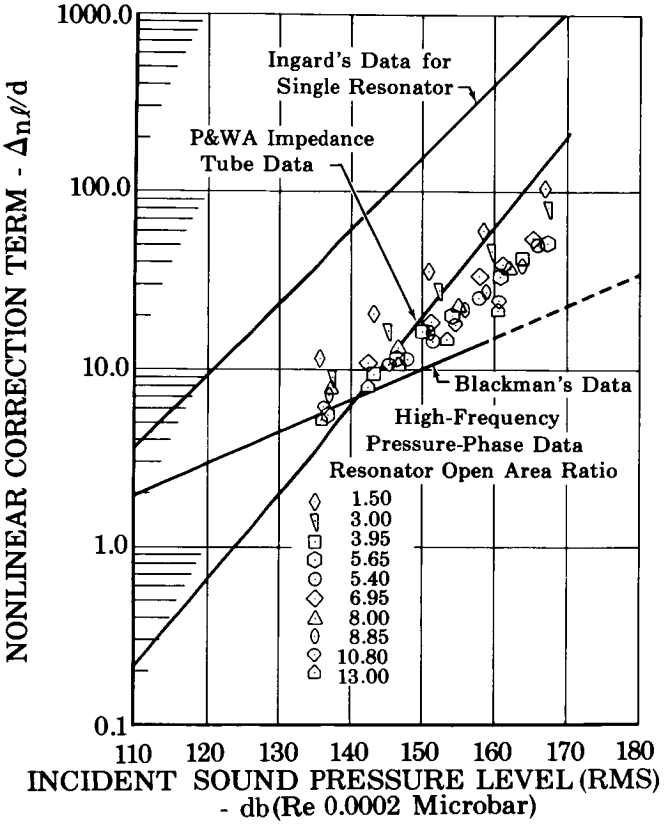

Figure III-14. Comparison of Nonlinear Correction Factors From High Frequency Experiments With Results From Impedance Tube Experiments FD 29175

Expressing the correction factor as a function of particle velocity has been attempted by Ingard (Reference 1), Blackman (Reference 6), Sirignano (Reference 7), and others; however, Ingard's and Blackman's corroboration with resonator array experiments has been rather poor.

The theory of Sirignano is unique in that he has corrected the defined $\Delta_{n\ell}$ to account not only for the incorrect frequency relation but also for the density and viscosity so that the proper functional relation for resistance in the nonlinear regime is obtained. This may be shown by the following.

Sirignano's theory states

$$\epsilon = \frac{u}{3\pi}\sqrt{\frac{2\rho}{\omega\mu}} \qquad \text{(III-16)}$$

where

$$\epsilon = (\Delta_{n\ell}/d) + 1 \qquad \text{(III-17)}$$

If equation (III-2) is written in the following form

$$R = \theta\rho c\sigma = (8\mu\rho\omega)^{1/2}\,(1 + t/d + \Delta_{n\ell}/d) \qquad \text{(III-18)}$$

and equation (III-16) is substituted, then

$$R = (8\mu\rho\omega)^{1/2}\,(t/d + \epsilon) \qquad \text{(III-19)}$$

In the nonlinear regime $\epsilon >> t/d$ is a reasonable assumption; hence, it can be neglected in the above equation. Replacing ϵ by equation (III-16) and simplifying produces

$$R = \frac{4\rho u}{3\pi} = 0.43\rho u \qquad \text{(III-20)}$$

which shows that even though Sirignano's defined nonlinear correction term, equation (III-16), is a function of both frequency and viscosity, when the term is used with equation (III-19) to compute the acoustic resistance the two variables cancel so that the resulting expression, equation (III-20), is correctly independent of both. However, comparison of equation (III-20) with equation (III-13) suggests that the Sirignano theory will not account for aperture edge effects and if the theory is modified by the flow coefficient to account for these effects in the following manner:

$$\epsilon_C = \epsilon C_f^{-2} \qquad \text{(III-21)}$$

then the values of ϵ_C will be, on the average, approximately 16% higher than experimental data.

To check the hypothesis, a comparison of the correction factor data with equation (III-16) was made. The results are shown in figure III-15 as the ratio of ϵ / ϵ_E where ϵ_E is the value of $(\Delta_n \ell/d + 1)$ computed from the resistance data (again using equation (III-15) and ϵ is computed using equation (III-16). As expected the resulting sample-to-sample differences appear similar to those found to be caused by aperture edge effects. (See figures III-7 and III-8.)

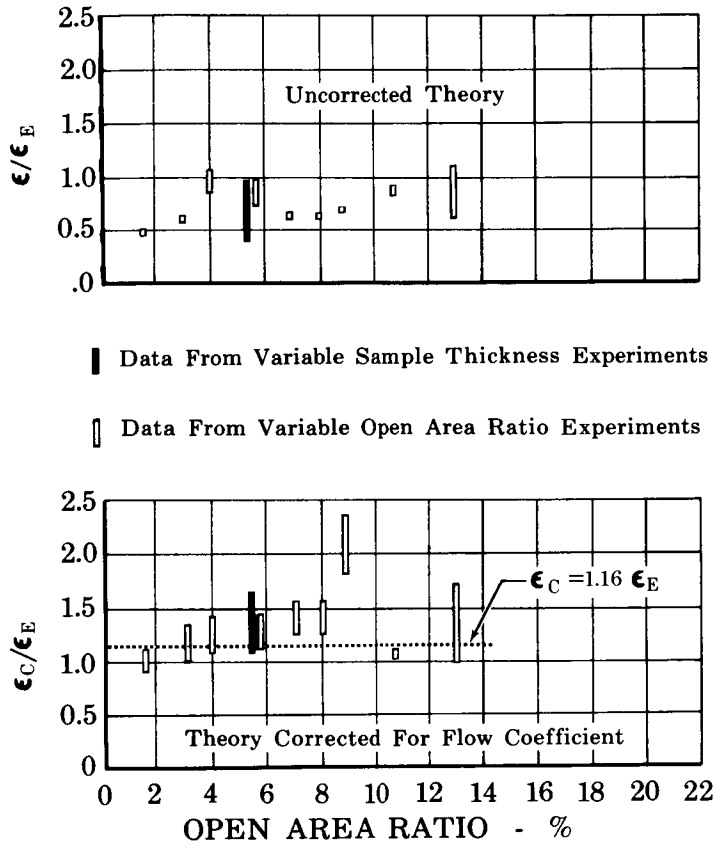

Figure III-15. Comparisons of Experimental Non-linear Resistance Correction Factors With Theory of Sirignano FD 31420

To correct for the edge effects the theoretical values of ϵ were multiplied by the value of C_f^{-2} for each facing sample; results are also shown in figure III-15, as a ratio of ϵ_C/ϵ_E where ϵ_C is the corrected value.

A decrease in sample-to-sample differences is observed, and a line representing a 16% difference between theory and experiment in figure III-15 may be noted to pass through most of the data. The variation with σ should not be mistaken as a possible result of variations in the thickness-to-diameter ratio; this ratio was essentially constant (≈ 2) for all but the shaded bar.

2. Acoustic Reactance Data

From the analysis of the nonlinear regime reactance data, it was found that the present theory is in good agreement with experiment; however, improvement was obtained by using a new simple expression for the effective aperture length. No aperture edge effects in the reactance data were noted and no improvement in the theory through the use of the flow coefficient could be obtained. A summary of this work, including the most significant results, are described in the following paragraphs.

To show a comparison of the reactance data with theory, the results from experiments with apertures of various thickness were used. The theoretical reactance was determined from the equation

$$\chi = \frac{2\pi}{c} \frac{\ell_{eff}}{\sigma} f - \frac{c}{2\pi} \frac{1}{L} \frac{1}{f} \qquad \text{(III-22)}$$

where the term containing ℓ_{eff} is the inertance, and the term containing L is the capacitance. The effective aperture length was determined from the equation

$$\ell_{eff} = t + 0.85\, d\, (1 - 0.7\sqrt{\sigma}). \qquad \text{(III-23)}$$

The experimental values of inertance, reactance, and effective length were determined using the pressure-phase data, as shown in Appendix B.

Only a comparison of the inertance data (figure III-16) need be made because the capacitance is an exact term. The agreement at high frequencies is of the same degree as at the low frequencies. Apparently, there is no need to improve the method of predicting inertance at high frequencies; however, the theory could be improved for better agreement at all frequencies by improving the expression for effective length. Additional analysis of the data with this objective was attempted.

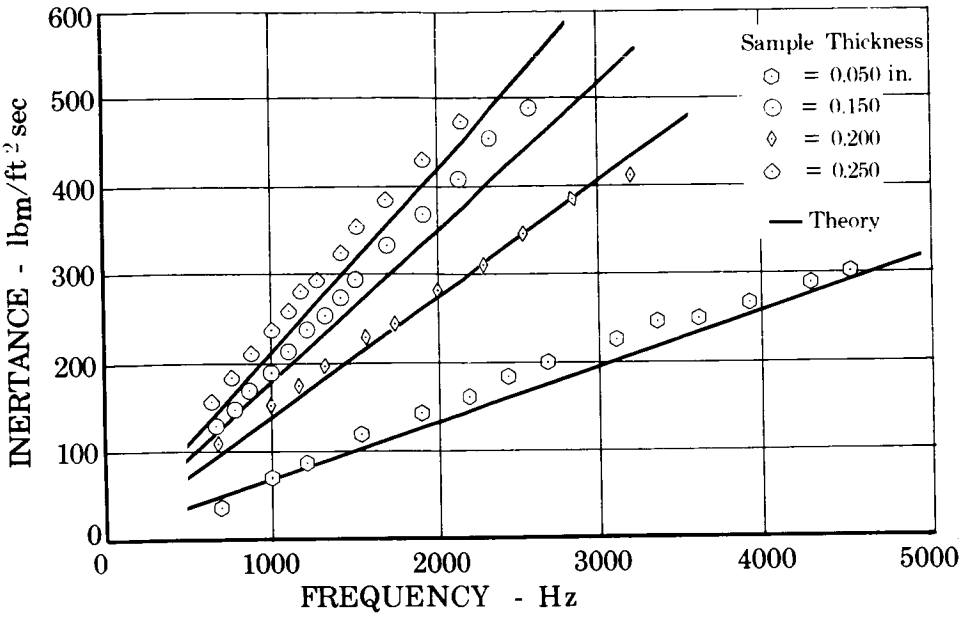

Figure III-16. Comparison of Inertance Data With Present Theory FD 29173A

Analysis of a large sample of effective length data led to the conclusion that the best representation for the effective length is simply

$$\ell_{eff} = t + d \qquad \text{(III-24)}$$

where t is the resonator facing thickness and d is the aperture diameter. The error in the use of the equation is demonstrated in figure III-17. It is worthy to note that except for the data from one particular facing, the maximum error is less than $\pm$ 20%. The use of equation (III-24) to predict the frequency of resonance

$$f_o = \frac{c}{2\pi}\sqrt{\frac{\sigma}{L\ell_{eff}}} \qquad \text{(III-25)}$$

will result in a much smaller error in f_o because ℓ_{eff} appears to the -1/2 power. The improvement in agreement between inertance data and theory using equation (III-24) may be noted by comparing figure III-16 with figure III-18.

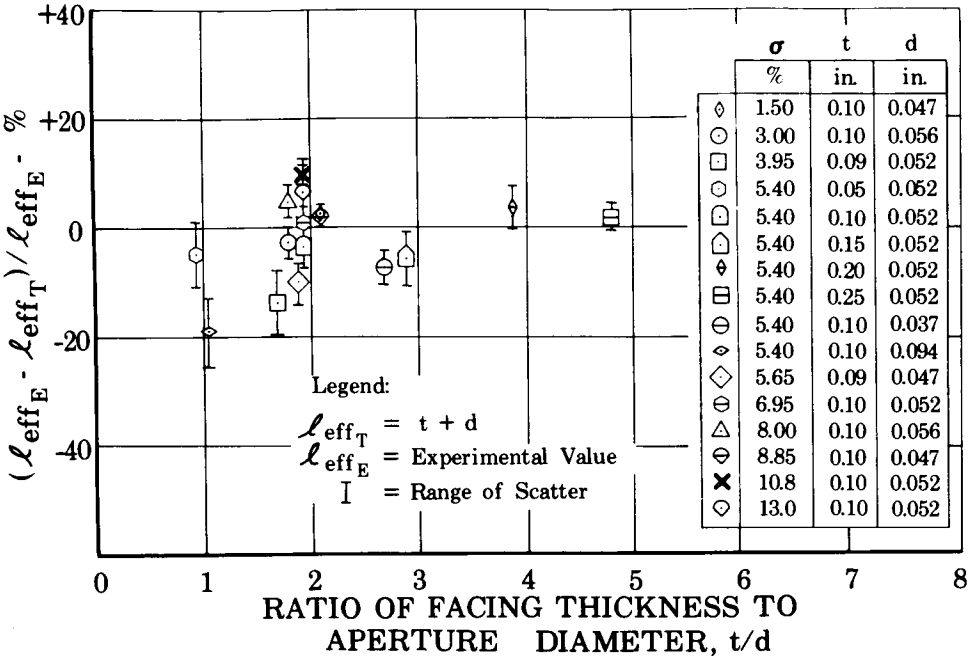

Figure III-17. Error in Theoretical Effective Length Term FD 31350

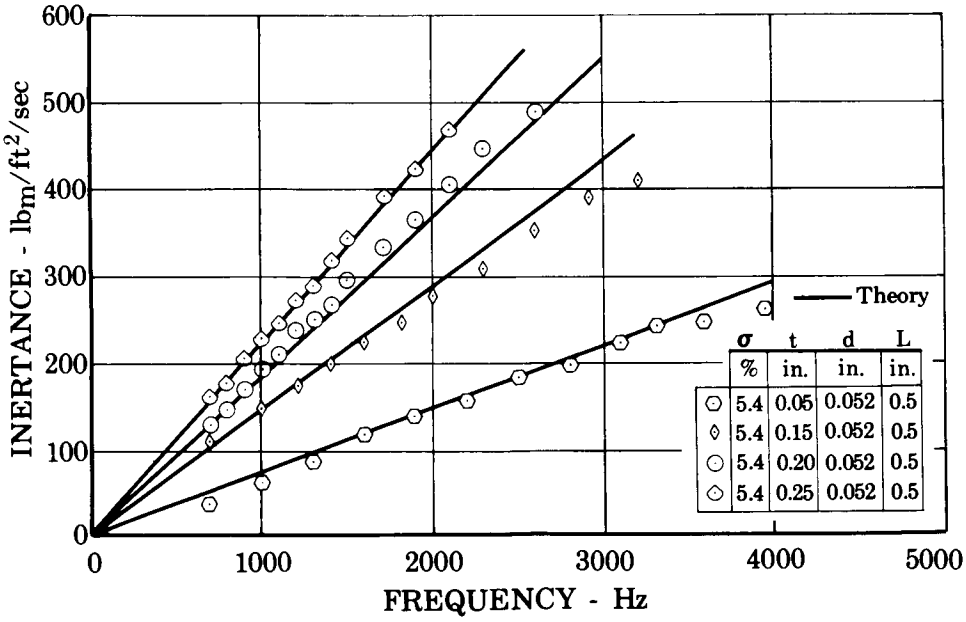

Figure III-18. Comparison of Inertance Data With Improved Theory FD 31378

SECTION IV
TASK II - CHAMBER SIMULATOR FABRICATION

The objective of the work performed under Task II was the fabrication and preliminary checkout of a cylindrical acoustic device that could be used to provide impedance data for an absorbing liner in a simulated rocket chamber. This type of experiment was necessary for the reason discussed below.

The theory used in the design of absorbing liners utilizes empirical correlations developed from impedance data obtained with ASTM-type impedance tubes. Impedance apparatus of this type use flatplate liner samples rigidly mounted at the end of a tube in which the only organized acoustic modes are longitudinal. In these types of tests both the incident, refracted and reflected waves must be normal to the liner surface; therefore, results obtained applied only to one-dimensional, normal reacting surfaces.

For such surfaces, the refracted pressure wave travels nearly normal to the surface, irrespective of the particular angle of incidence; hence, it is reasonable to assume that the ratio of acoustic pressure acting upon the surface to the fluid velocity normal to the surface will also be independent of the direction of the incident wave. Then the impedance of the surface, which by definition is the above ratio, can be expressed simply as the normal specific acoustic impedance.

Uncertainty in the formulation of the absorbing liner theory is introduced by the assumption that a cylindrical surface has the same acoustic characteristics as a one-dimensional normally reacting surface. To eliminate this uncertainty it was necessary to determine the acoustic characteristics of a cylindrical liner having obliquely incident sound waves and to determine if such a liner is a normally reacting surface.

A. APPARATUS

No design criteria have been set forth for the design of tangential and radial acoustic chambers; therefore, a static (i.e., without flow capabilities) tangential acoustic chamber was fabricated so that tests could be conducted to provide design information for the chamber simulator. (See figure IV-1.) This information would include the number of acoustic drivers necessary for nonlinear operation, the response characteristics

of the chamber, and an efficiency evaluation of the coupling device between the drivers and the chamber.

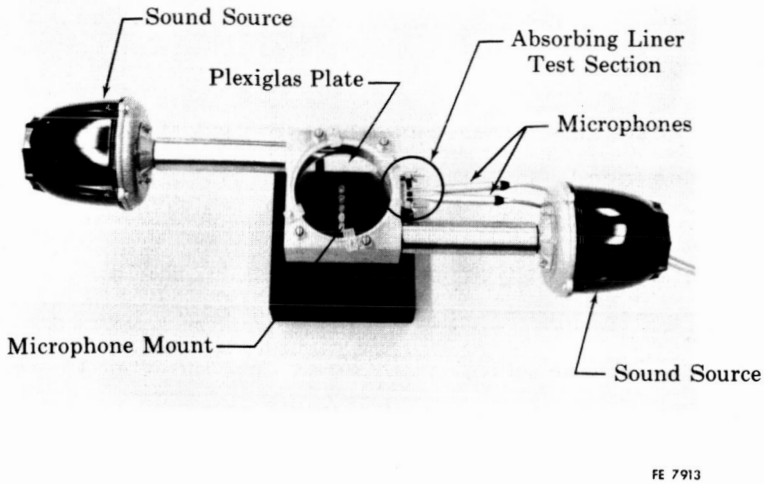

Figure IV-1. Static Tangential Chamber FD 25290

The cylindrical test chamber had a 5-in. internal diameter with an axial length of 1 in. The ends of the chamber were made of 1/2-in. Plexiglas plates to enable visual observation of pressure distributions when styrofoam pellets were placed in the test chamber. The top Plexiglas plate contained instrumentation ports for microphones and the plate was capable of being rotated so that any point in the chamber could be observed. Two Atlas Sound Driver Units, Model PD-60T, were used as sound sources; both were tangentially mounted on the test chamber. The liner test section occupied approximately 8% of the total surface area on the outer diameter chamber wall, and was located 45 deg from one of the sound inlets. Two Brüel & Kjaer, Model 4138, 1/8-in. condenser microphones were used in the absorbing liner test section. One microphone measured pressure oscillations in the chamber in front of the test section and the second, pressure oscillations in the resonator cavity. The outputs of both microphones were supplied to the pressure-phase impedance measuring apparatus described in Appendix B.

B. PRELIMINARY EXPERIMENTS

Preliminary response tests of the static tangential chamber showed that the first three tangential modes and the first two radial modes

could be excited. The first tangential mode corresponded to a frequency of 1572 Hz with a maximum amplitude of 165 db, well above the linear acoustic regime. The response characteristics of the chamber were good; i.e., no distortion of the standing wave pattern was observed on an oscilloscope used to monitor the output of a microphone, mounted through the Plexiglas endplate 1/2 in. from the outer chamber wall, as the plate and microphone were rotated 360 deg around the chamber.

The chamber simulator was modified to determine if transverse modes could be excited by locating the sound source near the outer edge of the endplate. (See figure IV-2.) The first five tangential modes were excited with maximum sound levels of 170, 172, 166, 161, and 160 db, respectively. Radial modes could not be detected within the chamber. The coupling device between the speakers and the chamber appeared to be better for this configuration because higher sound levels were reached with one sound source as compared to the first configuration which required two sound sources to reach an even lower level at the tangential modes. Another advantage of the second configuration is that the entire tangential standing wave could be rotated in the chamber by rotating the endplate in which the sound source is mounted. This enables the test section to be positioned at any point within the tangential wave, a distinct advantage over the first configuration which maintained a fixed relationship between one point on the standing wave and the test section.

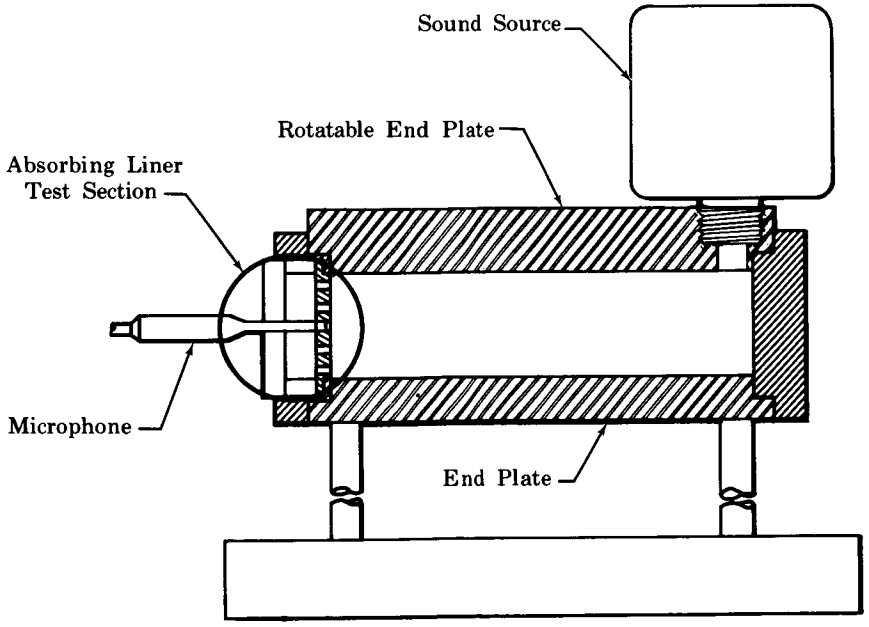

Figure IV-2. Modified Chamber Simulator FD 31419

A third configuration was tested in which the sound source was located in the center of the Plexiglas endplate. It was found that with this configuration radial modes could be easily generated but no tangential modes could be detected.

It was decided to use the first configuration for additional investigation of transverse modes because either tangential or radial standing waves could be generated within the test chamber. Additional studies were made to better understand the characteristics of the first tangential mode because it is primarily the type of instability encountered in rocket chambers and also because it is believed to be the source of obliquely incident waves.

An experiment was conducted in which a 1/4-in. Brüel & Kjaer condenser microphone was mounted flush with internal side of a Plexiglas endplate at a radius of 2.25 in. The plate was rotated in steps of 10 deg until the microphone made one full revolution around the chamber; at each step the rms sound pressure was recorded. Figure IV-3 shows that, as expected, the standing first tangential wave follows a sinusoidal pattern represented by $P = A \sin \xi$ where A is the peak amplitude at 90 and 270 deg which corresponded to the center of the two sound source discharge ports.

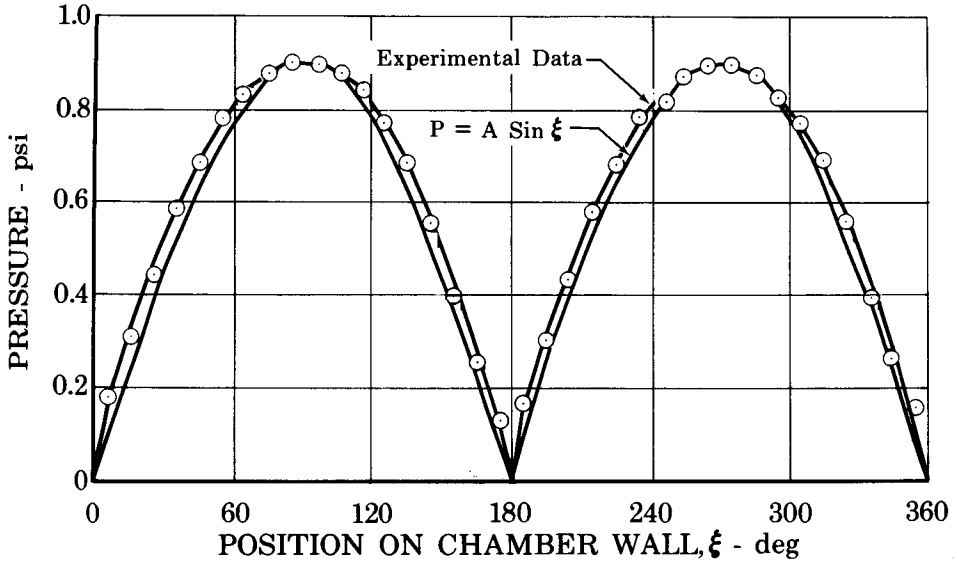

Figure IV-3. First Tangential Pressure Profile FD 31379A

The results of this testing can be used to determine the location and minimum number of pressure transducers necessary to measure the peak amplitude in a thrust chamber with a standing first tangential mode of instability. If only one transducer were used and if it were located so that a nodal point of the first tangential mode occurred at the same point, the instability would not be detected. To determine the minimum number of transducers and the locations that are needed to detect the maximum amplitude of the first tangential mode of instability, two pressure transducers located 90 deg apart can be used to provide data to calculate the peak pressure amplitude. The proof is as follows.

The equations $P_X = A \sin \xi$ and $P_Y = A \sin (\xi + 90 \text{ deg}) = \cos (\xi)$ represent the two measured pressures at any position on the circumference of the chamber wall where P_X and P_Y are 90 deg apart and A is the peak amplitude. Squaring both equations and adding gives

$$P_X^2 + P_Y^2 = A^2 (\sin^2 \xi + \cos^2 \xi) = A^2$$

Solving for A gives

$$A = \sqrt{P_X^2 + P_Y^2} \qquad \text{(IV-1)}$$

Therefore, the peak amplitude of the first transverse mode is easily determined by measuring the pressure at two points in the same cross section, 90 deg apart on the chamber walls. The results of this experiment can also be used to show that if the acoustical characteristics of an absorbing liner are to be measured, the minimum number of transducer pairs (one in the chamber wall and one in the liner cavity) is equal to one plus the mode number of the expected tangential instability.

To determine relationship between obliquely incident sound waves and the acoustic characteristics of a resonator configuration, each of the 5 resonator assemblies described in table IV-1 were installed in the absorbing liner test section (see figure IV-1) of the chamber simulator. The facing sample for each resonator had a curved surface with the same radius as the outer wall of the chamber. (See figure IV-4.) The backing cavity was formed by using Teflon spacer plates that conformed to the contour of the sample when the curved backing wall was secured to the assembly. (See figure IV-5.) In figure IV-5 the back of the liner sample and the

cavity space with the condenser microphones installed can be seen (a Plexiglas backing wall was used in this assembly for illustration purposes).

Table IV-1. Resonator Configurations Used in Chamber Simulator Impedance Experiments

Resonator Sample No.	Open Area Ratio, %	Sample Thickness, in.	Cavity Backing Depth, in.	Aperture Diameter, in.	Flow Coefficient
1	1.4	0.10	0.3	0.052	0.83
2	3.2	0.10	0.5	0.052	0.78
3	4.7	0.10	0.6	0.052	0.83
4	7.0	0.10	0.5	0.052	0.78
5	9.4	0.10	0.6	0.052	0.78

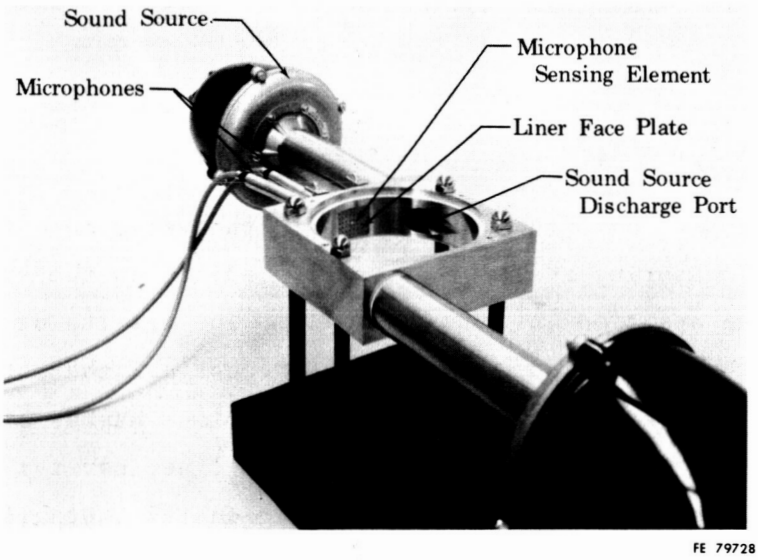

Figure IV-4. Instrumented Chamber Simulator FD 31996

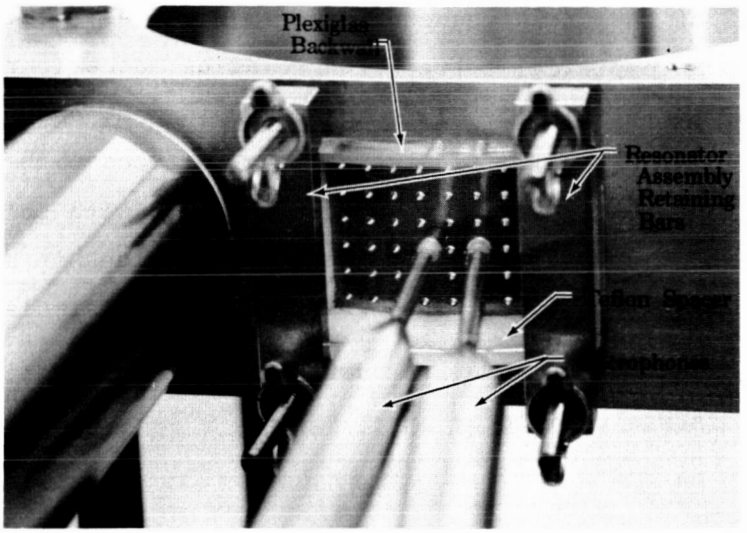

Figure IV-5. Illustration of Resonator Cavity And Instrumentation FD 31423

Data for determining acoustic properties of each resonator configuration was obtained at a frequency of 1572 Hz, which corresponded to the first tangential mode of the chamber, over a range of sound pressures from 135 to 165 db. The data obtained consisted of the measurement of the sound pressures in the chamber at the face of the liner sample and in the resonator cavity, and the phase angle between these two pressure waves.

C. ANALYSIS OF DATA

To determine the acoustic characteristics of each resonator assembly the equations derived in Appendix B were used to determine the components of impedance, absorption coefficient, and orifice particle velocities from the pressure-phase data.

1. Acoustic Resistance Data

The results of the high frequency experiments (see Section III) were used to develop an empirical correlation relating acoustic resistance with orifice particle velocity. The data used in that analysis was obtained from one-dimensional normally reacting surfaces with normal incident sound waves. To determine if a cylindrical surface with obliquely incident sound waves is characterized by the same relationship a similar analysis was performed with data obtained from the chamber simulator.

In the analysis of the simulator data the open area ratio (σ) of the sample resonators was defined as

$$\sigma = \frac{A_2 L}{V_c} \qquad \text{(IV-2)}$$

where A_2 is the total area of the apertures, and L and V_c are the length and volume, respectively, of the backing cavity. This equation must be used in place of the usual definition of σ because the cavity is wedge shaped causing the cross-sectional area to vary across the entire length of the cavity. (In the longitudinal test apparatus the cross-sectional area of the cavity (A_c) is constant , thus the volume can be defined as

$$V_c = A_c L \qquad \text{(IV-3)}$$

which when used in equation (IV-2) gives

$$\sigma = \frac{A_2}{A_c} \qquad \text{(IV-4)}$$

the usual definition of σ.) Equation (IV-3) does not apply to the volume of the resonator cavity in the cylindrical chamber, thus, equation (IV-2) must be used to calculate the open area ratio.

Correlation of the acoustic resistance (R) data with the flow coefficient (C_f) was made using the function obtained from the high frequency analysis, i.e.,

$$R = \frac{K_2 \rho u}{(C_f)^2} \qquad \text{(IV-5)}$$

Equation (IV-5) was used to calculate the values of K_2 for all data taken in the tangential tests where the particle velocities were in the non-linear regime, i.e., greater than 60 ft/sec. A comparison of the results with those of the high frequency analysis are shown in figure IV-6. It is worthy of note that the same average value of K_2, 0.37, was obtained for both flat and cylindrical surfaces. It is therefore concluded that the nonlinear acoustic resistance for both cases can be represented by the expression

$$R = 0.37\rho u(C_f)^{-2} \qquad \text{(IV-6)}$$

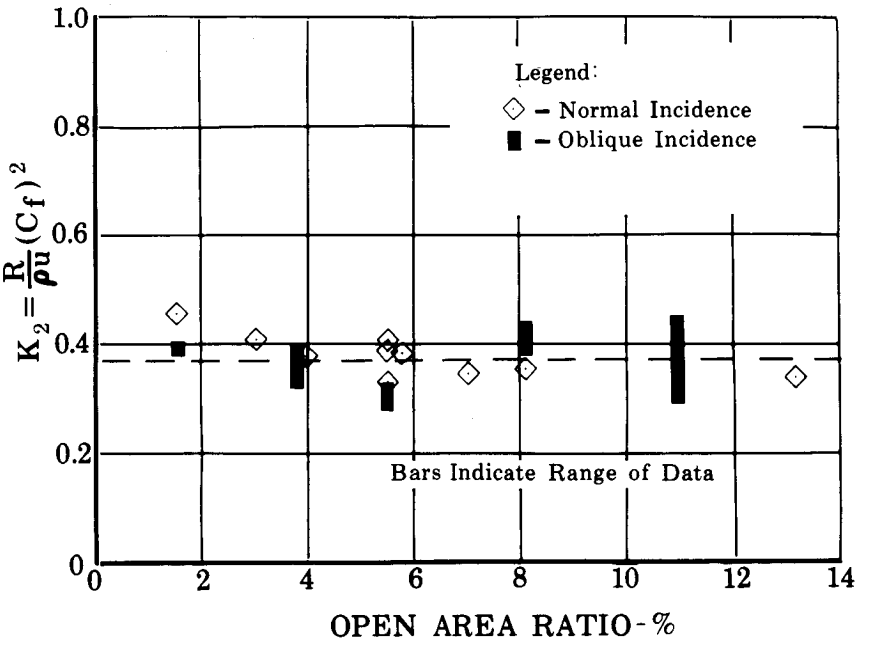

Figure IV-6. Comparison of Resistance Coefficient for Normal and Tangential Incidence

FD 31418

2. Acoustic Reactance Data

Comparison of the effective aperture length data from the static simulator experiments with the theory derived from the high-frequency experiments were made. Results are shown in figure IV-7 where the effective length data from the latter experiments have been included. With the exception of the data from one resonator sample (σ = 3.2%) the scatter in the data is seen to fall within the range of the high-frequency data. It is not known why the data from the single sample fall lower than

those of the other samples; however, it is evident that there are no essential differences in the effective length from either the cylindrical or flat facing samples.

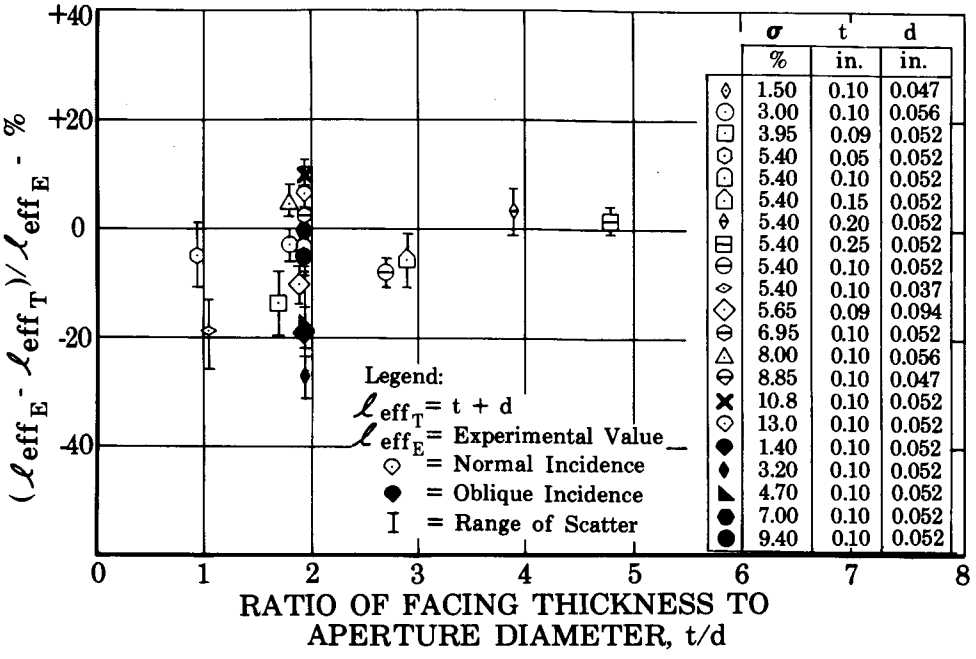

Figure IV-7. Comparison of Effective Length Data With Theory FD 31417

D. CONCLUSIONS AND RECOMMENDATIONS

Results of the chamber simulator experiments show that both one-dimensional and cylindrical liner surfaces are characterized by an identical relationship between the acoustic resistance and particle velocity. In the relationship developed with flat samples the particle velocity was normal to the liner surface, therefore it is only reasonable that the particle velocity is also normal to the surface of a cylindrical liner. Since the ratio of the driving pressure to the particle velocity normal to a surface is defined as the normal specific acoustic impedance then a cylindrical liner with a partitioned cavity having oblique incident sound waves has the same acoustic characteristics as a normally reacting surface.

From the results of the chamber simulator experiments it is concluded that either cylindrical or longitudinal impedance tubes can be used to provide data for the development of empirical correlations to be used in the

design of partitioned absorbing liners for rocket chambers. Absorbing liners used in rocket chambers are often unpartitioned and designed to give maximum absorption at frequencies near that of the first tangential mode. As shown in the preliminary experiments the first tangential mode forms a pressure profile around the chamber wall in the form of a sine wave with resulting severe pressure gradients around the liner facing. In equations used to determine the absorption coefficient of the liner, the impedance of the common backing cavity is based on a theory that assumes a uniform pressure distribution across the liner backing cavity. Analytical attempts have not been successful in developing an expression to describe the pressure distribution and impedance of an unpartitioned cavity with a pressure gradient across the liner surface.

It is recommended that additional research be conducted in an attempt to improve the absorbing liner design theory for unpartitioned liners. Until the theory can be improved it will be necessary to assume that the impedance of an unpartitioned cavity having a pressure gradient across it has the same acoustic characteristics as one which has a uniform pressure distribution.

SECTION V
TASK III - SIMULATOR EXPERIMENTS

Absorbing liners used in rocket engines always have gases flowing past, and, under some circumstances, a simultaneous flow of gases will occur in which the gases flow through, as well as past, the liner apertures. Previous experiments relating the effects of flow have shown wide differences in results. This is seen in the case of a recent publication by Ingard and Ising (Reference 3) in which the effects on the acoustic resistance due to flow through (no flow past) a single orifice were determined with the use of a hot-wire annemometer. A significant difference was found to exist between these results and those previously determined (Reference 2) by use of an ASTM-type impedance tube in which an array of orifices was tested.

In the past, the effects on resistance of flow past the apertures of flat facing samples could only be measured using modified ASTM-type impedance tubes. With such an apparatus a complete resonator assembly could not be used since a flow duct had to be installed in place of the resonator cavity. Hence, the effects on the absorption coefficient and reactance components could not be measured directly. The use of the pressure-phase impedance measuring technique imposes no such limitations and, in addition, permits the use of cylindrical test assemblies. It was originally planned to use a cylindrical test chamber for the flow experiments. Tests made with the static (no flow) chamber simulator (see Section IV) showed that a liner with a cylindrical surface and partitioned cavity is a normally reacting surface in which the effects of incidence angle are negligible. Therefore, the real and imaginary parts of impedance can be measured in either a cylindrical or longitudinal impedance apparatus so long as a uniform pressure distribution is maintained across the liner surface. Thus, for simplicity longitudinal impedance tubes were used in the flow experiments.

The objective of the flow experiments under Task III is to obtain, using the pressure-phase technique, impedance data and absorption coefficients with flow through (no flow past) the apertures and flow past (no flow through) the apertures of absorbing liner assemblies. Where possible, comparisons of the data with the existing empirical flow correlations were to be made to verify and/or improve the existing theory.

A. FLOW-THROUGH EXPERIMENTS

The static (no flow) high frequency impedance apparatus described in Appendix B was modified for the flow-through (no flow-past) tests. (See figure V-1.) In the experiment two samples having open area ratios of 3.94 and 10.8%, thickness of 0.10 in., aperture diameter of 0.052 in., and backing cavity depth of 0.5 in. were used. In order to determine the effects of net flow on the acoustic resistance each resonator assembly was tested at a constant frequency near resonance (resistance greater than reactance) and the average flow-through velocity was varied from near zero to 325 ft/sec. The same tests were made at two different sound pressure levels of 145 and 160 db. To determine the effects of flow through the apertures on the absorption coefficient, each resonator assembly was tested at a constant sound level of 160 db over a range of frequencies from 500 to 4000 Hz while the flow-through velocities were held constant at 136, 237, and 302 ft/sec.

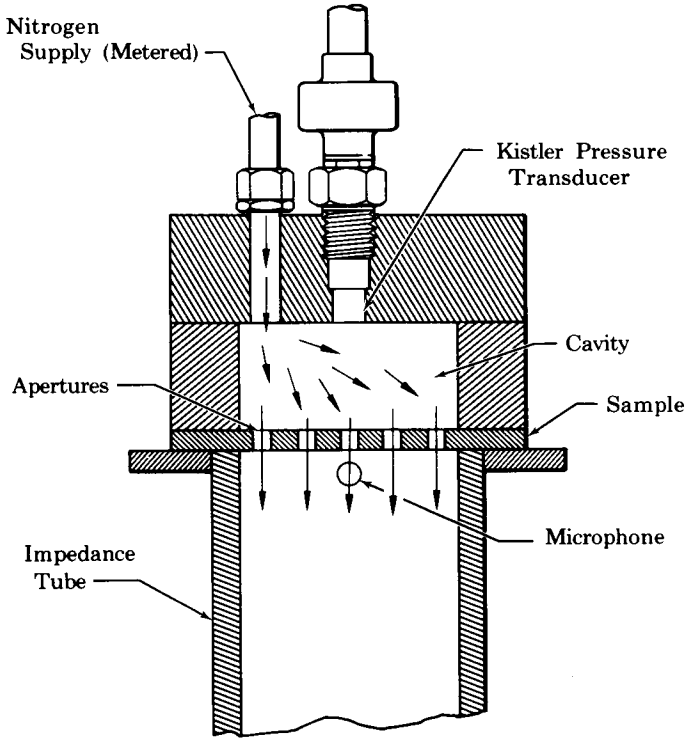

Figure V-1. Sketch of Test Section - Impedance Measuring Device Used With Flow Through Apertures FD 29176A

Results of the tests made at constant frequencies are shown in figure V-2, in which the ratio of the acoustic resistance with flow to that with no flow has been correlated with the average flow-through velocity and compared with previous data obtained with the ASTM-type impedance apparatus. The exact causes of the differences between the ASTM data and the pressure-phase data are not known; however, they are believed to be caused by several differences in the test procedures which are explained as follows. In the probe tube type experiments, the sample did not have a backing cavity, thus allowing the incident sound wave to pass through the apertures and out the flow duct instead of interacting in the cavity and reradiating back into the impedance tube as in the pressure-phase experiments. In the ASTM-type experiments, a probe tube was used to investigate the standing wave which is established in the gaseous media having a net flow towards the sample. It is known that this net flow can distort the standing wave pattern thus producing error of unknown magnitude in the data results. Also, based on previous experience with the probe tube investigations of the standing wave pattern, it has been found that precise impedance data for such an experiment are difficult to obtain. It does appear that the pressure-phase data is more accurate, especially because, as shown by results of the high frequency analysis in Section III, they are in good agreement with the hot-wire experiments of Ingard and Ising (Reference 3).

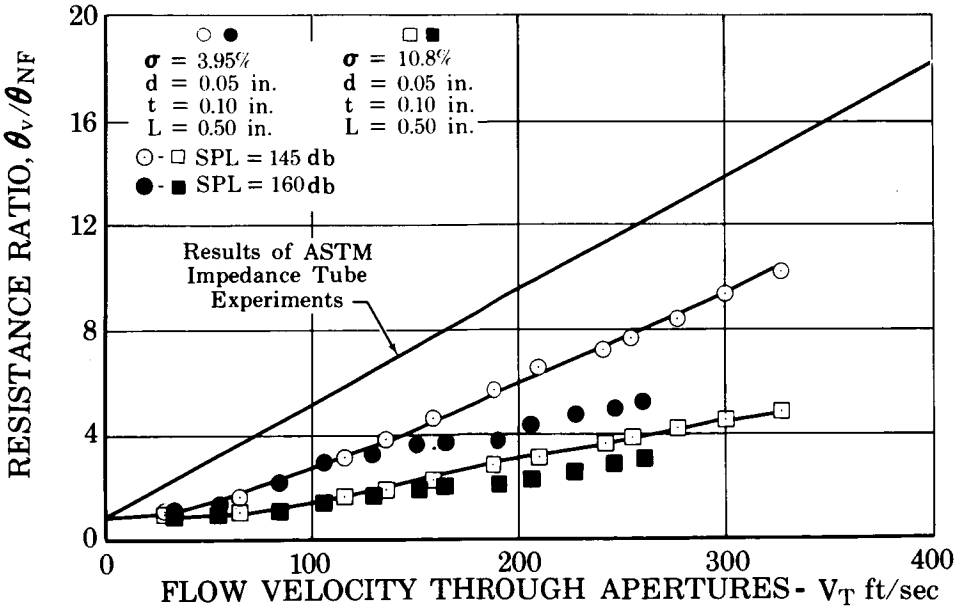

Figure V-2. Comparison of Data from the ASTM and the Pressure-Phase Experiments for Flow-Through Tests FD 31050 A

Investigations of the flow-through data was based upon the results of the high frequency analysis, as explained in Section III,i.e., the resistance is given by the empirical correlation

$$R = \frac{0.37\rho u}{C_f^2} \qquad (V\text{-}1)$$

and also upon the results of Ingard and Ising (Ref. 3), which suggests that for cases where the steady-flow through velocity (V_T) is greater than the particle velocity with no net flow then the resistance is given by

$$R = \lambda \rho V_T \qquad (V\text{-}2)$$

In equation (V-2) λ is a proportionality constant that Ingard and Ising found to have values between 1 and 1.5.

Combining equation (V-1) and (V-2) shows that the resistance can best be represented by the equation

$$R = \frac{\lambda\,(0.37)\rho V_T}{C_f^2} \qquad (V\text{-}3)$$

By letting $\tau = 0.37\lambda$ equation (V-3) becomes

$$R = \frac{\tau \rho V_T}{C_f^2} \qquad (V\text{-}4)$$

where τ is an empirical constant that must be experimentally determined. Using equation (V-4) in analyzing the data to determine the value of τ, two cases were considered. One in which the steady flow-through velocity was the average velocity (V_T) and not corrected for the flow coefficient

$$\tau_1 = \frac{RC_f^2}{\rho V_T}$$

and a second one in which the steady flow velocity was corrected for the flow coefficient, i.e., the average velocity is divided by the flow coefficient giving

$$\tau_2 = \frac{RC_f^3}{\rho V_T}$$

The results are shown in figure V-3 in which the constants (τ_1 and τ_2) have been correlated with the ratio of the steady flow-through velocity to the peak velocity (u_{NF}) amplitude with zero net flow. The results show that when the net flow velocity is greater than the one-half of the peak acoustic velocity with no net flow, a good approximation for both τ_1 and τ_2 would be unity. In figure V-3, the correlation using τ_2 is noted to be better than τ_1, i.e., less scatter; therefore, it is concluded that the effects of flow-through can best be represented by the following:

$$R = \frac{\rho V_T}{C_f^3} \quad \text{where } V_T > 0.5\ u_{NF} \tag{V-5}$$

where V_T is the average flow velocity and the term C_f^3 is used to account for the aperture edge effects on both the acoustic peak velocity and the net flow velocity.

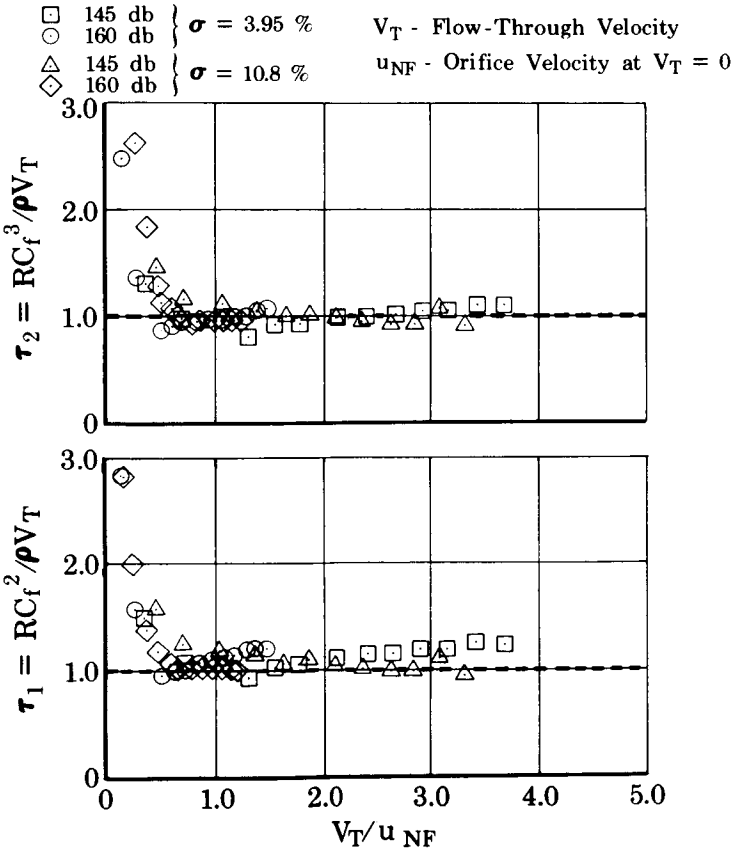

Figure V-3. Correlation of Data for Constant Frequency Experiments with the Ratio of the Net Flow-Through Velocity to the Peak Orifice Velocity for No Net Flow

FD 31265

The dimensionless resistance is defined as

$$\theta = \frac{R}{\sigma \rho c} \qquad \text{(V-6)}$$

therefore, equation (V-5) may be written in the form

$$\theta = \frac{V_T}{C_f^3 \sigma c} = \frac{M_T}{C_f^3 \sigma} \quad \text{where } M_T > 0.5\, M_{NF} \qquad \text{(V-7)}$$

In equation (V-7) M_T is the Mach No. of the net flow through the apertures.

Equation (V-5) is seen to be independent of frequency. This means that for a given net flow velocity greater than $0.5u_{NF}$, the resistance of an acoustic liner is independent of frequency; confirmation follows. The results of the constant flow-through experiments with variable frequencies are shown in figure V-4 where the absorption coefficient is correlated with frequency as a function of net flow velocity. In the two cases for net velocities greater than $0.5\ u_{NF}$, i.e., net velocities of 237 and 302 ft/sec, almost no resonance effects are observed in the absorption curves.

Referring to equation (B-10) in Appendix B, it is clear that if the absorption coefficient is constant over a range of frequencies and if the resistance is much greater than the reactance, as was the case for frequencies greater than 1500 Hz, then the resistance must remain a constant value over the same range of frequencies. Thus the results of the variable frequency tests further substantiate the empirical correlation given in equation (V-5).

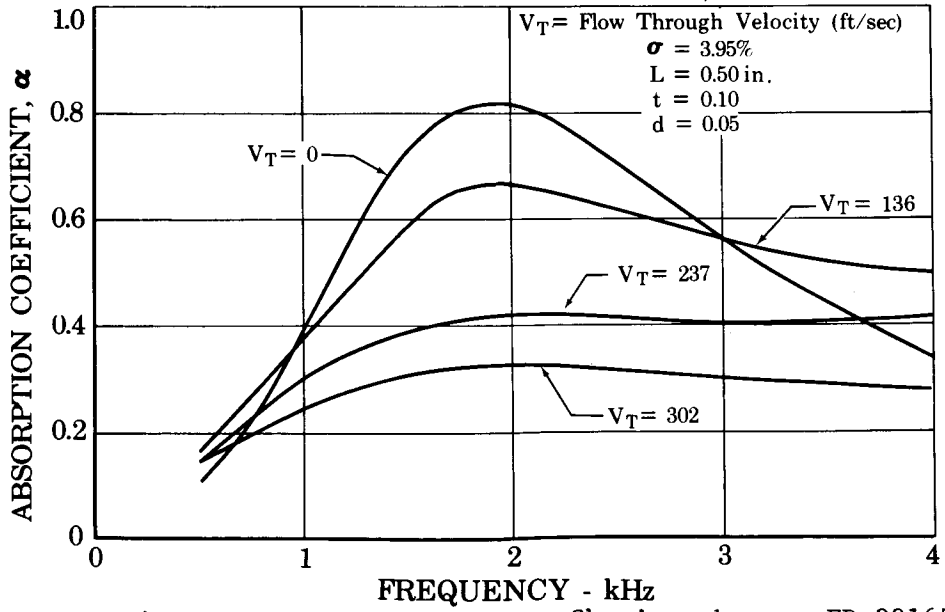

Figure V-4. Summary of Experiments Showing the Effects of Flow-Through the Apertures on the Absorption Coefficient FD 29165

It was observed that the effective length decreases with an increase in the net flow-through velocity, however as shown in figure V-5 this was only true for a sound pressure level of 145 db. For a sound pressure level of 160 db which is of more interest for acoustic liner design purposes, the effects of flow through the apertures on effective length, and therefore acoustic reactance, were found to be negligible.

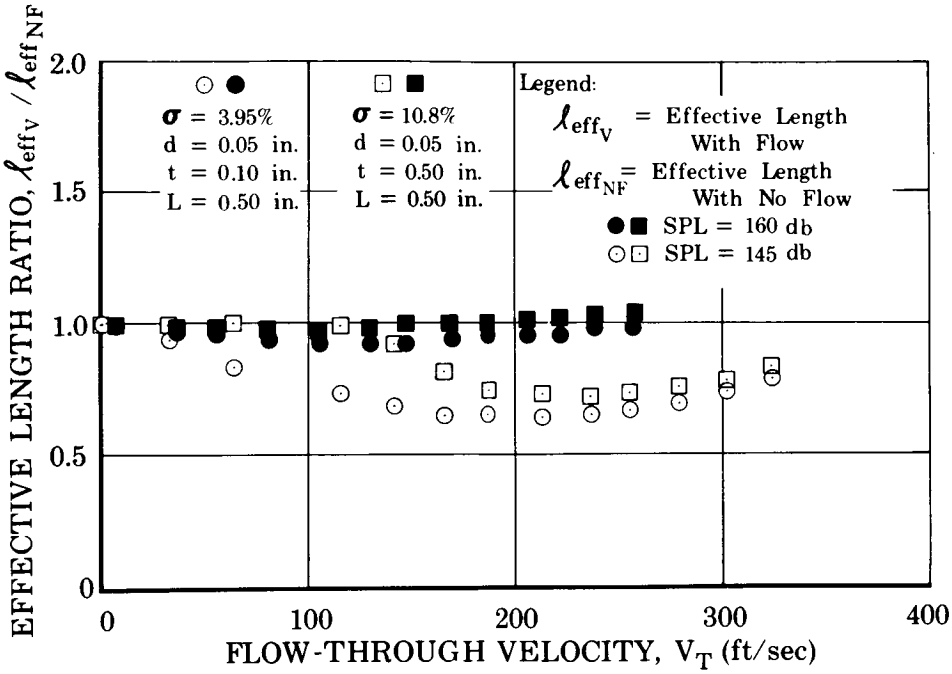

Figure V-5. Effects of Flow Through Apertures on Effective Length FD 31412A

B. FLOW-PAST EXPERIMENTS

The cold flow apparatus shown in figure V-6 was fabricated for the flow-past experiments. The apparatus, theoretically capable of producing sound pressure levels in excess of 170 db at frequencies of 100 to 2000 Hz for flows up to 400 fps consists of:

1. A Ling 94-B electropneumatic transducer
2. An expansion horn
3. A 2-in. dia standing wave tube
4. A circular absorbing liner test section
5. Two Atlantic Research pressure transducers
6. A tube extension
7. A reflection plate.

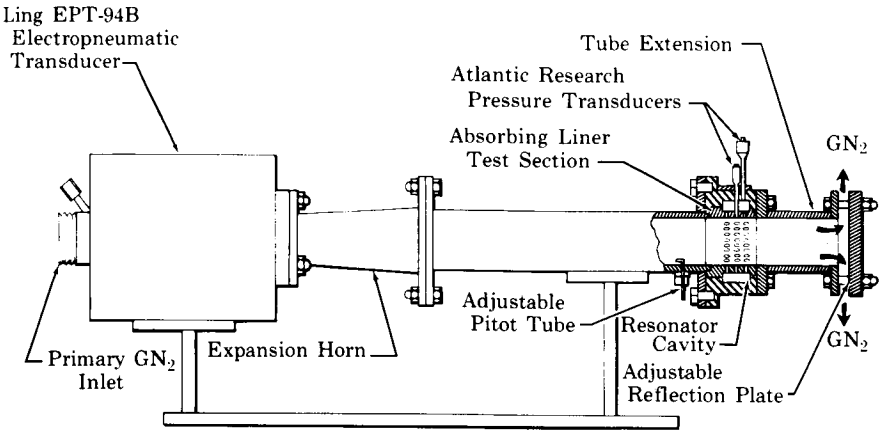

Figure V-6. Flow-Past Apparatus FD 31411

Briefly, the operation of the apparatus is as follows: sound waves, along with a metered supply of gaseous nitrogen, enter the tube through the Ling transducer. The nitrogen gas flows through the tube section parallel to the perforated face of the test section and exits through a gap between the reflection plate and the end of the tube extension. A pitot tube is located just upstream of the test section in order to determine the velocity profile approaching the liner sample. The sound waves moving down the tube are reflected at the end plate and a standing wave is produced. The absorption characteristics of the test section are then determined as explained in Appendix B by measuring the sound pressures and phase angles with the pressure transducers.

Two cylindrical samples were tested, one with an open area ratio of 0.027 and an aperture diameter of 0.099 in.; and one with an open area ratio of 0.021 and an aperture diameter of 0.050 in. Each sample was 0.030-in. thick and had a backing cavity of 0.51 in. The tests were conducted at a constant frequency near resonance to determine the effects of flow on the acoustic resistance of each resonator configuration. The tests were originally planned to be conducted using a full 360-deg test section with a full annular backing cavity; however, severe distortion of the pressure wave was found to exist in the cavity. In order to reduce this effect, the cavity was partitioned and some of the apertures sealed off

so that acoustical data were measured only in a 45-deg test section. A tube extension, two tube diameters long, was also added to reduce the distortion effects caused by the flow being exhausted into the atmosphere.

The range of flow velocities tested was significantly restricted because of the minimum and maximum operating pressure range allowable with the Ling electropneumatic transducer. Flow-past velocities lower than 80 ft/sec could not be achieved unless gaseous nitrogen was allowed to bleed off upstream of the sample; however, this caused severe changes in the standing wave pattern produced in the tube and the resulting acoustic data could not be reproduced on successive tests. The upper velocity range was limited to approximately 300 ft/sec by the flowrate that could be obtained at the maximum transducer inlet pressure.

1. Acoustical Resistance Data

The results of the tests are shown in figures V-7 and V-8, in which the ratio of the acoustic resistance with flow to that with no flow has been correlated with the average flow-past velocity and with the average Mach number.

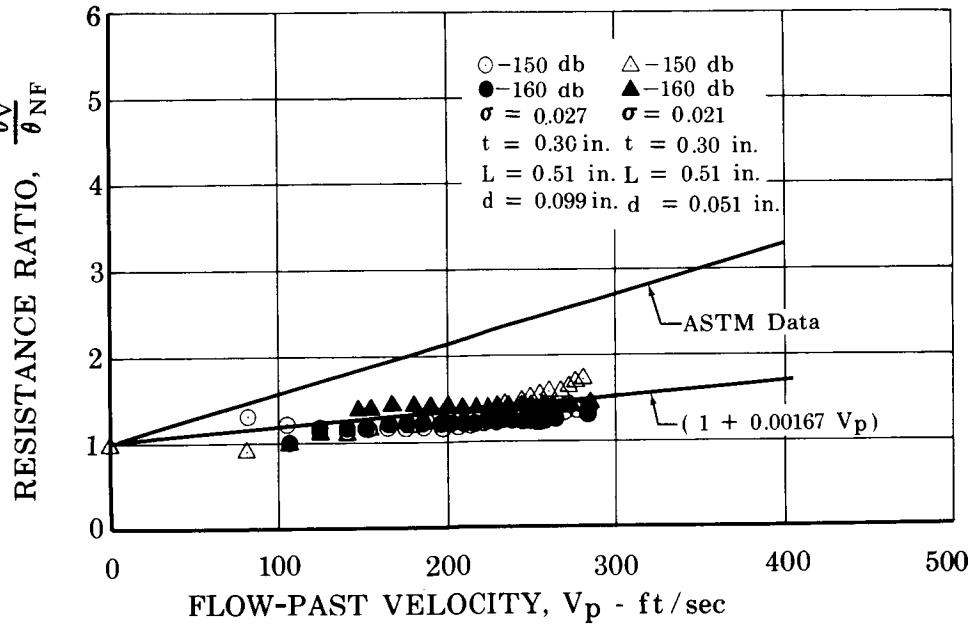

Figure V-7. Correlation of Acoustic Resistance Data with Velocity of the Flow Past the Apertures

FD 31187A

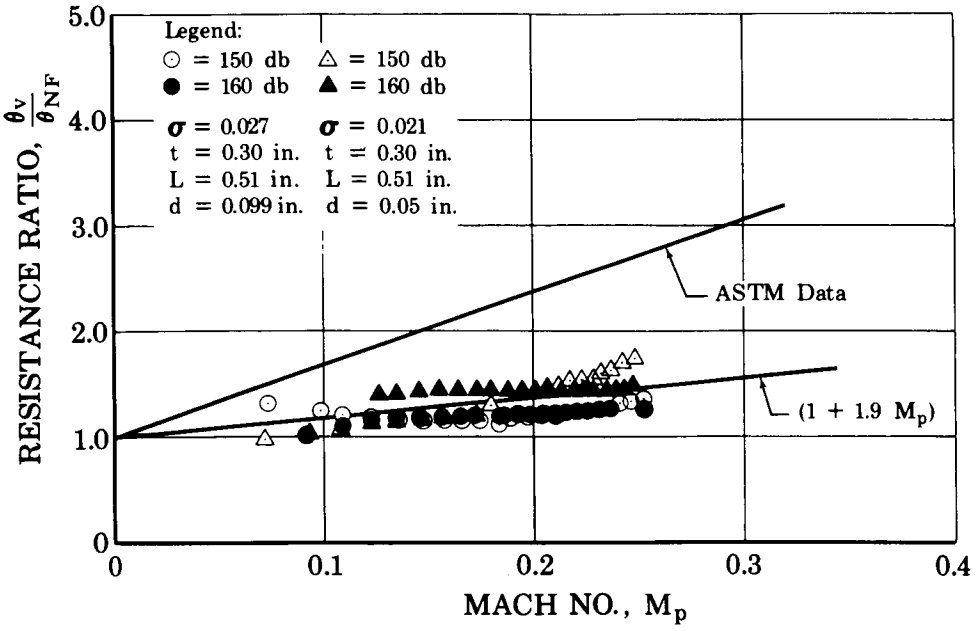

Figure V-8. Correlation of Acoustic Resistance Data with Mach Number of Flow Past the Apertures FD 31407A

The following empirical equations were developed relating the change in acoustic resistance with the average flow past:

$$\theta_V = \theta_{NF} (1 + 0.00167\ V_p) \quad \text{(V-8)}$$

$$\theta_V = \theta_{NF} (1 + 1.9\ M_p) \quad \text{(V-9)}$$

Figures V-7 and V-8 contain previous data obtained with the ASTM-type impedance apparatus for the purposes of comparison. The data clearly shows that the average flow past the sample has a much smaller effect on the resistance than has been previously determined with the ASTM impedance apparatus.

2. Acoustical Reactance Data

It has been shown in the past that the acoustic reactance for no flow can be determined by the equation:

$$\chi_{NF} = \frac{2\pi}{c} \frac{\ell_{eff}}{\sigma} f - \frac{c}{2\pi Lf} \quad \text{(V-10)}$$

The term containing ℓ_{eff} is the inertance, and the term containing L is the capacitance. To determine a correlation of reactance to velocity

past only the inertance data need be used since the capacitance is an exact term. Furthermore, only the effective aperture length need be correlated with the flow-past, because it is the only part of the inertance that is not exact. The results of this comparison are shown in figure V-9. An empirical equation relating the effective aperture length with flow velocity was found to be as follows:

$$\left(\ell_{eff}\right)_V = \ell_{eff_{NF}} (1 - 0.00143\ V_p) \qquad \text{(V-11)}$$

where

$$\left(\ell_{eff}\right)_{NF} = t + d$$

If the media is other than air, equation (V-11), written in terms of the Mach number, should be used, i.e.,

$$\left(\ell_{eff}\right)_V = \ell_{eff_{NF}} (1 - 1.65\ M_p) \qquad \text{(V-12)}$$

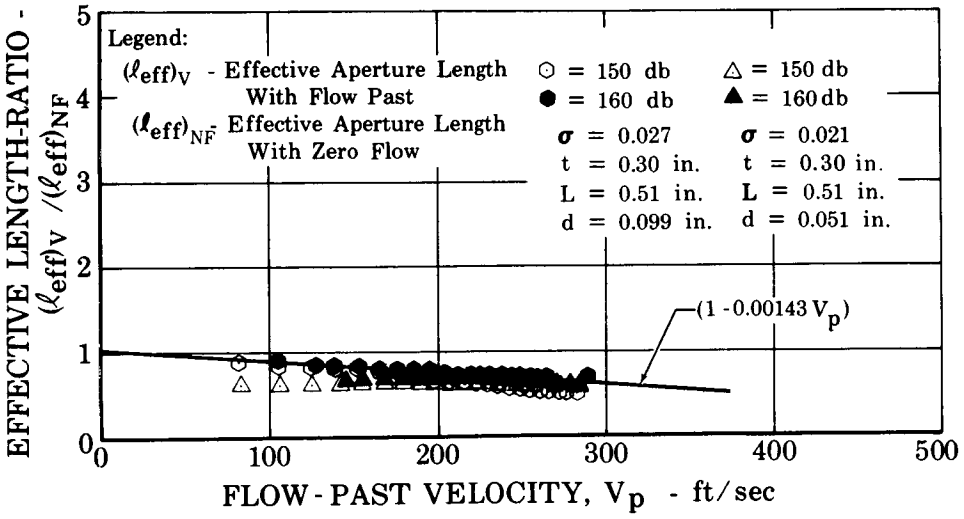

Figure V-9. Effects of Velocity Past Apertures on Effective Aperture Length FD 31408A

Figures V-10 and V-11 show a comparison of the reactance data computed using equation (V-11) substituted for ℓ_{eff} of equation (V-10) and the experimental reactance determined by the pressure phase data. A significant amount of data scatter was found to exist with the maximum error being 23.2%. It was concluded from the results that further experiments should be conducted with samples or various thickness, open area, and aperture to determine a more acceptable correlation.

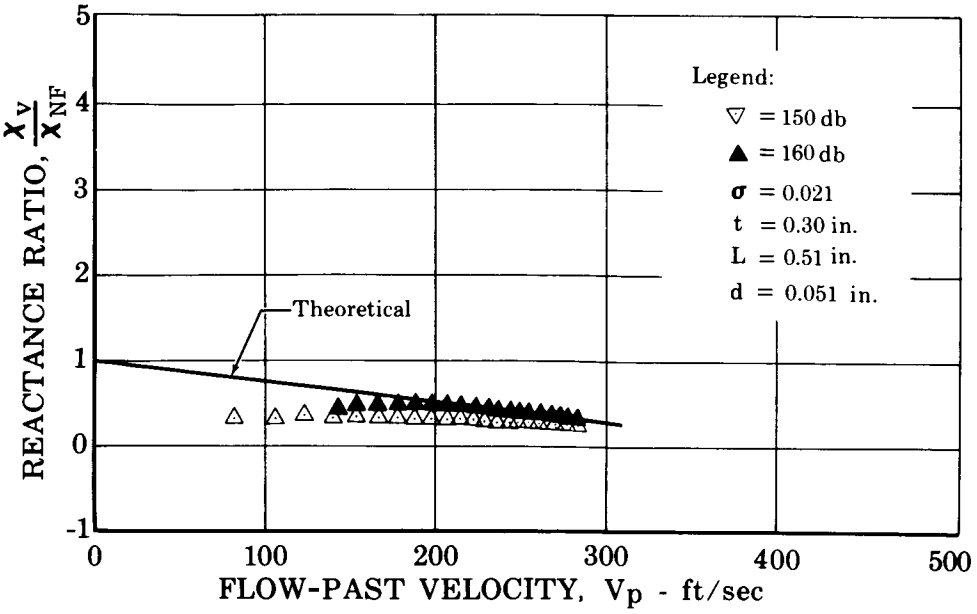

Figure V-10. Comparison of Reactance Data With Theory for Sample With 0.05-in. Diameter Apertures FD 31410A

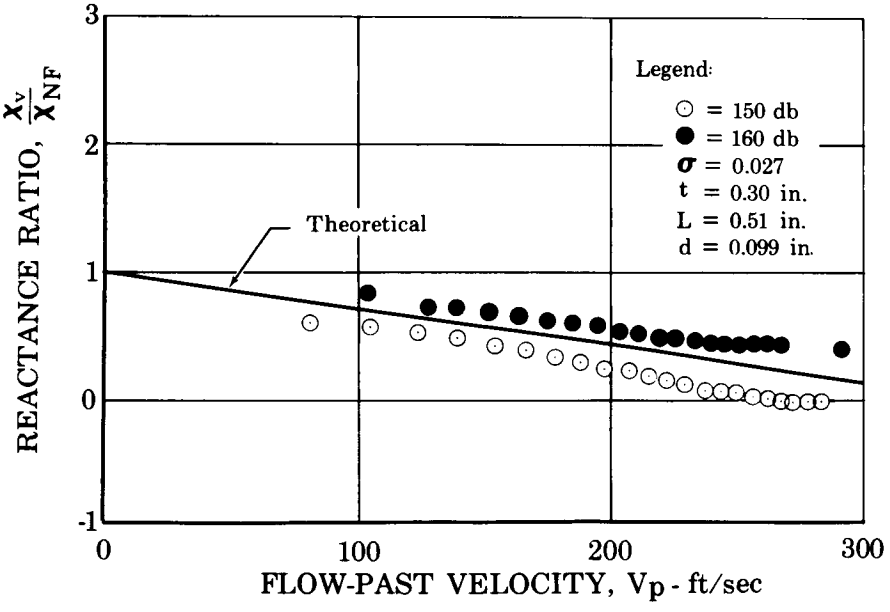

Figure V-11. Comparison of Reactance Data With Theory for Sample With 0.1-in. Diameter Apertures FD 31409A

The exact causes of the differences between the earlier data and the pressure-phase velocity data are not presently known; however, they are believed to be due to the differences in the test procedures. The earlier data were obtained with an ASTM-type impedance apparatus in which the test sample was a flat plate and did not have a closed volume backing cavity. (See figure V-12.) This allowed the incident sound

wave to pass through the apertures of the sample and be carried out the flow-duct instead of interacting in the cavity and reradiating back into the impedance tube. Also, in the ASTM-type experiments a probe tube was used to investigate the standing wave which is established in a gaseous media flowing toward the sample. This flow toward the sample can distort the standing wave pattern along the length of the tube. Since the acoustic characteristics depend on the probe tube measuring the pressure maximum and minimum and their distances from the sample, the wave distortion can cause errors of unknown magnitude in the data.

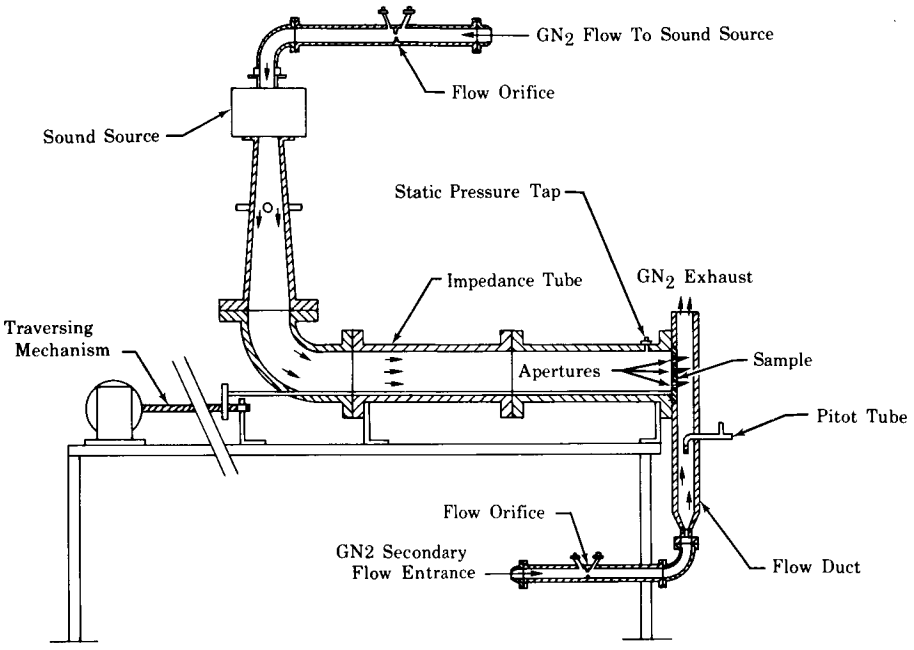

Figure V-12. Simultaneous Flow Apparatus FD 21980

It is recommended that further experiments should be conducted to better define the effect of higher gas velocities on the acoustic characteristic of a resonator. The experiments should be conducted with flow of different density to determine if the flow effects are dependent upon velocity or Mach No. and with samples of various thickness, open area ratio, backing cavity depth, and aperture diameter.

SECTION VI
REFERENCES

1. Ingard, U., "On the Theory and Design of Acoustic Resonators," JASA, Volume 25, No. 6, November 1953.

2. "A Study of the Suppression of Combustion Oscillations With Mechanical Damping Devices," Pratt & Whitney Aircraft Report No. PWA FR-2596, November 20, 1967.

3. Ingard, U., and H. Ising, "Acoustic Nonlinearity of an Orifice," JASA, Volume 42, No. 1, July 1967.

4. Bies, D. A., and O. B. Wilson, Jr., JASA, Volume 29, pp. 711-714 (1957).

5. Ingard, U., and S. Labate, "Acoustic Circulation Effects and the Nonlinear Impedance of Orifices," JASA, Volume 22, No. 2, March 1950.

6. Blackman, A. W., "Effect of Non-Linear Losses on the Design of Absorbers for Combustion Instabilities," Journal American Rocket Society, Volume 30, No. 11, pp. 1022-1028, November 1960.

7. Sirignano, L., L. Crocco, and D. T. Hanje, "Acoustic Liner Studies," 3rd ICRPG Conference, CPIA Publication No. 138, Volume I, October 1966.

8. "A Study of the Suppression of Combustion Oscillations with Mechanical Damping Devices," Phase II Summary Report, PWA FR-1922, 15 July 1966.

9. "Use of Partial Derivatives in Variation Analysis," Pratt & Whitney Aircraft Report No. PWA FR-1993, 30 September 1966.

10. "Suppression of Combustion Oscillations with Mechanical Damping Devices," Quarterly Progress Report, Pratt & Whitney Aircraft Report No. PWA FR-3101, 15 January 1969.

11. Dodge, Barnett F., Chemical Engineering Thermodynamics, McGraw-Hill Book Company, Inc., New York and London, 1944, p. 328.

12. Kinsler, L. E., and A. R. Frey, "Fundamentals of Acoustics," Second Edition, John Wiley & Sons, Inc., New York, New York, 1962, pp. 225 and 241.

13. Phillips, B., "Recent Advances in Acoustic Liner Technology," 5th ICRPG Conference CPIA Publication No. 183, December 1968.

APPENDIX A
APPLICATION OF THEORY

1. DEVELOPMENT OF DESIGN EQUATIONS

An absorbing liner may consist of a perforated cylindrical element that is concentric to, and separated from, the combustion chamber pressure shell by support rings. In principle, the liner is composed of a parallel array of Helmholtz-type resonators that when properly designed can absorb large amounts of energy. In the following paragraphs the phenomenological correlation predicting the acoustic resistance as a function of particle velocity is used to develop equations for a new liner design technique. This technique produces the optimized liner design for a given case of instability.

The specific impedance of a Helmholtz resonator (Reference 12) is defined as:

$$Z = \frac{g}{\rho c} \frac{P_1}{u} \tag{A-1}$$

for an array of resonators equation (A-1) becomes

$$Z = \frac{g}{\rho c} \frac{P_1}{\sigma_1 u} \tag{A-2}$$

where (Reference 2)

$$\sigma_1 = \frac{\sigma}{1 - \sigma^2} \tag{A-3}$$

which is a correction for high open area ratios. The specific impedance is made up of real and imaginary components in the following manner:

$$Z = (\theta + i\chi), \tag{A-4}$$

Substituting equation (A-4) into equation (A-1) and solving for the particle velocity, u, gives

$$u = \frac{g}{\sigma_1 \rho c} \frac{P_1}{(\theta + i\chi)} \tag{A-5}$$

Using the phenomenological correlation for the acoustic resistance (Section III)

$$R = \frac{0.37\,\rho u}{C_f^{\,2}} \tag{A-6}$$

and converting to specific acoustic resistance by use of the relationship

$$\theta = \frac{R}{\sigma_1 \rho c} \tag{A-7}$$

gives

$$\theta = \frac{0.37\,u}{\sigma_1\, cC_f^{\,2}} \tag{A-8}$$

Substituting equation (A-5) into equation (A-8), squaring to eliminate the imaginary term, and rearranging gives

$$u^4 + (2.7\sigma_1\, cC_f^{\,2}\, u\chi)^2 = \left(\frac{P_1 C_f^{\,2} g}{0.37\rho}\right)^2 \tag{A-9}$$

At resonance the reactance (χ) is zero, therefore, equation (A-9) reduces to

$$u_o = \sqrt{\frac{P_1 C_f^{\,2} g}{0.37\rho}}\ . \tag{A-10}$$

It is important to note that the particle velocity at resonance is independent of the liner configuration and depends only on the total pressure; experimental results from the present program are in excellent agreement with equation (A-10). (See figure A-1.)

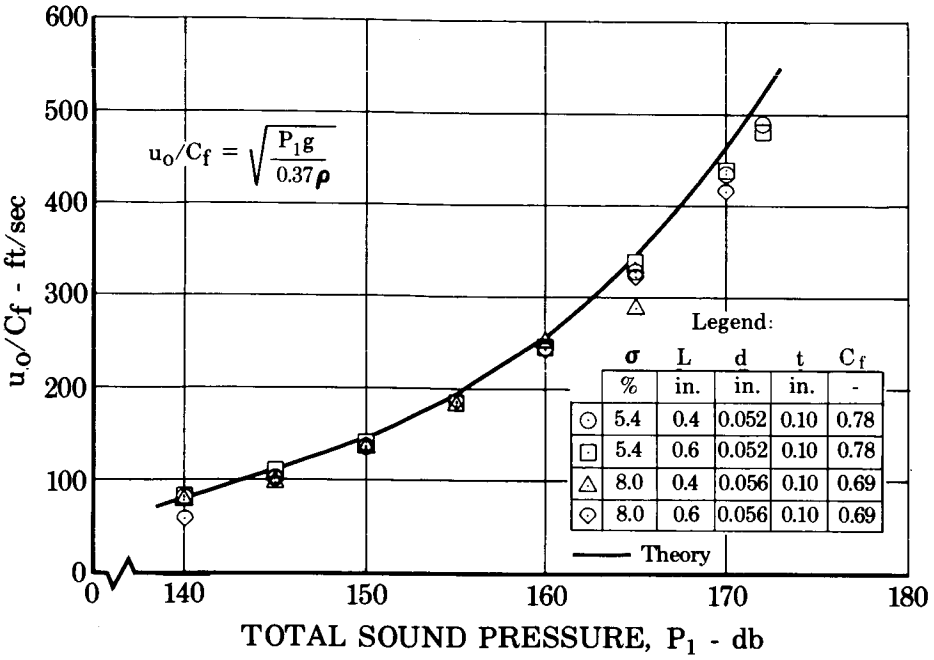

Figure A-1. Correlation of the Orifice Particle Velocity at Resonance with the Total Sound Pressure FD 31186

2. ABSORBING LINER CALCULATIONS

The following calculations illustrate a method that gives the optimized liner design for an assumed level of absorption desired at the frequency of instability. The gas properties and flow coefficient assumed for this example are

$\rho = 0.075\ lb_m/ft^3$

$c = 1130$ ft/sec

$C_f = 0.78$

It is assumed that the flow coefficient can be controlled when the liner is fabricated. The peak combustion pressure oscillation amplitude is assumed to be 159 db* (Reference 0.0002 microbar) occurring at a frequency of 2000 Hz.

*A low sound pressure was assumed so that the resulting configuration could be tested with the high frequency impedance measuring apparatus. In normal application to rocket chambers this value would correspond to a sound level of 180 to 190 decibels.

A. No Flow or Flow Past Calculations

1. Conditions at Resonance

The resonant frequency of the liner design is taken to be the frequency at which the highest level of instability is expected to occur. Assume the amount of absorption that is required at resonance to stabilize combustion is 90%. It is believed that 50% absorption in a rocket chamber is sufficient to suppress most instabilities to an acceptable level. If higher absorption values (above 80%) are desired at sound levels greater than 170 db, large open area ratios (25% or greater) are necessary which are impractical for applications to rocket engines. If, however, the liner is to be used under conditions where high open area ratios are acceptable, then high absorption values can be assumed.

The absorption coefficient is defined as

$$\alpha = \frac{4\theta}{(\theta + 1)^2 + \chi^2} \quad . \tag{A-11}$$

For 90% absorption at resonance ($\chi = 0$) the required resistance can be solved for

$$0.90 = \frac{4\theta_o}{(\theta_o + 1)^2}$$

$$\theta_o^2 - 2.44\ \theta_o + 1 = 0$$

$$\theta_o = 1.92;\ 0.02^*$$

With a steady flow (M_p) of gas past the liner it is necessary to determine the resistance of the liner if no flow were present by using the relationship developed in Section V, which describes the effects of flow past on the resistance.

$$\theta_{NF} = \theta_{M_p}/(1 + 1.9\ M_p) \tag{A-12}$$

*According to Reference (13), only values of $\theta \geq 1$ should be used in this type of design analysis; therefore, the lower value of θ_o should be ignored.

where θ_{MP} is θ_o, the resistance required for 90% absorption at resonance. In the example calculations $M_P = 0$ then

$$\theta_{NF} = \theta_{MP} = 1.92$$

The particle velocity at resonance is given by equation (A-10)

$$u_o = \sqrt{\frac{P_1 C_f^2 g}{0.37 \rho}}$$

where P_1 is 159 db (Reference 0.0002 microbar) or 53-lb_f/ft^2

$$u_o = \sqrt{\frac{(53)(0.78)^2(32.2)}{(0.37)(0.075)}}$$

$$u_o = 191 \text{ ft/sec}$$

Now the resistance and particle velocity at resonance are known and the required open area ratio satisfying these values are obtained from equation (A-8)

$$\theta_{NF} = \frac{0.37\ u_o}{C_f^2\ \sigma_{1c}}$$

$$\sigma_1 = \frac{0.37\ u_o}{C_f^2\ c\ \theta_{NF}}$$

$$= \frac{(0.37)(191)}{(0.78)^2(1130)(1.92)}$$

$$= 0.054$$

using equation (A-3) gives

$$0.054 = \frac{\sigma}{1 - \sigma^2}$$

$$\sigma^2 + 18.5\sigma - 1 = 0$$

$$\sigma = 0.054$$

At this point it is necessary to assume a liner aperture diameter and liner thickness:

$d = 0.052$ in.

$t = 0.10$ in.

Using the expression for the effective length (see Section V) with flow past the liner gives

$$\ell_{eff} = \left(\frac{t}{12} + \frac{d}{12}\right)\left(1 - 1.6\ M_P\right) \qquad \text{(A-13)}$$

$= 0.013$ ft where for this case $M_P = 0$.

Now the required backing distance of the liner cavity is calculated from the equation for resonant frequency.

$$f_o = \frac{c}{2\pi}\sqrt{\frac{\sigma_1}{L\,\ell_{eff}}} \qquad \text{(A-14)}$$

$$L = \left(\frac{c}{2\pi f_o}\right)^2 \frac{\sigma_1}{\ell_{eff}}$$

$$L = \left(\frac{1130}{2(3.14)(2000)}\right)^2 \left(\frac{0.054}{0.013}\right)$$

$L = 0.035$ ft

$L = 0.415$ in.

This sets all liner parameters to give 90% absorption at 2000 Hz, with no flow past the liner. A summary of the liner design shows

$\sigma = 5.4\%$

$L = 0.415$ in.

$d = 0.052$ in.

$t = 0.10$ in.

$u_o = 191$ ft/sec

2. Nonresonant Conditions

It is necessary to investigate if this liner has sufficient absorption at frequencies other than that of resonance. The maximum particle velocity occurs at resonance, therefore, a particle velocity which is

less than the value calculated at resonance can be chosen and used in equation (A-9) to compute the reactance. This technique applies only for particle velocities that are in the nonlinear range; i.e., $\geq$ 60 ft/sec.

To determine the reactance, use equation (A-9) and substitute the results of equation (A-10), giving

$$u^4 + \left(\frac{\sigma_1 C_f^2 cu\chi}{0.37} \right)^2 = u_o^4 \qquad \text{(A-15)}$$

Assume a particle velocity less than that at resonance

$$u = 180 \text{ ft/sec}$$

Solving equation (A-15) for the specific reactance (χ) gives

$$(180)^4 + \left(\frac{0.054\ (0.78)^2\ (1130)\ (180)}{0.37} \right)^2 \chi^2 = (191)^4$$

$$\chi = \pm 0.92$$

where the negative reactance corresponds to a frequency below resonance and the positive value to a frequency above resonance. Using a definition for specific reactance (Reference 2) the frequencies for the above values are calculated

$$\chi = \frac{2\pi}{c} \frac{\ell_{eff}}{\sigma_1} f - \frac{c}{2\pi} \frac{1}{L} \frac{1}{f} \qquad \text{(A-16)}$$

$$\pm 0.92 = \frac{2\ (3.14)}{1130} \left(\frac{0.013}{0.054} \right) f - \left(\frac{1130}{2(3.14)\ (0.035)} \right) \frac{1}{f}$$

$$f = 1651 \text{ for } \chi = -0.92$$

$$f = 2409 \text{ for } \chi = +0.92$$

Now the resistance with a particle velocity of 180 ft/sec is determined from equation (A-8)

$$\theta = \frac{0.37\ u}{\sigma_1\ cC_f^2}$$

$$= \frac{0.37(180)}{(0.054)(1130)(0.78)^2}$$

$$\theta = 1.8$$

The resistance is now corrected to account for the effects of flow past the liner

$$\theta_{M_P} = \theta_{NF}(1 + 1.9\ M_P) \qquad \text{(A-17)}$$

$$\theta_{M_P} = \theta_{NF} = 1.8 \text{ since } M_P = 0$$

The absorption coefficient at both frequencies is determined from equation (A-11)

$$\alpha = \frac{4\theta}{(\theta + 1)^2 + x^2}$$

$$= \frac{4\ (1.8)}{(1.8 + 1)^2 + (0.92)^2}$$

$$= 0.83$$

$$\alpha = 83\%$$

The absorption coefficient at frequencies farther from resonance is determined by assuming increasingly smaller particle velocities below the maximum value at resonance and repeating the process which follows equation A-15.

The liner designed for the no flow case ($M_P = 0$) was tested with the high frequency impedance apparatus so that a comparison of the design results with the actual experimental results could be made. Figure A-2 shows the absorption coefficient versus frequency for the experimental results compared with the new design theory and old theory which calculated the resistance by use of the nonlinear correction term. A comparison of the individual acoustic components are shown in table A-1 where the subscript E refers to the experimental results.

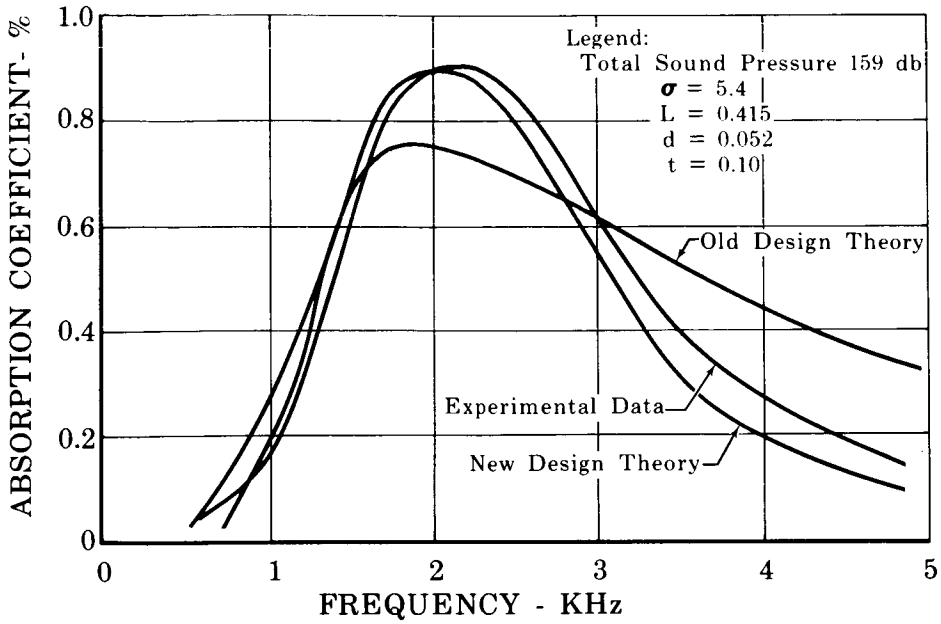

Figure A-2. Comparison of Experimental Results With the New and Old Design Theories FD 31185

Table A-1. Comparison of Design Theory With Experimental Results

f, Hz	u, ft/sec	ue, ft/sec	θ	θ_E	χ	χ_E	α, %	α_E, %
645	50	46	0.5	0.9	-7.3	-8.0	4	5
835	70	62	0.7	1.0	-5.2	-5.8	10	10
995	90	80	0.9	1.0	-4.0	-4.4	19	16
1135	110	99	1.1	1.2	-3.1	-3.4	29	29
1260	130	115	1.3	1.3	-2.5	-2.9	46	38
1401	150	135	1.5	1.6	-1.9	-2.1	61	56
1561	170	151	1.7	1.7	-1.3	-1.6	76	68
1651	180	160	1.8	1.8	-0.9	-1.3	83	76
2000	191	179	1.9	1.9	0.0	-0.1	90	90
2409	180	173	1.8	1.8	0.9	0.7	83	86
2561	170	173	1.6	1.7	1.3	1.0	76	82
2856	150	150	1.5	1.4	1.9	1.6	61	67
3165	130	130	1.3	1.1	2.5	2.0	46	53
3525	110	113	1.1	0.9	3.1	2.4	29	37
4795	70	68	0.7	0.5	5.2	3.2	10	16

B. FLOW-THROUGH CALCULATIONS

For an example calculation assume a Mach number of net flow through the apertures

$$M_T = 0.10$$

and use the same design requirements as used for the flow-past calculations.

1. Conditions at Resonance

In the flow-past calculations the particle velocity at resonance was calculated to be

$$u_o = 191 \text{ ft/sec}$$

For air the particle velocity Mach number is

$$M_o = 0.17$$

Before making additional calculations it is necessary that the following condition (see Section V) be satisfied

$$M_T > 0.5M_o \qquad \text{(A-18)}$$

if this condition is not met then the design calculations should be made in the same manner as for the no-flow case. Using equation (A-18), it is seen that for the sample calculation the above requirement is satisfied

$$0.1 > 0.5(0.17) = 0.085$$

The resistance at resonance was found as

$$\theta_o = 1.92.$$

Now the resistance at resonance and the flow through Mach number are known and the required open area ratio satisfying these values can be determined from equation (V-7).

$$\theta_o = \frac{M_T}{\sigma_1 C_f^3} \qquad \text{(A-19)}$$

$$\sigma_1 = \frac{M_T}{\theta_o C_f^3}$$

$$= \frac{0.1}{1.92(0.78)3}$$

$$= 0.11$$

Using equation (A-3) gives

$$\sigma = 0.109.$$

At this point it is necessary to assign a liner aperture diameter and liner thickness

$$d = 0.052 \text{ in.}$$

$$t = 0.10 \text{ in.}$$

The effective length is determined as

$$\ell_{eff} = \frac{t}{12} + \frac{d}{12}$$

$$= 0.013 \text{ ft}$$

Now the required backing distance of the liner cavity is calculated as in equation (A-14)

$$L = 0.68 \text{ ft.}$$

$$L = 0.82 \text{ in.}$$

This sets all liner parameters to give 90% absorption at 2000 Hz with flow through Mach number of 0.1. A summary of the liner design shows

$$\sigma = 10.9\%$$

$$L = 0.82 \text{ in.}$$

$$d = 0.052 \text{ in.}$$

$$t = 0.10 \text{ in.}$$

$$M_o = 0.17$$

2. Nonresonant Conditions

When condition A-18 is satisfied the resistance is determined by equation (A-19) and since the flow through is assumed to be constant then the resistance is constant over all frequencies (see Section V).

$$\theta = 1.92.$$

The reactance is calculated from equation (A-16) by assuming a frequency

$$f = 1700 \text{ Hz}$$

then $$\chi = -0.32$$

The absorption coefficient is calculated from equation (A-11) and

$$\alpha = \frac{4\theta}{(\theta + 1)^2 + \chi^2}$$

$$= \frac{4(1.92)}{(1.92 + 1)^2 + (0.32)^2}$$

$$\alpha = 0.83$$

$$\alpha = 83\%$$

Since the resistance is constant it is seen from equation (A-11) that the absorption coefficient is only effected by changes in reactance. To determine the absorption coefficient over a band of frequencies it is necessary to choose the frequencies, calculate the corresponding reactance and use equation (A-11) to determine the respective absorption coefficients.

APPENDIX B
PRESSURE-PHASE IMPEDANCE MEASURING TECHNIQUE

This appendix is divided into four sections; in the first a description of the basic impedance measuring apparatus is given and the necessary impedance relations are derived in the second. The error analysis of the experiment appears in the third part, and a description of the ancillary components follows.

1. BASIC APPARATUS

The pressure-phase impedance device is shown in figure 3-1. The device consists of a square duct of fixed length and uniform cross section, which unlike the ASTM impedance tube, can be made as short as desired without imposing a frequency limit on the apparatus. At one end of the duct, a source of sound waves is placed, and at the other end, the specimen to be tested. An audio oscillator (signal generator) drives the speakers causing plane waves to be transmitted longitudinally along the tube.

When the longitudinal wave is incident on the sample at the end of the tube part of its energy is reflected back up the tube in the form of another pressure wave. The incident and reflected waves set up a standing wave in the tube that has a maximum pressure amplitude at the sample face, a small microphone mounted flush in the side wall of the tube at the sample is used to measure the pressure.

The portion of the incident sound energy that is not reflected back up the tube is transmitted through the apertures and into the resonator cavity. The energy in the cavity, also in the form of sound pressure, is measured with a second microphone located on the back wall of the cavity. (See figure B-2.) The outputs of both microphones are fed through a wave analyzer to a millivolt meter so that the pressure amplitudes of the sound level in front of the sample and in the cavity can be read. In addition, as shown in the schematic of figure A-3, the outputs of both microphones are connected to a synchronous filter and phase meter to determine the phase difference between the incident and transmitted waves.

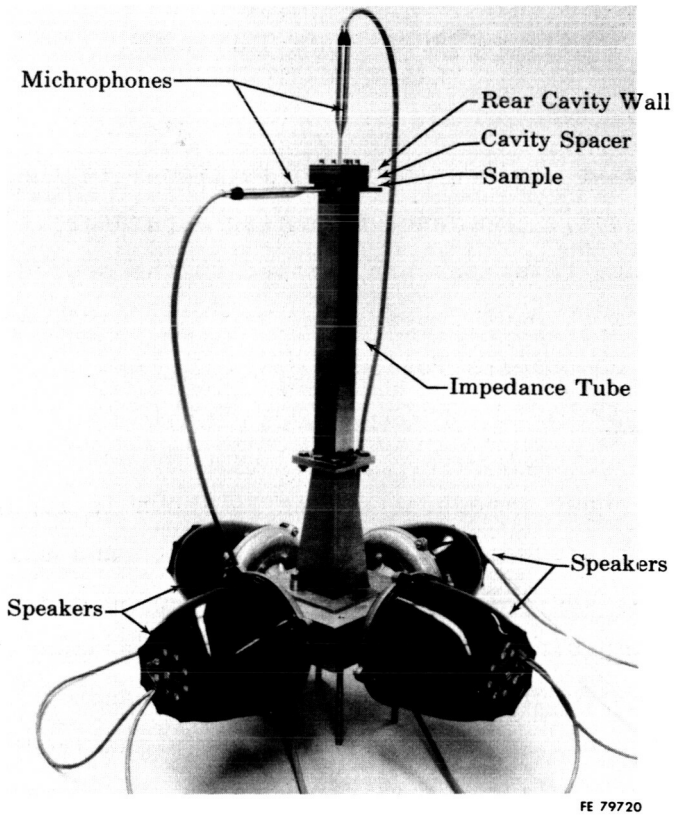

Figure B-1. High Frequency and High-Sound Pressure-Phase Angle Impedance Tube FD 25289

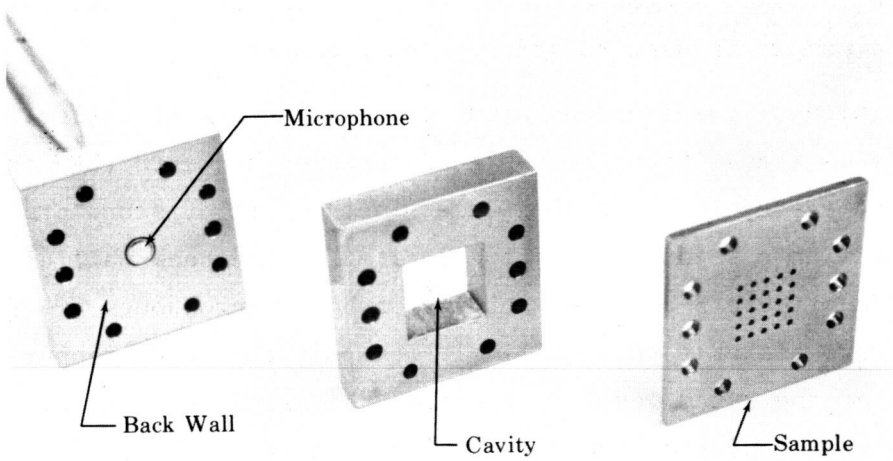

Figure B-2. Resonator Test Section FD 23078

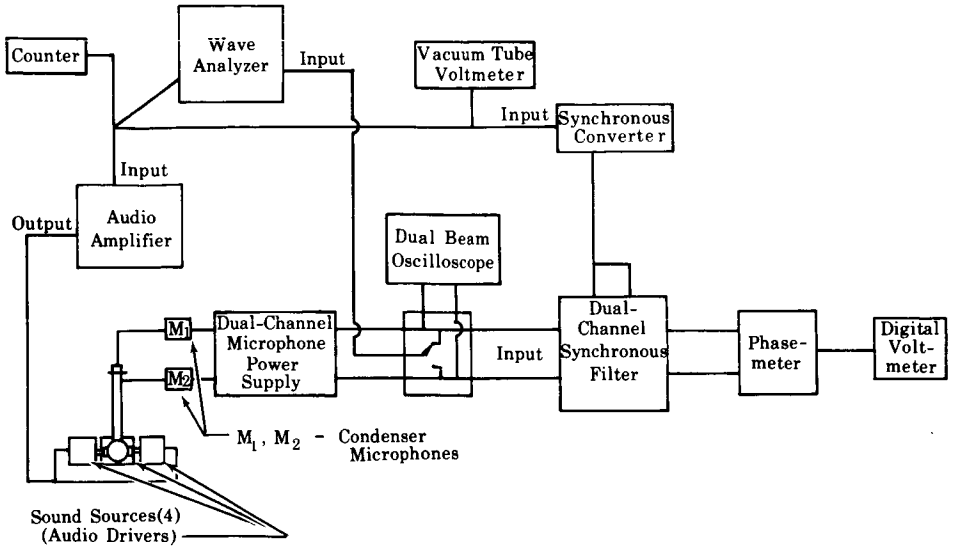

Figure B-3. Schematic of Pressure-Phase Impedance Measuring Apparatus FD 29167

2. DERIVIATION OF IMPEDANCE RELATIONS

A typical Helmholtz resonator at the end of a tube is shown in figure B-4. Also shown are two microphones, one mounted in the side wall to measure the sound pressure in front of the sample, P_1, and one on the rear wall to measure the sound pressure in the cavity, P_2. With the signals from both microphones the phase difference, ϕ, between the two pressures can be determined.

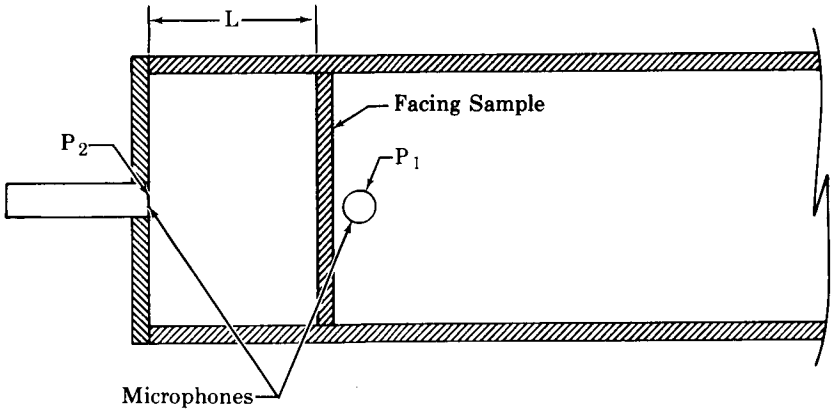

Figure B-4. Helmholtz Resonator in Impedance Tube FD 23080

The total impedance of a resonator assembly is composed of two parts

$$Z_{total} = Z_{plate} + Z_{air\ cavity} \tag{B-1}$$

If u is the oscillatory gas velocity amplitude in the apertures and ρ and c are the density and sonic velocity, respectively of the test media, σ is the ratio of the area of the apertures to the cross-sectional area of the tube, by definition the impedance is the complex ratio of the pressure difference and the particle velocity

$$Z_{plate} = \frac{\bar{P}_1 - \bar{P}_2}{\sigma \rho cu} \tag{B-2}$$

and also for a partitioned cavity

$$Z_{air\ cavity} = \frac{P_2}{\sigma cu\rho} = \frac{i}{kL} \tag{B-3}$$

Solving equation (B-2) for u, substituting into equation (B-3) and solving for Z_{plate} gives:

$$Z_{plate} = \frac{i}{kL}\left[\frac{P_1}{P_2} - 1\right] \tag{B-4}$$

where k, the wave number, is defined as $k = \omega/c$.

Using a mathematical identity, the ratio of the complex pressures can be expressed as:

$$\frac{P_1}{P_2} = \left[\frac{P_1}{P_2}\right] e^{-i\phi} = \left[\frac{P_1}{P_2}\right] \cos \phi - i\left[\frac{P_1}{P_2}\right] \sin \phi$$

Substituting the identity into equation (B-4)

$$Z_{plate} = \frac{1}{kL}\left[\frac{P_1}{P_2}\right] \sin \phi - \frac{i}{kL}\left[1 - \frac{P_1}{P_2} \cos \phi\right]$$

Solving equation (B-1) for Z_{total} gives:

$$Z_{total} = \frac{1}{kL}\left[\frac{P_1}{P_2}\right] \sin \phi - \frac{i}{kL}\left[1 - \left|\frac{P_1}{P_2}\right| \cos \phi\right] + \frac{i}{kL} \tag{B-5}$$

or

$$Z_{total} = \frac{1}{kL}\left[\frac{P_1}{P_2}\right] \sin \phi + i \left[\frac{1}{kL}\left|\frac{P_1}{P_2}\right| \cos \phi\right] \qquad \text{(B-6)}$$

The total impedance is a complex sum; the real part is the resistance, θ, and the imaginary part is the reactance, χ. By inspection of equation (A-6) it is evident that the resistance can be determined from

$$\theta = \frac{1}{kL}\left[\frac{P_1}{P_2}\right] \sin \phi \qquad \text{(B-7)}$$

and the reactance from

$$\chi = -\frac{1}{kL}\left[\frac{P_1}{P_2}\right] \cos \phi \qquad \text{(B-8)}$$

As shown in Reference 5, the normal incident sound pressure can be obtained from

$$P_i = P_1 \Big/ \left[1 + \frac{Z-1}{Z+1}\right] = P_1 \Big/ \left[1 + \left(\frac{(\theta - 1)^2 + \chi^2}{(\theta + 1)^2 + \chi^2}\right)^{\frac{1}{2}}\right] \qquad \text{(B-9)}$$

Additional acoustic parameters that can now be computed are:

Absorption coefficient

$$\alpha = \frac{4\theta}{(\theta + 1)^2 + \chi^2} \qquad \text{(B-10)}$$

Nonlinear resistance correction factor

$$\Delta_n \ell/d = \frac{\theta \sigma c}{\sqrt{8 \nu \omega}} - (t/d + 1) \qquad \text{(B-11)}$$

where

σ is the open area ratio of the facing,

υ is the kinematic viscosity of the media and

ω is the angular frequency

In addition, the oscillatory flow velocity in apertures is computed using equation (B-3)

$$u = kLP_2/(\sigma \rho c) \qquad \text{(B-12)}$$

and the aperture effective length is obtained by setting the inertance of the sample (Reference 5) equal to the impedance of the plate (equation B-4)

$$\ell_{eff} = \frac{\sigma c Z_{plate}}{2\pi f} = \frac{\sigma c}{2\pi f k L}\left[\frac{P_1}{P_2} - 1\right] \qquad \text{(B-13)}$$

3. ERROR ANALYSIS OF TECHNIQUE

An error analysis of the pressure-phase angle method of determining the acoustical properties of a liner was performed using the "method of partial derivatives." (See Reference 9.) According to this method, the error in a calculated value may be approximated as

$$\sigma_F^2 = \left(\frac{\partial F}{\partial X_1}\right)^2 \sigma_{X_1}^2 + \left(\frac{\partial F}{\partial X_2}\right)^2 \sigma_{X_2}^2 + \cdots \left(\frac{\partial F}{\partial X_n}\right)^2 \sigma_{X_n}^2 \qquad \text{(B-14)}$$

where F is the calculated function

$X_1, X_2, \ldots X_n$ are the variables used in calculating the function

$\frac{\partial F}{\partial X_1}, \frac{\partial F}{\partial X_2}, \ldots \frac{\partial F}{\partial X_n}$ are the partial derivatives of the calculated function with respect to the variables $X_1, X_2, \ldots X_n$

$\sigma_{X_1}, \sigma_{X_2}, \ldots \sigma_{X_n}$ are the estimated errors in measurement of the variables $X_1, X_2, \ldots X_n$

and σ_F is the estimated error in the calculated function due to the errors in the measurement of the variables $X_1, X_2, \ldots X_n$.

In using the pressure-phase angle method for determining the acoustical properties of a liner the following variables must be measured:

1. Sound pressure level in front of the liner
2. Sound pressure level in the cavity
3. Frequency of the sound pressure oscillations
4. Phase angle between these sound pressures
5. Gas properties of the system
6. Geometry of the system.

For this analysis, it was assumed that there was no error in measuring the geometry of the system and that the gas properties contributed no

error. Thus, only the two sound pressure levels and the phase angle between them were considered in estimating errors.

It is believed that these are valid assumptions for impedance tube testing or other experiments where the geometry and gas properties are well known. For hot testing, an analysis should be carried out which considers all of the variables because gas properties and even parts of the geometry may not be well known.

The following calculated values were analyzed:

1. Gas particle velocity in the aperture, u
2. Resistance, R
3. Reactance, X
4. Impedance, Z
5. Absorption coefficient, α
6. Incident Pressure, P_i.

Each of these parameters were analyzed in the same fashion. An equation for the parameter was written in terms of the variables listed above, and then the appropriate partial derivatives were taken and inserted in the general equation (B-14). The results are given below.

a. Gas Particle Velocity in the Aperture, u

$$\sigma_u = (0.115\ \sigma_{db_2})\ u \qquad \text{(B-15)}$$

where σ_u is the estimated error in u

and σ_{db_2} is the estimated error in measurement of cavity SPL in db.

Thus, an error of 11.5% per db of error in measuring cavity SPL is estimated. If an error of 0.5 db is estimated in cavity SPL measurement, then the estimated error in u is 5.75%.

b. Resistance, R

$$\sigma_R = \sqrt{\sigma^2_{(R/phase)} + \sigma^2_{(R/SPL)}} \qquad \text{(B-16)}$$

where

σ_R is the estimated error in R

$\sigma_{(R/phase)}$ is the estimated error in R due to error in phase angle measurement

$\sigma_{(R/SPL)}$ is the estimated error in R due to error in SPL measurement;

and

$$\sigma_{(R/SPL)} = \left(0.115\sqrt{\sigma^2_{db_1} + \sigma^2_{db_2}}\right)R \qquad \text{(B-17)}$$

$$\sigma_{(R/phase)} = \left[0.0174\ (\cot\phi)\sigma\phi\right]R \qquad \text{(B-18)}$$

where

ϕ is the phase angle

$\sigma\phi$ is the estimated error in phase angle measurement

σ_{db_1} is the estimated error in measurement of SPL in front of the liner

σ_{db_2} is the estimated error in measurement of cavity SPL.

The $\sigma_{(R/phase)}$ is negligible except below 10 deg and above 170 deg. (See figure B-5.) Between 10 deg and 170 deg, σ_R is approximately equal to $\sigma_{(R/SPL)}$, which for $\sigma_{db_1} = \sigma_{db_2} = 0.5$ yields an estimated error of 8.1% in R.

c. Reactance, X

$$\sigma_X = \sqrt{\sigma^2_{(X/SPL)} + \sigma^2_{(X/Phase)}} \qquad \text{(B-19)}$$

where the terminology is the same as above for resistance

and

$$\sigma_{(X/SPL)} = \left(0.115\sqrt{\sigma^2_{db_1} + \sigma^2_{db_2}}\right)X \qquad \text{(B-20)}$$

$$\sigma_{(X/phase)} = \left[0.0174\ (\tan\phi)\sigma\phi\right]X. \qquad \text{(B-21)}$$

The error indicated here is similar to that given above for resistance, except that the region of high error here is between 80 deg and 100 deg because of the tan ϕ term. (See figure B-6).

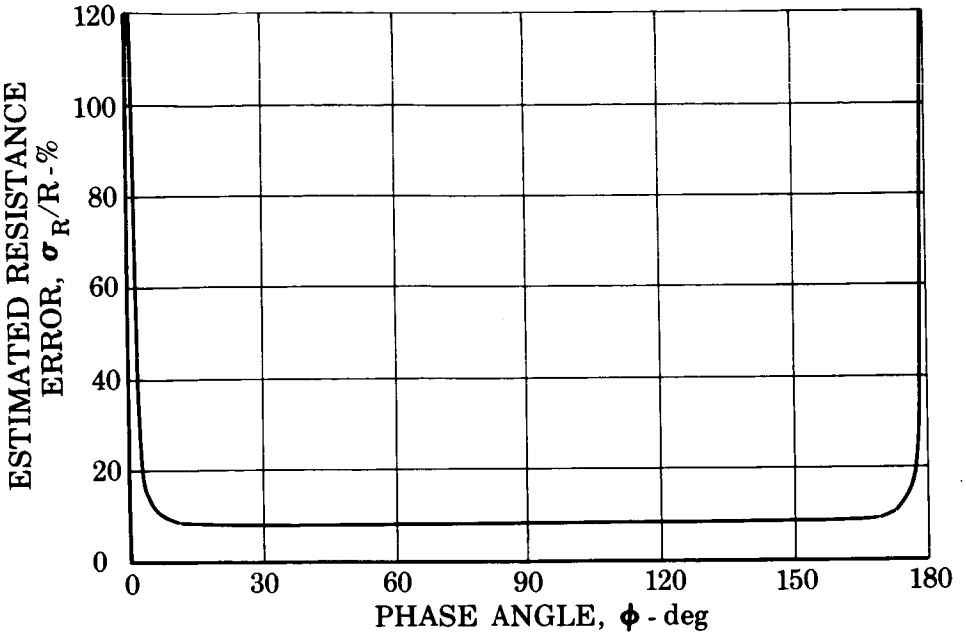

Figure B-5. Estimated Resistance Error as a Function of Phase Angle FD 29169

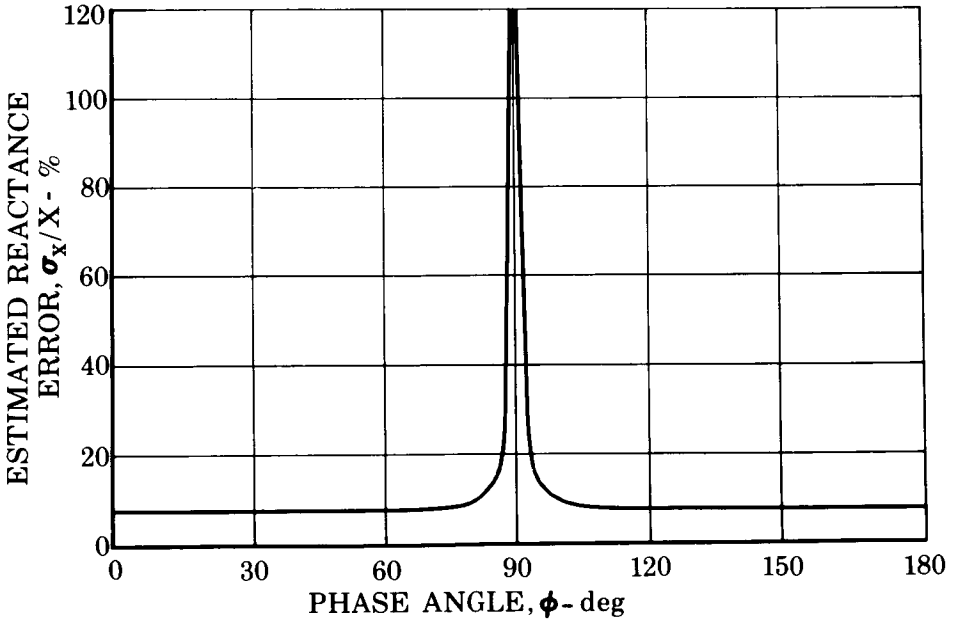

Figure B-6. Estimated Reactance Error as a Function of Phase Angle FD 29170

d. Impedance, Z

$$\sigma_Z = \left(0.115 \sqrt{\sigma^2_{db_1} + \sigma^2_{db_2}}\right) Z \qquad \text{(B-22)}$$

where σ_Z (the estimated error in calculating Z (is 11.5% per unit value of the radical. For $\sigma_{db_1} = \sigma_{db_2} = 0.5$, we get an estimated error of 8.1%.

e. Absorption Coefficient, α

$$\sigma_\alpha = \left[0.115 \left(\frac{Z - 1}{Z + 1}\right)\sqrt{\sigma^2_{db_1} + \sigma^2_{db_2}}\right]\alpha \qquad \text{(B-23)}$$

since Z is positive, σ_α (the estimated error in α) should always be less than or equal to 11.5% per unit value of the radical. For $\sigma_{db_1} = \sigma_{db_2} = 0.5$, the estimated error always is less than or equal to 8.1%.

f. Incident Pressure, P_i

$$\sigma_{P_i} = \sqrt{\sigma^2_{(P_i/db_1)} + \sigma^2_{(P_i/Z)}} \qquad \text{(B-24)}$$

where

σ_{P_i} is the estimated error in P_i

$\sigma_{(P_i/db_1)}$ is the estimated error in P_i because of errors in measuring sound pressure level in front of the liner

$\sigma_{(P_i/Z)}$ is the estimated error in P_i due to errors in calculating Z

and

$$\sigma_{(P_i/db_1)} = 0.115\ \sigma_{db_1}\ P_1 \qquad \text{(B-25)}$$

$$\sigma_{(P_i/Z)} = \frac{\sigma_Z}{Z\ (Z + 1)}\ P_i \qquad \text{(B-26)}$$

Combining these equations we have

$$\sigma_{P_i} = 0.115\ P_i \sqrt{\sigma^2_{db_1} + \frac{\sigma^2_{db_1} + \sigma^2_{db_2}}{\left[Z\ (Z + 1)\right]^2}}$$

Using $\sigma_{db_1} = \sigma_{db_2} = 0.5$, we have

$$\sigma_{P_i} = \left(0.115\sqrt{0.25 + \frac{0.5}{\left[Z\ (Z + 1)\right]^2}}\right) P_i \qquad \text{(B-27)}$$

The second term under the radical is negligible when $Z > 1$. So the estimated error in P_i is approximately 5.75% for $Z > 1$. For $0.5 < Z < 1$, the estimated error is less than 12.5%. For $Z \leq 0.5$ the error increases rapidly. (See figure B-7.)

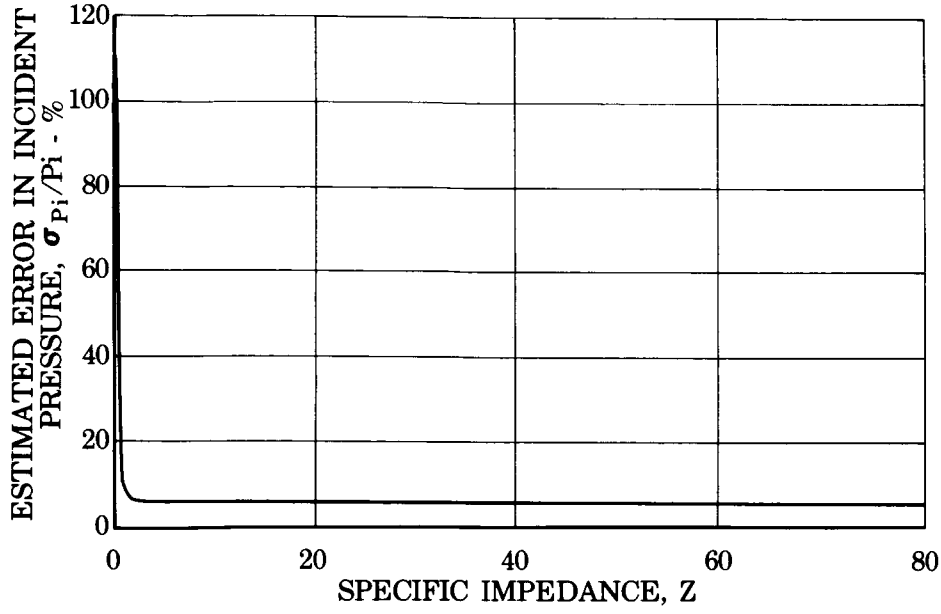

Figure B-7. Estimated Error in Incident Sound Pressure as a Function of Impedance FD 29174

g. Conclusions

It can be concluded from this analysis that in impedance tube testing or other cold flow experiments in which the gas properties and geometry are well known, error in acquisition of data should not prevent good calculated results if care is taken to assure that no large errors are incurred in sound pressure or phase angle measurement. Exceptions are given below. Large estimated errors occur when calculating

1. Resistance at phase angles of less than 10 deg or more than 170 deg
2. Reactance at phase angles between 80 deg and 100 deg
3. Incident pressure when the calculated impedance is less than 0.5.

4. ANCILLARY COMPONENTS

The ancillary components used with the apparatus are:

Component	Manufacturing and Model Number
Wave Analyzer	General Radio - Model 1900-A
Audio Amplifier	Harman Kardon - Model BA-150 Watt
Electronic Counter	Hewlett Packard - Model 521CR
Condenser Microphones	M_1 & M_2 - Brüel & Kjaer - Model 4138, plus UA 0036 adapter, also 2615 cathode follower
Dual-Channel Power Supplies	Brüel & Kjaer - Model 2803

Component	Manufacturing and Model Number
Dual-Beam Oscilloscope	Hewlett Packard - Model 132A
Vacuum Tube Voltmeter	Hewlett Packard - Model 400DR
Dual-Channel Synchronous Filter	AD-YU Electronics - Model 1034
Synchronous Converter	AD-YU Electronics - Model 1036
Digital Phase Computer	AD-YU Electronics - Model 524A3
Precisions DC Voltmeter	Honeywell - Model DC-110BR, or optional Digital Voltmeter.
Pistonphone	Brüel & Kjaer - Model 4220 (for microphone calibrations)
Sound Sources	Atlas Sound Driver Unit - Model PD-60T

The function of each component is as follows:

1. The GR1900-A Wave Analyzer measures the output of the microphones through an adjustable narrow (± 3, 10 or 50 Hz) band-pass filter. The analyzer's tracking generator output provides the driving signal.
2. The Counter and Vacuum Tube Voltmeter are used to monitor the frequency and amplitude of the driving signal.
3. The Audio Amplifier boosts the power of the driving signal to the level required.
4. The Audio Driver converts the electrical signal to sound.
5. The Condenser Microphones provide electrical signals equivalent to sound pressure level.
6. The Microphone Power Supply provides the polarization voltage to the microphones and contains an attenuator for standardization and an emitter follower for isolation.
7. The Dual Beam Scope is used to monitor microphone outputs for approximate level and phase and for distortion.

8. The block diagram of the Type 1034 Dual-Channel Syncronous Filter is shown in figure B-8. Since both channels are identical, only channel 1 is shown and described.

   The distorted, and/or noisy signal is amplified before being applied to the balanced mixer circuitry through an emitter-follower. The balanced mixer also receives signals from an emitter-follower, the frequency of which is the syncronized input (a 2.4 volt signal containing the carrier frequency mixed with an audio frequency which is the fundamental frequency of the distorted signal input. Both input circuits contain emitter-followers in order to provide high input impedances. The output of the balanced mixes is fed to the crystal filter, from which only the recovered carrier frequency (with amplitude proportional to the fundamental component of the distorted signal input, and with phase angle equal to that input) is allowed to emerge. After two stages of amplification an LC filter circuit is used to provide even greater purity of the recovered carrier. One stage of the output amplifier provides voltage amplification, while the other stage provides three low impedance outputs; both "HI" and "LO" outputs and a selectable D.C. metering circuit.

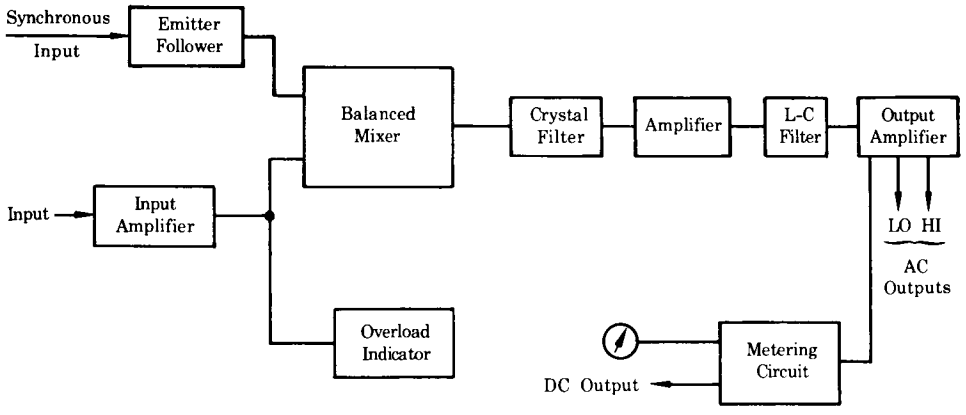

Figure B-8. Block Diagram of One Channel of Model 1034 Dual-Channel Synchronous Filter FD 29168

9. Type 1036 Synchronous Converter is especially designed to be used together with Type 1034 Dual-Channel Synchronous Filter. Figure B-9 shows a block diagram of Type 1036. (E_a is a synchronized audio signal. The output signal has constant amplitude and frequency equal to crystal frequency plus input signal frequency.) The input amplifier provides a high input impedance. The wideband 90-deg phase shifter produces two signals, E_a and $E_a + 90^o$. These two signals have exactly 90-deg phase difference and equal amplitude. The frequency equals that of the input audio signal, f_a, and changes as the frequency of the input signal changes. The two balanced mixers produce E_1 and E_2, containing only

the upper and lower sidebands of their inputs (suppressed carrier). The crystal oscillator supplies signal, E_c, at the exact center frequency of the crystal filters used in Type 1034 Dual-Channel Synchronous Filter. The 90-deg phase shifter generates two outputs, E_c and $E_c + 90^o$, with equal amplitude. Since the amplitudes of E_a and E_a + 90-deg are equal and their frequencies always follow the input audio frequency, W_a, one can write two expressions for the output of the balanced mixers, E_1 and E_2, as follows:

$$E_1 = kE_aE_c \sin (W_c + W_a)t - \sin (W_c - W_a)\, t$$
$$E_2 = kE_aE_c \sin (W_c + W_a)t + \sin (W_c - W_a)\, t$$

The sum amplifier accepts E_1 and E_2 and produces its algebraic sum, E_3, such as $E_3 = E_1 + E_2 = 2kE_aE_c \sin (W_c + W_a)\, t$. The output amplifier provides low output impedance to drive up to 40 channels of Type 1034 Synchronous Filter. The voltmeter circuit can be switched by panel control to read the amplitude of either the output signal or input signal on the panel meter.

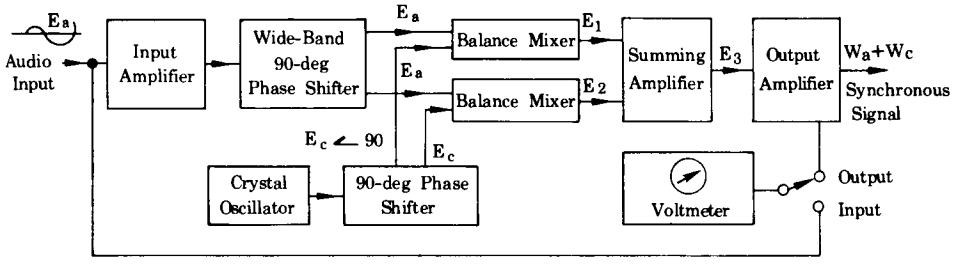

Figure B-9. Block Diagram of Type 1036 Synchronous Connecter FD 29163

10. The Type 524A Phase Meter provides a D.C. level output proportional to the phase difference between it's inputs.

11. The Digital Voltmeter measures the phase meter output and by means of an AC to DC converter can read the synchronous filter's outputs as an additional measure of sound pressure level.

APPENDIX C
FLOW COEFFICIENT EXPERIMENTS

In order to explain the high frequency test results, an experiment was performed to determine if the hydraulic flow coefficient of the sample orifices was related to the sample-to-sample differences in the acoustic resistance and particle velocity data. The flow coefficient (C_f) of each sample was calculated from the following equation (Reference 11).

$$w = C_f \, A_2 \, Y_1 \sqrt{\frac{2g\rho_1\Delta p}{1 - \beta^4}} \qquad \text{(C-1)}$$

where

w = mass flowrate
A_2 = orifice flow area
Y_1 = expansion factor accounting for effects of compressive flow
g = gravitational constant
ρ_1 = upstream fluid density
Δp = pressure differential across the orifice
β = ratio of upstream to orifice diameters.

A flow rig (figure C-1) was fabricated for the experiment. The rig consisted of a plenum chamber supplied with a metered quantity of nitrogen which was allowed to vent through the sample apertures. A static pressure tap was located upstream of the sample. A spacer plate which formed the cavity side walls in the high frequency tests was installed downstream of the sample to simulate any wall effects on the flow exhausting from the apertures.

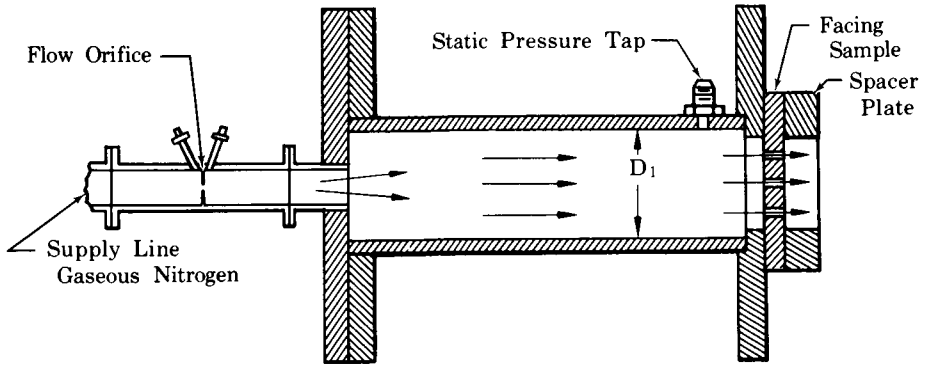

Figure C-1. Apparatus for Measuring Resonator Facing Flow Coefficient FD 29164

The following procedure was used in evaluating the flow coefficient by use of equation C-1. The mass flowrate was determined by use of a calibrated flowmeter. The orifice flow area, A_2, was taken to be that of a single orifice having the same area as the total area of all the small apertures in the sample. The expansion factor was calculated from the following equation (Reference 11).

$$Y_1 = \sqrt{\frac{\left[\gamma/(\gamma-1)\right] r^{2/\gamma}\left[1 - r^{(\gamma-1)/\gamma}\right]}{1 - r}} \qquad (C-2)$$

where

$$r = P_2/P_1$$

is the ratio of the upstream static pressure to the downstream ambient pressure. By measuring the static pressure upstream of the sample in the plenum chamber the pressure differential across the orifice was known. The diameter ratio, β , was calculated as the ratio of the upstream diameter, D_1, to the effective diameter of the sample apertures where effective diameter was calculated as the diameter of a single orifice of area A_2. Sufficient flow was supplied to the sample apertures to produce velocities of the same magnitude as the peak velocities obtained in the high frequency tests. A list of the flow coefficient and the velocity range over which they were measured appears in the table below.

σ	t in.	Minimum Velocity ft/sec	Flow Coefficient	Maximum Velocity ft/sec	Flow Coefficient	Average Flow Coefficient
1.5	0.10	433	0.68	447	0.70	0.69
3.0	0.10	447	0.76	493	0.71	0.73
3.95	0.09	443	0.86	519	0.86	0.86
5.65	0.09	334	0.86	456	0.84	0.85
6.95	0.10	284	0.67	349	0.67	0.67
8.00	0.10	293	0.68	384	0.68	0.68
8.85	0.10	242	0.61	325	0.60	0.61
10.8	0.10	301	0.93	348	0.91	0.92
13.0	0.10	276	0.85	290	0.81	0.83
5.4	0.05	363	0.70	430	0.66	0.68
5.4	0.10	356	0.78	424	0.78	0.78
5.4	0.15	340	0.71	410	0.71	0.71
5.4	0.20	311	0.60	381	0.64	0.62
5.4	0.25	337	0.68	405	0.69	0.69

APPENDIX D
ACOUSTIC DATA

Acoustic data obtained under the present program are listed in the following tables. For simplicity, the IBM printouts from the data reduction deck are used.

A brief title describing the type of data precedes each individual listing. Next the properties of the gaseous medium and the dimensions of the resonator assembly that are input into the deck are listed. The following list identifies each header.

DEN	Density (Cavity Gas), lb_m/ft^3
SONIC	Sonic Velocity (Cavity Gas), ft/sec
VIS	Dynamic Viscosity (Cavity Gas), $lb_m/ft/sec$
CF	Flow Coefficient
SIG	Open Area Ratio
XL	Cavity Backing Distance, in.
T	Liner Thickness (aperture length), in.
D	Aperture Diameter, in.

Then a listing of the experimental data and results follows:

Data	FREQ	Frequency, Hz
	PA1	Chamber Pressure Amplitude RMS, lb_f/in^2
	PA2	Cavity Pressure Amplitude RMS, lb_f/in^2
	PHASE	Phase Angle, deg
Results	INERT	Specific Acoustic Inertance
	REACT	Specific Acoustic Reactance
	RESIS	Specific Acoustic Resistance
	IMPED	Specific Acoustic Impedance
	ABSOR	Absorption Coefficient
	SPL	Incident Pressure Amplitude, db

DNLD	Nonlinear Correction Term
UORF	Particle Velocity in Apertures, ft/sec
LEFF	Effective Length of Aperture, in.
K2RES	K_2 Resistance Proportionality Coefficient = RESIS $\sigma c C_f^2$/UORF
DNLDK	Comparison of Nonlinear Correction Term with Sirignano Theory
VELTH	Velocity of Steady Flow-Through the Aperture, ft/sec
VELPT	Velocity of Steady-Flow Past the Apertures, ft/sec

I. DATA USED IN THE HIGH FREQUENCY ANALYSIS

RESONATOR CONFIGURATION NO. 1

DEN	SONIC	VIS	CF	SIG	XL	T	D
0.0750	1129.0	0.12200E-04	0.686	0.0150	0.500	0.100	0.047

FREQ	PA1	PA2	PHASE	INERT	REACT	RESIS	IMPED	ABSOR	SPL	DNLD	CORF	LEFF	K2RES	DNLDK
1200.0	0.002	0.003	159.5	6.267	2.673	0.999	2.85	0.358	114.89	2.27	5.24	0.169	1.51	4.61
1200.0	0.003	0.004	158.6	6.251	2.657	1.041	2.85	0.370	116.92	2.50	6.60	0.168	1.25	3.91
1200.0	0.004	0.005	157.0	6.191	2.597	1.102	2.82	0.394	119.00	2.83	8.40	0.166	1.04	3.36
1200.0	0.005	0.007	155.3	6.128	2.534	1.165	2.78	0.419	121.08	3.17	10.70	0.165	0.86	2.87
1200.0	0.007	0.009	152.9	6.077	2.483	1.270	2.78	0.448	123.17	3.74	13.48	0.163	0.75	2.59
1200.0	0.009	0.011	150.6	6.138	2.544	1.433	2.92	0.462	125.22	4.62	16.20	0.165	0.70	2.56
1200.0	0.011	0.014	147.3	5.995	2.402	1.542	2.85	0.504	127.37	5.21	20.88	0.161	0.58	2.19
1200.0	0.014	0.018	142.6	5.887	2.293	1.753	2.88	0.546	129.52	6.35	25.98	0.158	0.53	2.08
1200.0	0.018	0.022	137.5	5.772	2.178	1.996	2.95	0.581	131.66	7.66	31.96	0.155	0.49	2.00
1200.0	0.023	0.026	132.1	5.716	2.122	2.349	3.16	0.597	133.73	9.57	37.56	0.154	0.49	2.07
1200.0	0.029	0.030	126.9	5.630	2.037	2.713	3.39	0.605	135.76	11.54	44.13	0.151	0.48	2.09
1200.0	0.045	0.040	119.2	5.560	1.967	3.519	4.03	0.579	139.65	15.90	58.84	0.149	0.47	2.12
1200.0	0.072	0.054	113.7	5.542	1.948	4.438	4.84	0.531	143.47	20.87	77.57	0.149	0.45	2.08
1200.0	0.115	0.068	109.0	5.557	1.964	5.704	6.03	0.467	147.24	27.72	98.79	0.149	0.46	2.14
1200.0	0.182	0.089	105.3	5.529	1.936	7.077	7.33	0.410	151.05	35.14	128.74	0.149	0.43	2.07
1200.0	0.290	0.111	102.8	5.663	2.070	9.112	9.34	0.342	154.84	46.14	160.22	0.152	0.45	2.17
1200.0	0.459	0.142	102.0	6.011	2.417	11.374	11.62	0.286	158.68	58.38	204.05	0.162	0.44	2.14
1200.0	0.728	0.176	101.5	6.546	2.952	14.512	14.80	0.232	162.53	75.35	253.94	0.176	0.45	2.21
1200.0	1.265	0.225	101.2	7.518	3.925	19.824	20.20	0.176	167.19	104.07	323.40	0.202	0.48	2.39

RESONATOR CONFIGURATION NO. 2

DEN	SONIC	VIS	CF	SIG	XL	T	D
0.0750	1129.0	0.12200E-04	0.730	0.0300	0.500	0.100	0.056

FREQ	PA1	PA2	PHASE	INERT	REACT	RESIS	IMPED	ABSOR	SPL	DNLD	UORF	LEFF	K2RES	DNLDK
1500.0	0.002	0.007	153.7	3.810	0.935	0.462	1.04	0.613	115.80	1.69	7.17	0.164	1.16	3.09
1500.0	0.003	0.010	152.8	3.803	0.928	0.477	1.04	0.627	117.85	1.83	9.02	0.164	0.95	2.58
1500.0	0.004	0.012	151.4	3.802	0.927	0.505	1.05	0.646	119.94	2.10	11.23	0.164	0.81	2.28
1500.0	0.005	0.015	149.3	3.772	0.897	0.532	1.04	0.675	122.08	2.37	14.30	0.162	0.67	1.94
1500.0	0.007	0.019	144.8	3.737	0.862	0.608	1.05	0.730	124.36	3.10	17.80	0.161	0.61	1.90
1500.0	0.009	0.024	140.8	3.722	0.847	0.690	1.09	0.772	126.61	3.90	21.65	0.160	0.57	1.86
1500.0	0.011	0.029	137.0	3.692	0.818	0.762	1.11	0.807	128.84	4.59	26.64	0.159	0.51	1.73
1500.0	0.014	0.035	133.4	3.679	0.804	0.850	1.17	0.835	131.04	5.45	32.03	0.158	0.47	1.66
1500.0	0.018	0.043	128.2	3.616	0.741	0.941	1.19	0.872	133.34	6.33	39.41	0.156	0.43	1.53
1500.0	0.023	0.052	122.5	3.557	0.682	1.070	1.26	0.901	135.62	7.57	46.84	0.153	0.41	1.51
1500.0	0.029	0.059	119.1	3.551	0.676	1.216	1.39	0.905	137.67	8.98	53.77	0.153	0.40	1.53
1500.0	0.045	0.078	112.1	3.504	0.629	1.550	1.67	0.898	141.59	12.22	70.89	0.151	0.39	1.53
1500.0	0.072	0.099	107.3	3.501	0.626	2.011	2.10	0.850	145.15	16.68	89.25	0.151	0.40	1.63
1500.0	0.115	0.126	103.8	3.500	0.625	2.546	2.62	0.785	148.69	21.86	113.66	0.151	0.40	1.65
1500.0	0.182	0.164	101.0	3.483	0.608	3.130	3.18	0.718	152.30	27.51	148.12	0.150	0.38	1.58
1500.0	0.290	0.207	98.7	3.482	0.607	3.968	4.01	0.633	155.88	35.62	186.47	0.150	0.38	1.62
1500.0	0.459	0.258	96.2	3.427	0.552	5.082	5.11	0.545	159.52	46.41	232.07	0.147	0.39	1.68
1500.0	0.728	0.321	95.2	3.465	0.590	6.484	6.51	0.460	163.21	59.97	288.81	0.149	0.40	1.74
1500.0	1.154	0.395	95.2	3.635	0.760	8.353	8.38	0.379	166.95	78.07	355.32	0.156	0.42	1.83
1500.0	1.265	0.409	95.2	3.680	0.805	8.847	8.88	0.362	167.70	82.86	367.80	0.158	0.43	1.88

RESONATOR CONFIGURATION NO. 3

DEN	SONIC	VIS	CF	SIG	XL	T	D
0.0750	1129.0	0.12200E-04	0.864	0.0395	0.500	0.090	0.052

FREQ	PA1	PA2	PHASE	INERT	REACT	RESIS	IMPED	ABSOR	SPL	DNLD	UORF	LEFF	K2RES	DNLDK
1800.0	0.029	0.083	103.5	2.589	0.193	0.807	0.83	0.977	138.78	6.67	68.44	0.122	0.39	1.01
1800.0	0.045	0.105	99.1	2.561	0.165	1.032	1.04	0.993	143.31	9.29	86.16	0.121	0.39	1.07
1800.0	0.072	0.134	97.7	2.570	0.174	1.289	1.30	0.978	146.80	12.28	109.73	0.121	0.39	1.09
1800.0	0.115	0.168	95.7	2.558	0.162	1.630	1.63	0.938	150.08	16.25	138.14	0.121	0.39	1.12
1800.0	0.182	0.222	93.0	2.498	0.103	1.967	1.96	0.892	153.53	20.17	182.10	0.118	0.35	1.05
1800.0	0.290	0.267	92.8	2.522	0.126	2.593	2.59	0.802	156.80	27.46	218.94	0.119	0.39	1.17
1800.0	0.459	0.336	95.2	2.692	0.296	3.255	3.26	0.715	160.28	35.17	275.62	0.127	0.39	1.18
1800.0	0.728	0.454	95.6	2.770	0.374	3.822	3.84	0.653	163.97	41.77	371.81	0.131	0.34	1.03
1800.0	1.089	0.578	92.2	2.569	0.173	4.509	4.51	0.593	167.21	49.77	473.50	0.121	0.31	0.96

RESONATOR CONFIGURATION NO. 4

DEN	SONIC	VIS	CF	SIG	XL	T	D
0.0750	1129.0	0.12200E-04	0.780	0.0540	0.500	0.100	0.052

FREQ	PA1	PA2	PHASE	INERT	REACT	RESIS	IMPED	ABSOR	SPL	DNLD	UORF	LEFF	K2RES	DNLDK
2000.0	0.002	0.010	155.5	2.709	0.552	0.252	0.60	0.538	115.49	0.88	6.84	0.157	1.36	2.62
2000.0	0.003	0.012	155.1	2.713	0.557	0.258	0.61	0.546	117.52	0.99	8.51	0.158	1.12	2.22
2000.0	0.004	0.016	154.5	2.711	0.554	0.264	0.61	0.555	119.56	1.07	10.72	0.157	0.91	1.84
2000.0	0.005	0.020	153.5	2.693	0.537	0.268	0.60	0.565	121.60	1.12	13.81	0.156	0.71	1.46
2000.0	0.007	0.026	151.8	2.685	0.529	0.283	0.60	0.588	123.69	1.36	17.38	0.156	0.60	1.29
2000.0	0.009	0.031	149.3	2.690	0.534	0.317	0.62	0.628	125.86	1.87	21.14	0.156	0.55	1.29
2000.0	0.011	0.039	144.3	2.667	0.510	0.367	0.62	0.689	128.15	2.62	26.32	0.155	0.51	1.31
2000.0	0.014	0.050	138.6	2.622	0.466	0.411	0.62	0.744	130.44	3.29	33.51	0.152	0.45	1.22
2000.0	0.018	0.060	134.1	2.609	0.453	0.467	0.65	0.792	132.74	4.14	40.29	0.151	0.43	1.21
2000.0	0.023	0.073	129.7	2.586	0.430	0.518	0.67	0.832	135.02	4.91	49.01	0.150	0.39	1.15
2000.0	0.029	0.087	128.6	2.601	0.445	0.558	0.71	0.850	137.15	5.51	58.24	0.151	0.35	1.06
2000.0	0.045	0.118	118.4	2.555	0.398	0.737	0.83	0.928	141.93	8.23	78.57	0.148	0.34	1.11
2000.0	0.072	0.153	111.3	2.526	0.370	0.950	1.02	0.964	146.50	11.44	102.39	0.147	0.34	1.15
2000.0	0.115	0.200	106.0	2.498	0.342	1.192	1.24	0.968	150.58	15.11	133.44	0.145	0.3[illegible]	1.15
2000.0	0.182	0.255	102.3	2.485	0.328	1.508	1.54	0.942	154.13	19.88	169.93	0.144	0.32	1.17
2000.0	0.290	0.325	98.8	2.450	0.293	1.899	1.92	0.894	157.55	25.79	216.41	0.142	0.32	1.17
2000.0	0.459	0.414	96.5	2.426	0.270	2.376	2.39	0.828	160.99	33.00	275.60	0.141	0.31	1.17
2000.0	0.728	0.527	95.4	2.436	0.280	2.963	2.97	0.750	164.48	41.88	350.98	0.141	0.31	1.16
2000.0	1.052	0.[illegible]34	94.6	2.443	0.286	3.566	3.57	0.681	167.31	51.00	421.97	0.142	0.31	1.17

RESONATOR CONFIGURATION NO. 5

DEN	SONIC	VIS	CF	SIG	XL	T	D
0.0750	1129.0	0.12200E-04	0.850	0.0565	0.500	0.090	0.047

FREQ	PA1	PA2	PHASE	INERT	REACT	RESIS	IMPED	ABSOR	SPL	DNLD	UORF	LEFF	K2RES	DNLDK
2100.0	0.029	0.099	105.3	2.211	0.158	0.577	0.59	0.919	137.82	6.00	66.34	0.128	0.40	1.03
2100.0	0.045	0.125	99.1	2.172	0.119	0.744	0.75	0.974	142.70	8.58	83.52	0.126	0.41	1.12
2100.0	0.072	0.161	97.0	2.166	0.113	0.920	0.92	0.994	147.39	11.30	107.60	0.125	0.39	1.11
2100.0	0.115	0.212	95.0	2.150	0.097	1.111	1.11	0.995	151.41	14.24	141.84	0.124	0.36	1.04
2100.0	0.182	0.261	92.2	2.108	0.055	1.436	1.43	0.967	154.55	19.26	174.51	0.122	0.37	1.13
2100.0	0.290	0.325	90.4	2.066	0.012	1.830	1.83	0.913	157.76	25.34	217.18	0.119	0.38	1.18
2100.0	0.459	0.404	89.0	2.012	-0.040	2.330	2.33	0.840	161.07	33.07	270.28	0.116	0.39	1.23
2100.0	0.728	0.527	88.2	1.964	-0.089	2.833	2.83	0.770	164.60	40.84	352.22	0.114	0.37	1.15
2100.0	0.917	0.552	87.5	1.904	-0.148	3.404	3.40	0.701	166.21	49.66	368.82	0.110	0.42	1.34

RESONATOR CONFIGURATION NO. 6

DEN	SONIC	VIS	CF	SIG	XL	T	D
0.0750	1129.0	0.12000E-04	0.672	0.0695	0.500	0.100	0.052

FREQ	PA1	PA2	PHASE	INERT	REACT	RESIS	IMPED	ABSOR	SPL	DNLD	UORF	LEFF	K2RES	DNLDK
2100.0	0.029	0.097	105.9	2.221	0.167	0.589	0.61	0.923	137.87	8.38	52.70	0.158	0.39	1.72
2100.0	0.045	0.128	101.1	2.195	0.141	0.723	0.73	0.967	142.56	10.95	69.48	0.156	0.36	1.66
2100.0	0.072	0.166	98.2	2.181	0.127	0.887	0.89	0.991	147.25	14.09	90.54	0.155	0.34	1.61
2100.0	0.115	0.212	96.3	2.175	0.122	1.108	1.11	0.993	151.35	18.35	115.31	0.155	0.34	1.62
2100.0	0.182	0.270	94.2	2.155	0.101	1.384	1.38	0.972	154.66	23.64	146.85	0.153	0.33	1.62
2100.0	0.235	0.300	92.9	2.135	0.081	1.610	1.61	0.944	156.36	27.97	162.88	0.152	0.35	1.72
2100.0	0.290	0.340	91.5	2.099	0.045	1.747	1.74	0.925	157.90	30.59	184.87	0.149	0.33	1.65
2100.0	0.365	0.377	90.1	2.057	0.003	1.983	1.98	0.891	159.52	35.13	205.06	0.146	0.34	1.70
2100.0	0.459	0.428	89.5	2.034	-0.019	2.200	2.20	0.859	161.23	39.29	232.74	0.145	0.33	1.67
2100.0	0.578	0.492	89.5	2.032	-0.021	2.412	2.41	0.828	162.99	43.36	267.22	0.145	0.31	1.60
2100.0	0.817	0.565	88.6	1.981	-0.072	2.967	2.96	0.753	165.50	54.00	306.82	0.141	0.34	1.73

RESONATOR CONFIGURATION NO. 7

DEN	SONIC	VIS	CF	SIG	XL	T	D
0.0750	1129.0	0.12200E-04	0.684	0.0800	0.500	0.100	0.056

FREQ	PA1	PA2	PHASE	INERT	REACT	RESIS	IMPED	ABSOR	SPL	DNLD	UORF	LEFF	K2RES	DNLDK
2200.0	0.002	0.015	147.0	2.262	0.302	0.196	0.36	0.516	115.41	1.42	7.78	0.177	1.06	3.11
2200.0	0.003	0.018	146.0	2.273	0.313	0.211	0.37	0.539	117.50	1.74	9.35	0.178	0.95	2.93
2200.0	0.004	0.023	144.8	2.272	0.312	0.220	0.38	0.555	119.56	1.93	11.64	0.178	0.79	2.52
2200.0	0.005	0.029	142.9	2.268	0.308	0.233	0.38	0.577	121.64	2.21	14.48	0.177	0.68	2.21
2200.0	0.007	0.035	140.0	2.266	0.306	0.257	0.40	0.614	123.80	2.72	17.61	0.177	0.61	2.11
2200.0	0.009	0.044	134.5	2.240	0.280	0.285	0.40	0.659	126.00	3.33	22.18	0.175	0.54	1.95
2200.0	0.011	0.053	127.9	2.220	0.260	0.334	0.42	0.723	128.33	4.38	26.36	0.174	0.53	2.04
2200.0	0.014	0.065	123.1	2.197	0.236	0.363	0.43	0.759	130.53	5.00	32.43	0.172	0.47	1.84
2200.0	0.018	0.075	120.0	2.198	0.237	0.411	0.47	0.803	132.81	6.04	37.23	0.172	0.46	1.89
2200.0	0.023	0.091	116.7	2.181	0.221	0.439	0.49	0.829	134.99	6.64	45.28	0.171	0.4.	1.68
2200.0	0.029	0.106	112.8	2.167	0.206	0.492	0.53	0.867	137.30	7.75	52.59	0.169	0.39	1.66
2200.0	0.045	0.143	106.5	2.138	0.178	0.601	0.62	0.926	141.91	10.10	70.95	0.167	0.35	1.56
2200.0	0.072	0.180	102.5	2.131	0.170	0.770	0.78	0.974	146.70	13.73	89.32	0.167	0.36	1.64
2200.0	0.115	0.233	101.2	2.148	0.188	0.952	0.97	0.990	151.17	17.63	115.07	0.168	0.34	1.61
2200.0	0.182	0.300	98.4	2.134	0.174	1.182	1.19	0.986	155.05	22.54	148.24	0.167	0.33	1.58
2200.0	0.290	0.382	94.8	2.084	0.124	1.481	1.48	0.959	158.41	28.97	188.79	0.163	0.33	1.58
2200.0	0.459	0.475	92.3	2.036	0.075	1.892	1.89	0.904	161.65	37.76	234.95	0.159	0.34	1.64
2200.0	0.498	0.498	92.3	2.038	0.078	1.958	1.96	0.894	162.25	39.19	246.02	0.159	0.33	1.63

RESONATOR CONFIGURATION NO. 8

DEN	SONIC	VIS	CF	SIG	XL	T	D
0.0750	1129.0	0.12200E-04	0.607	0.0885	0.500	0.100	0.047

FREQ	PA1	PA2	PHASE	INERT	REACT	RESIS	IMPED	ABSOR	SPL	DNLD	UORF	LEFF	K2RES	DNLDK
2350.0	0.029	0.116	97.0	1.890	0.055	0.452	0.45	0.856	137.20	7.26	55.68	0.153	0.29	1.53
2350.0	0.045	0.157	94.8	1.879	0.044	0.533	0.53	0.906	141.68	9.12	75.12	0.152	0.26	1.39
2350.0	0.072	0.200	93.4	1.874	0.039	0.665	0.66	0.959	146.39	12.15	95.66	0.152	0.25	1.41
2350.0	0.115	0.258	92.4	1.869	0.034	0.818	0.81	0.989	151.16	15.68	123.24	0.151	0.24	1.39
2350.0	0.145	0.286	92.4	1.874	0.038	0.929	0.93	0.998	153.64	18.22	136.70	0.152	0.25	1.45
2350.0	0.182	0.317	92.5	1.881	0.046	1.054	1.05	0.998	155.70	21.10	151.62	0.152	0.25	1.50
2350.0	0.235	0.356	92.6	1.890	0.054	1.211	1.21	0.990	157.38	24.69	170.12	0.153	0.26	1.56
2350.0	0.290	0.400	92.2	1.886	0.051	1.328	1.32	0.979	158.84	27.39	190.88	0.153	0.25	1.53
2350.0	0.365	0.454	91.7	1.878	0.043	1.473	1.47	0.963	160.47	30.73	216.65	0.152	0.25	1.51
2350.0	0.459	0.521	90.3	1.843	0.008	1.616	1.61	0.944	162.16	34.01	248.75	0.149	0.23	1.45
2350.0	0.578	0.585	89.3	1.812	-0.022	1.813	1.81	0.916	163.79	38.54	279.10	0.147	0.23	1.46

RESONATOR CONFIGURATION NO. 9

DEN	SONIC	VIS	CF	SIG	XL	T	D
0.0750	1129.0	0.12200E-04	0.916	0.1080	0.500	0.100	0.052

FREQ	PA1	PA2	PHASE	INERT	REACT	RESIS	IMPED	ABSOR	SPL	DNLD	UORF	LEFF	K2RES	DNLDK
2450.0	0.002	0.023	136.2	1.916	0.156	0.149	0.21	0.445	115.16	1.20	9.60	0.182	1.59	2.42
2450.0	0.003	0.030	134.6	1.910	0.150	0.152	0.21	0.451	117.18	1.27	12.22	0.181	1.27	1.96
2450.0	0.004	0.037	133.0	1.906	0.145	0.156	0.21	0.460	119.21	1.39	15.39	0.181	1.04	1.63
2450.0	0.005	0.047	130.8	1.901	0.141	0.163	0.21	0.476	121.27	1.59	19.15	0.180	0.87	1.42
2450.0	0.007	0.058	127.6	1.893	0.133	0.173	0.21	0.497	123.34	1.86	23.84	0.180	0.74	1.26
2450.0	0.009	0.071	123.1	1.884	0.123	0.189	0.22	0.530	125.46	2.31	28.99	0.179	0.67	1.20
2450.0	0.011	0.085	116.3	1.865	0.105	0.212	0.23	0.574	127.63	2.94	34.86	0.177	0.62	1.19
2450.0	0.014	0.105	107.8	1.834	0.074	0.231	0.24	0.608	129.77	3.45	42.89	0.174	0.55	1.09
2450.0	0.018	0.126	104.1	1.822	0.061	0.246	0.25	0.633	131.88	3.87	51.56	0.173	0.48	0.99
2450.0	0.023	0.147	101.5	1.815	0.054	0.270	0.27	0.668	134.05	4.52	59.89	0.172	0.46	0.97
2450.0	0.029	0.153	103.3	1.836	0.076	0.322	0.33	0.735	136.39	5.97	62.71	0.174	0.52	1.17
2450.0	0.045	0.207	97.9	1.813	0.053	0.385	0.38	0.802	140.80	7.71	84.60	0.172	0.46	1.08
2450.0	0.072	0.261	94.7	1.800	0.040	0.488	0.49	0.881	145.42	10.54	106.51	0.171	0.46	1.14
2450.0	0.115	0.336	92.6	1.787	0.027	0.602	0.60	0.938	150.07	13.69	137.21	0.169	0.44	1.12
2450.0	0.182	0.433	90.8	1.770	0.010	0.742	0.74	0.978	154.80	17.53	176.76	0.168	0.42	1.10
2450.0	0.290	0.540	89.0	1.743	-0.016	0.945	0.94	0.999	159.74	23.12	219.98	0.165	0.43	1.15

RESONATOR CONFIGURATION NO. 10

DEN	SONIC	VIS	CF	SIG	XL	T	D
0.0750	1129.0	0.12200E-04	0.831	0.1300	0.500	0.100	0.052

FREQ	PA1	PA2	PHASE	INERT	REACT	RESIS	IMPED	ABSOR	SPL	DNLD	UORF	LEFF	K2RES	DNLDK
2600.0	0.002	0.031	69.2	1.603	-0.054	0.144	0.15	0.440	115.14	1.76	11.16	0.172	1.31	2.68
2600.0	0.003	0.038	69.0	1.602	-0.056	0.146	0.15	0.444	117.16	1.81	13.88	0.172	1.06	2.19
2600.0	0.004	0.048	68.7	1.601	-0.056	0.145	0.15	0.443	119.15	1.80	17.48	0.172	0.84	1.74
2600.0	0.005	0.059	68.7	1.599	-0.058	0.151	0.16	0.454	121.19	1.96	21.26	0.172	0.71	1.51
2600.0	0.007	0.071	69.0	1.597	-0.060	0.158	0.16	0.470	123.25	2.20	25.56	0.172	0.62	1.36
2600.0	0.009	0.083	69.3	1.594	-0.064	0.170	0.18	0.495	125.33	2.58	30.03	0.171	0.57	1.29
2600.0	0.011	0.096	68.8	1.586	-0.072	0.185	0.19	0.526	127.45	3.09	34.48	0.171	0.54	1.29
2600.0	0.014	0.114	67.0	1.576	-0.082	0.194	0.21	0.542	129.51	3.37	40.99	0.170	0.48	1.18
2600.0	0.018	0.131	65.7	1.563	-0.095	0.211	0.23	0.578	131.68	3.81	47.86	0.168	0.43	1.13
2600.0	0.023	0.159	66.6	1.563	-0.095	0.220	0.23	0.587	133.69	4.20	57.23	0.168	0.38	0.98
2600.0	0.029	0.182	74.5	1.588	-0.070	0.253	0.26	0.643	135.93	5.27	65.71	0.171	0.39	1.03
2600.0	0.045	0.238	73.2	1.566	-0.092	0.306	0.31	0.714	140.27	6.98	85.64	0.168	0.36	1.01
2600.0	0.059	0.280	72.3	1.552	-0.106	0.333	0.35	0.745	142.65	7.89	100.61	0.167	0.33	0.95
2600.0	0.072	0.310	71.9	1.537	-0.120	0.369	0.38	0.782	144.67	9.04	111.60	0.165	0.33	0.97
2600.0	0.092	0.356	71.7	1.523	-0.135	0.409	0.43	0.816	147.00	10.33	128.13	0.164	0.32	0.96
2600.0	0.115	0.395	71.9	1.508	-0.150	0.459	0.48	0.854	149.19	11.96	142.12	0.162	0.32	0.99
2600.0	0.145	0.454	72.4	1.498	-0.160	0.505	0.53	0.882	151.43	13.45	163.18	0.161	0.31	0.96
2600.0	0.182	0.527	73.0	1.490	-0.168	0.549	0.57	0.905	153.66	14.88	189.53	0.160	0.29	0.91
2600.0	0.235	0.598	72.7	1.464	-0.194	0.623	0.65	0.932	156.19	17.25	215.11	0.157	0.29	0.92
2600.0	0.290	0.679	72.9	1.450	-0.208	0.676	0.70	0.948	158.21	18.97	244.16	0.156	0.28	0.88
2600.0	0.365	0.771	72.7	1.425	-0.233	0.749	0.78	0.962	160.45	21.33	277.12	0.153	0.27	0.87

RESONATOR CONFIGURATION NO. 11

DEN	SONIC	VIS	CF	SIG	XL	T	D
0.0750	1129.0	0.12200E-04	0.676	0.0540	0.500	0.050	0.052

FREQ	PA1	PA2	PHASE	INERT	REACT	RESIS	IMPED	ABSOR	SPL	DNLD	UORF	LEFF	K2RES	DNLDK
2300.0	0.030	0.089	106.8	2.056	0.181	0.601	0.62	0.926	138.21	6.51	68.54	0.104	0.24	1.12
2300.0	0.047	0.108	99.5	2.010	0.135	0.807	0.81	0.983	143.23	9.42	83.36	0.101	0.26	1.27
2300.0	0.075	0.138	95.5	1.972	0.097	1.013	1.01	0.997	147.88	12.33	106.16	0.099	0.26	1.28
2300.0	0.094	0.150	94.2	1.961	0.086	1.179	1.18	0.991	149.53	14.67	115.07	0.099	0.28	1.39
2300.0	0.119	0.168	93.3	1.951	0.076	1.325	1.32	0.979	151.13	16.72	129.11	0.098	0.28	1.40
2300.0	0.150	0.187	92.6	1.943	0.068	1.505	1.50	0.958	152.69	19.25	143.21	0.098	0.29	1.44
2300.0	0.189	0.210	92.3	1.942	0.067	1.689	1.69	0.933	154.31	21.85	160.68	0.098	0.29	1.45
2300.0	0.238	0.235	92.2	1.947	0.072	1.895	1.89	0.903	155.95	24.76	180.29	0.098	0.29	1.45
2300.0	0.300	0.261	92.2	1.957	0.082	2.151	2.15	0.865	157.59	28.36	199.97	0.099	0.29	1.50
2300.0	0.377	0.290	92.7	1.990	0.115	2.440	2.44	0.823	159.25	32.45	221.81	0.100	0.30	1.54
2300.0	0.475	0.325	93.4	2.037	0.162	2.736	2.74	0.782	160.97	36.62	248.87	0.103	0.30	1.54
700.0	0.300	0.317	9.9	0.431	-5.729	0.999	5.81	0.108	154.52	23.59	74.02	0.071	0.37	1.87
1000.0	0.300	0.332	22.0	0.707	-3.604	1.456	3.88	0.306	155.03	29.18	110.72	0.082	0.36	1.83
1300.0	0.300	0.336	38.1	0.990	-2.326	1.824	2.95	0.544	155.82	32.25	145.61	0.088	0.34	1.75
1600.0	0.300	0.325	56.7	1.330	-1.365	2.078	2.48	0.733	156.68	33.17	173.13	0.096	0.33	1.68
1900.0	0.300	0.300	72.1	1.572	-0.697	2.159	2.26	0.825	157.26	31.54	189.67	0.096	0.31	1.59
2200.0	0.300	0.270	85.9	1.804	-0.155	2.168	2.17	0.861	157.55	29.30	198.00	0.095	0.30	1.52
2500.0	0.300	0.249	101.0	2.120	0.395	2.035	2.07	0.868	157.61	25.57	207.58	0.098	0.27	1.36
2800.0	0.300	0.219	111.4	2.307	0.766	1.956	2.10	0.838	157.36	23.04	204.83	0.095	0.26	1.32
3100.0	0.300	0.193	122.6	2.551	1.160	1.815	2.15	0.783	156.97	20.08	199.81	0.095	0.25	1.25
3300.0	0.300	0.168	129.8	2.794	1.487	1.785	2.32	0.716	156.59	19.05	185.25	0.098	0.26	1.32
3600.0	0.300	0.159	137.7	2.866	1.668	1.518	2.25	0.665	156.33	15.15	190.79	0.092	0.22	1.08
3950.0	0.300	0.140	146.7	3.042	1.950	1.281	2.33	0.568	155.91	11.82	184.43	0.089	0.19	0.93
4300.0	0.300	0.119	154.6	3.278	2.275	1.080	2.51	0.454	155.49	9.18	170.89	0.088	0.17	0.83
4700.0	0.300	0.102	162.0	3.463	2.545	0.827	2.67	0.336	155.12	6.19	160.82	0.085	0.14	0.65
5100.0	0.300	0.084	168.3	3.783	2.937	0.608	3.00	0.216	154.79	3.79	143.49	0.086	0.11	0.50

RESONATOR CONFIGURATION NO. 12

DEN	SONIC	VIS	CF	SIG	XL	T	D
0.0750	1129.0	0.12200E-04	0.710	0.0540	0.500	0.150	0.052

FREQ	PA1	PA2	PHASE	INERT	REACT	RESIS	IMPED	ABSOR	SPL	DNLD	UORF	LEFF	K2RES	DNLDK
1700.0	0.029	0.092	117.3	2.900	0.363	0.704	0.79	0.927	137.93	7.67	52.44	0.198	0.41	1.45
1700.0	0.045	0.122	110.2	2.865	0.329	0.894	0.95	0.967	142.56	10.78	69.13	0.196	0.39	1.49
1700.0	0.072	0.163	105.2	2.833	0.297	1.093	1.13	0.978	146.80	14.04	92.19	0.194	0.36	1.43
1700.0	0.091	0.185	103.2	2.823	0.286	1.223	1.25	0.973	148.69	16.18	104.64	0.193	0.35	1.44
1700.0	0.115	0.207	101.4	2.815	0.278	1.382	1.41	0.961	150.43	18.78	117.40	0.192	0.36	1.48
1700.0	0.145	0.235	99.8	2.802	0.266	1.541	1.56	0.944	152.15	21.39	133.26	0.192	0.35	1.47
1700.0	0.182	0.264	98.3	2.790	0.253	1.736	1.75	0.919	153.83	24.59	149.52	0.191	0.35	1.50
1700.0	0.230	0.303	96.9	2.767	0.231	1.910	1.92	0.896	155.57	27.44	171.67	0.189	0.34	1.45
1700.0	0.290	0.336	95.9	2.761	0.224	2.172	2.18	0.859	157.23	31.74	190.41	0.189	0.35	1.51
1700.0	0.365	0.377	94.9	2.746	0.209	2.441	2.45	0.821	158.93	36.15	213.65	0.188	0.35	1.52
1700.0	0.459	0.433	94.0	2.724	0.187	2.680	2.68	0.789	160.71	40.07	245.30	0.186	0.33	1.47
1700.0	0.728	0.552	92.6	2.688	0.151	3.340	3.34	0.708	164.24	50.90	312.39	0.184	0.32	1.45
700.0	0.290	0.356	12.8	1.277	-4.883	1.109	5.00	0.156	154.34	24.46	83.05	0.212	0.41	1.72
1000.0	0.290	0.404	32.6	1.710	-2.601	1.663	3.08	0.480	155.28	31.69	134.66	0.199	0.37	1.63
1200.0	0.290	0.414	51.5	2.028	-1.565	1.968	2.51	0.699	156.20	34.53	165.36	0.196	0.36	1.58
1400.0	0.290	0.395	70.4	2.323	-0.757	2.126	2.25	0.821	156.94	34.54	184.24	0.193	0.35	1.53
1600.0	0.290	0.356	88.0	2.618	-0.076	2.189	2.19	0.860	157.24	33.12	189.83	0.190	0.35	1.53
1700.0	0.290	0.598	91.9	2.577	0.040	1.227	1.22	0.989	159.14	16.24	338.61	0.176	0.11	0.44
1800.0	0.290	0.317	102.6	2.872	0.476	2.132	2.18	0.849	157.15	30.10	190.33	0.185	0.34	1.47
2000.0	0.290	0.276	118.2	3.223	1.066	1.989	2.25	0.789	156.72	26.20	184.19	0.187	0.33	1.40
2300.0	0.290	0.225	135.2	3.588	1.713	1.702	2.41	0.664	156.03	20.11	172.18	0.181	0.30	1.25
2600.0	0.290	0.168	148.5	4.088	2.429	1.488	2.84	0.492	155.32	15.85	145.95	0.183	0.31	1.25
2900.0	0.290	0.132	158.8	4.520	3.033	1.176	3.25	0.337	154.82	10.88	127.83	0.181	0.28	1.06
3200.0	0.290	0.110	164.9	4.769	3.422	0.923	3.54	0.239	154.55	7.15	117.32	0.173	0.24	0.83

RESONATOR CONFIGURATION NO. 13

DEN	SONIC	VIS	CF	SIG	XL	T	D
0.0750	1129.0	0.12200E-04	0.618	0.0540	0.500	0.200	0.052

FREQ	PA1	PA2	PHASE	INERT	REACT	RESIS	IMPED	ABSOR	SPL	DNLD	UORF	LEFF	K2RES	DNLDK
1400.0	0.029	0.092	108.9	3.392	0.311	0.911	0.96	0.971	138.65	11.61	43.19	0.282	0.49	2.32
1400.0	0.045	0.120	102.1	3.325	0.245	1.145	1.17	0.982	142.92	15.84	56.28	0.276	0.47	2.38
1400.0	0.072	0.159	98.0	3.276	0.195	1.394	1.40	0.966	146.53	20.35	74.19	0.272	0.46	2.29
1400.0	0.091	0.182	96.3	3.249	0.169	1.534	1.54	0.951	148.26	22.88	85.18	0.270	0.41	2.23
1400.0	0.115	0.202	95.0	3.233	0.152	1.745	1.75	0.923	149.87	26.70	94.48	0.269	0.43	2.33
1400.0	0.145	0.230	93.9	3.212	0.132	1.939	1.94	0.896	151.57	30.19	107.24	0.267	0.42	2.31
1400.0	0.182	0.258	92.8	3.196	0.106	2.178	2.18	0.861	153.25	34.51	120.33	0.265	0.42	2.35
1400.0	0.230	0.290	92.1	3.169	0.089	2.445	2.44	0.823	154.95	39.34	135.01	0.263	0.42	2.38
1400.0	0.290	0.329	91.6	3.156	0.075	2.712	2.71	0.786	156.70	44.18	153.24	0.262	0.41	2.35
1400.0	0.365	0.373	91.0	3.132	0.052	3.009	3.01	0.748	158.47	49.54	173.93	0.260	0.40	2.31
1400.0	0.459	0.424	90.4	3.103	0.023	3.338	3.33	0.709	160.25	55.49	197.41	0.258	0.39	2.28
1400.0	0.578	0.476	89.9	3.073	-0.006	3.746	3.74	0.665	162.03	62.85	221.50	0.255	0.39	2.29
1400.0	0.728	0.533	89.9	3.072	-0.007	4.203	4.20	0.620	163.83	71.11	248.53	0.255	0.39	2.31
1400.0	0.917	0.598	90.1	3.088	0.008	4.716	4.71	0.577	165.64	80.38	278.85	0.257	0.39	2.32
1400.0	1.154	0.672	90.4	3.117	0.036	5.291	5.29	0.534	167.48	90.78	312.88	0.259	0.39	2.33
1400.0	1.470	0.762	92.0	3.287	0.207	5.933	5.93	0.493	169.43	102.38	355.12	0.273	0.38	2.32
700.0	0.290	0.365	18.0	1.506	-4.654	1.512	4.89	0.216	154.49	33.80	84.98	0.250	0.41	2.30
800.0	0.290	0.382	26.3	1.724	-3.665	1.811	4.08	0.339	154.83	38.46	101.70	0.251	0.41	2.33
900.0	0.290	0.395	36.5	1.968	-2.822	2.088	3.51	0.477	155.27	42.23	118.44	0.254	0.41	2.33
1000.0	0.290	0.404	47.2	2.214	-2.098	2.266	3.08	0.601	155.74	43.60	134.66	0.257	0.39	2.23
1100.0	0.290	0.404	58.4	2.449	-1.471	2.391	2.80	0.699	156.20	43.90	148.13	0.259	0.37	2.14
1200.0	0.290	0.391	71.4	2.743	-0.849	2.524	2.66	0.768	156.58	44.44	156.11	0.266	0.37	2.14
1300.0	0.290	0.365	80.7	2.891	-0.425	2.600	2.63	0.791	156.73	43.92	157.83	0.259	0.38	2.18
1400.0	0.290	0.344	90.4	3.098	0.018	2.591	2.59	0.803	156.81	41.99	160.46	0.257	0.37	2.13
1500.0	0.290	0.317	102.4	3.438	0.563	2.560	2.62	0.788	156.71	39.86	158.61	0.267	0.37	2.12
1700.0	0.290	0.264	118.5	3.863	1.327	2.444	2.78	0.717	156.29	35.24	149.52	0.264	0.38	2.12
1900.0	0.290	0.225	132.1	4.230	1.960	2.169	2.92	0.624	155.84	28.80	142.23	0.259	0.35	1.94
2100.0	0.290	0.185	145.5	4.705	2.651	1.822	3.21	0.486	155.30	22.04	129.26	0.261	0.32	1.74
2300.0	0.290	0.145	151.8	5.172	3.297	1.767	3.74	0.381	154.96	20.08	111.16	0.261	0.37	1.93
2600.0	0.290	0.112	160.3	5.672	4.013	1.437	4.26	0.260	154.61	14.21	97.55	0.254	0.34	1.69

RESONATOR CONFIGURATION NO. 14

DEN	SONIC	VIS	CF	SIG	XL	T	D
0.0750	1129.0	0.12200E-04	0.686	0.0540	0.500	0.250	0.052

FREQ	PA1	PA2	PHASE	INERT	REACT	RESIS	IMPED	ABSOR	SPL	DNLD	UORF	LEFF	K2RES	DNLDK
1300.0	0.029	0.106	109.1	3.612	0.295	0.853	0.90	0.969	138.59	10.19	46.04	0.323	0.53	1.86
1300.0	0.045	0.143	103.8	3.570	0.253	1.030	1.06	0.984	142.98	13.51	62.11	0.319	0.47	1.79
1300.0	0.072	0.187	99.7	3.534	0.217	1.272	1.29	0.976	146.76	18.05	80.94	0.316	0.45	1.80
1300.0	0.091	0.214	98.1	3.516	0.199	1.400	1.41	0.965	148.51	20.46	92.93	0.315	0.43	1.77
1300.0	0.115	0.241	96.5	3.497	0.179	1.577	1.58	0.945	150.17	23.77	104.27	0.313	0.43	1.82
1300.0	0.145	0.273	95.0	3.470	0.153	1.754	1.76	0.922	151.86	27.09	118.35	0.311	0.42	1.82
1300.0	0.182	0.307	93.7	3.444	0.127	1.971	1.97	0.891	153.52	31.17	132.80	0.308	0.42	1.86
1300.0	0.230	0.352	92.6	3.415	0.098	2.164	2.16	0.863	155.27	34.78	152.47	0.306	0.40	1.80
1300.0	0.290	0.395	91.7	3.389	0.072	2.429	2.43	0.825	156.97	39.76	171.08	0.303	0.40	1.83
1300.0	0.365	0.444	90.9	3.360	0.042	2.727	2.72	0.785	158.69	45.34	191.95	0.301	0.40	1.85
1300.0	0.459	0.509	90.0	3.317	-0.000	2.990	2.99	0.751	160.48	50.28	220.39	0.297	0.38	1.78
1300.0	0.578	0.558	89.3	3.275	-0.041	3.433	3.43	0.698	162.19	58.58	241.65	0.293	0.40	1.89
1300.0	0.728	0.641	88.4	3.212	-0.105	3.763	3.76	0.663	164.02	64.77	277.45	0.287	0.38	1.82
1300.0	0.917	0.720	87.8	3.155	-0.162	4.221	4.22	0.618	165.82	73.36	311.31	0.282	0.38	1.83
1300.0	1.154	0.798	87.6	3.116	-0.200	4.790	4.79	0.570	167.62	84.03	345.30	0.279	0.3[illegible]	1.89
1300.0	1.453	0.906	89.6	3.280	-0.037	5.318	5.31	0.532	169.47	93.93	391.92	0.293	0.38	1.86
1300.0	1.788	1.141	92.0	3.498	0.181	5.194	5.19	0.541	171.30	91.60	493.40	0.313	0.30	1.44
700.0	0.290	0.395	17.6	1.857	-4.303	1.365	4.51	0.226	154.51	29.08	92.12	0.309	0.42	1.84
800.0	0.290	0.419	26.7	2.058	-3.331	1.675	3.72	0.367	154.91	34.25	111.51	0.299	0.43	1.90
900.0	0.290	0.449	38.7	2.377	-2.414	1.934	3.09	0.535	155.48	37.79	134.43	0.307	0.41	1.84
1000.0	0.290	0.464	51.4	2.634	-1.678	2.102	2.68	0.675	156.08	39.14	154.61	0.306	0.39	1.74
1100.0	0.290	0.464	65.0	2.886	-1.033	2.216	2.44	0.776	156.63	39.37	170.07	0.305	0.37	1.67
1200.0	0.290	0.433	79.7	3.164	-0.429	2.363	2.40	0.822	156.94	40.32	173.15	0.307	0.39	1.76
1300.0	0.290	0.400	90.7	3.346	0.029	2.402	2.40	0.829	157.00	39.25	173.06	0.299	0.39	1.78
1400.0	0.290	0.365	103.6	3.655	0.575	2.378	2.44	0.810	156.85	37.17	169.97	0.304	0.40	1.79
1500.0	0.290	0.325	115.6	3.982	1.107	2.310	2.56	0.758	156.52	34.53	162.31	0.309	0.40	1.80
1700.0	0.290	0.258	134.0	4.513	1.977	2.047	2.84	0.620	155.83	27.77	146.11	0.309	0.40	1.72
1900.0	0.290	0.205	145.7	4.918	2.648	1.806	3.20	0.485	155.30	22.21	129.72	0.301	0.39	1.66
2100.0	0.290	0.163	157.7	5.432	3.378	1.385	3.65	0.324	154.78	14.63	113.88	0.301	0.34	1.34

RESONATOR CONFIGURATION NO. 15

DEN	SONIC	VIS	CF	SIG	XL	T	D
0.0750	1129.0	0.12200E-04	0.831	0.1300	0.150	0.100	0.052

FREQ	PA1	PA2	PHASE	INERT	REACT	RESIS	IMPED	ABSOR	SPL	DNLD	UORF	LEFF	K2RES	DNLDK
1000.0	0.093	0.093	2.0	0.008	-14.366	0.501	14.37	0.009	144.20	23.26	3.88	0.002	13.07	42.04
2000.0	0.093	0.112	4.8	1.230	-5.957	0.500	5.97	0.053	144.29	15.54	9.35	0.172	5.42	16.85
3000.0	0.093	0.153	8.7	1.904	-2.887	0.441	2.92	0.169	144.57	10.39	19.14	0.178	2.33	6.94
4100.0	0.094	0.296	22.0	2.466	-1.039	0.420	1.12	0.542	145.81	7.91	50.42	0.168	0.84	2.41
4500.0	0.093	0.409	38.6	2.622	-0.571	0.456	0.73	0.745	146.65	8.31	76.39	0.163	0.60	1.74
4700.0	0.093	0.503	54.7	2.729	-0.329	0.464	0.56	0.824	147.16	8.27	98.15	0.162	0.47	1.37
4800.0	0.093	0.515	64.5	2.760	-0.234	0.491	0.54	0.862	147.46	8.79	102.58	0.161	0.48	1.40
4900.0	0.093	0.540	75.0	2.801	-0.131	0.492	0.50	0.877	147.59	8.69	109.65	0.160	0.45	1.31
5000.0	0.045	0.325	91.3	2.884	0.009	0.405	0.40	0.821	140.93	6.55	67.42	0.161	0.61	1.68
5150.0	0.047	0.321	114.5	2.962	0.171	0.375	0.41	0.781	140.97	5.72	68.64	0.161	0.55	1.49
5200.0	0.059	0.369	115.8	2.959	0.195	0.403	0.44	0.803	143.11	6.31	79.58	0.159	0.51	1.41
5500.0	0.081	0.344	143.3	3.110	0.496	0.370	0.61	0.697	145.19	5.32	78.55	0.158	0.47	1.27
5600.0	0.093	0.356	147.5	3.136	0.569	0.362	0.67	0.665	146.23	5.08	82.79	0.157	0.44	1.17
5700.0	0.093	0.303	155.2	3.229	0.707	0.326	0.77	0.578	145.85	4.22	71.73	0.158	0.46	1.17
5800.0	0.093	0.267	159.8	3.294	0.815	0.300	0.86	0.509	145.58	3.58	64.30	0.159	0.47	1.15
5000.0	0.023	0.225	101.0	2.933	0.058	0.298	0.30	0.707	134.54	4.05	46.64	0.164	0.64	1.63
5000.0	0.026	0.235	100.2	2.932	0.057	0.321	0.32	0.734	135.69	4.57	48.84	0.164	0.66	1.71
5000.0	0.030	0.258	98.9	2.926	0.051	0.329	0.33	0.744	136.74	4.77	53.55	0.164	0.62	1.62
5000.0	0.033	0.280	97.3	2.918	0.043	0.342	0.34	0.759	137.83	5.08	58.04	0.163	0.59	1.57
5000.0	0.037	0.296	95.7	2.911	0.036	0.364	0.36	0.782	138.97	5.58	61.48	0.163	0.60	1.61
5000.0	0.042	0.321	93.6	2.898	0.023	0.378	0.37	0.796	140.06	5.90	66.64	0.162	0.57	1.56
5000.0	0.047	0.336	92.0	2.889	0.014	0.405	0.40	0.821	141.23	6.55	69.79	0.162	0.58	1.63
5000.0	0.053	0.369	90.4	2.877	0.002	0.415	0.41	0.829	142.29	6.77	76.52	0.161	0.55	1.53
5000.0	0.055	0.386	90.1	2.875	0.000	0.410	0.41	0.825	142.56	6.66	80.13	0.161	0.51	1.44

RESONATOR CONFIGURATION NO. 16

DEN	SONIC	VIS	CF	SIG	XL	T	D
0.0750	1129.0	0.12200E-04	0.916	0.1080	0.150	0.100	0.052

FREQ	PA1	PA2	PHASE	INERT	REACT	RESIS	IMPED	ABSOR	SPL	DNLD	UORF	LEFF	K2RES	DNLDK
1000.0	0.093	0.094	2.2	0.175	-14.199	0.545	14.21	0.010	144.20	20.61	4.73	0.040	11.78	30.75
2000.0	0.094	0.116	6.3	1.380	-5.806	0.641	5.84	0.070	144.43	16.63	11.65	0.160	5.62	14.42
3000.0	0.093	0.174	10.9	2.264	-2.526	0.486	2.57	0.226	144.71	9.19	26.14	0.175	1.90	4.55
3500.0	0.093	0.244	18.8	2.611	-1.495	0.509	1.57	0.451	145.38	8.81	42.60	0.173	1.22	2.90
3900.0	0.094	0.348	34.2	2.855	-0.830	0.564	1.00	0.719	146.60	9.40	67.82	0.170	0.85	2.04
4100.0	0.093	0.404	48.7	2.969	-0.536	0.610	0.81	0.847	147.33	10.08	82.81	0.168	0.75	1.82
4200.0	0.093	0.433	58.1	3.031	-0.391	0.628	0.74	0.896	147.77	10.30	90.90	0.168	0.70	1.71
4300.0	0.081	0.409	69.5	3.109	-0.233	0.624	0.66	0.927	146.92	10.07	87.86	0.168	0.72	1.76
4400.0	0.057	0.336	81.6	3.185	-0.081	0.555	0.56	0.915	143.78	8.49	73.92	0.168	0.76	1.81
4500.0	0.064	0.356	95.5	3.249	0.055	0.571	0.57	0.924	144.79	8.71	80.08	0.168	0.73	1.73
4600.0	0.052	0.300	112.4	3.334	0.209	0.507	0.54	0.876	142.58	7.29	68.88	0.168	0.75	1.73
4800.0	0.093	0.373	128.4	3.462	0.467	0.589	0.75	0.859	147.43	8.68	89.45	0.168	0.67	1.59
5000.0	0.093	0.310	144.1	3.578	0.703	0.509	0.86	0.734	146.59	6.90	77.50	0.166	0.67	1.53
5200.0	0.093	0.235	157.6	3.781	1.017	0.419	1.10	0.550	145.74	5.01	61.14	0.169	0.70	1.51

RESONATOR CONFIGURATION NO. 17

DEN	SONIC	VIS	CF	SIG	XL	T	D
0.0750	1129.0	0.12200F-04	0.916	0.1080	0.200	0.100	0.052

FREQ	PA1	PA2	PHASE	INERT	REACT	RESIS	IMPED	ABSOR	SPL	DNLD	UORF	LEFF	K2RES	DNLDK
1000.0	0.093	0.100	1.8	0.724	-10.056	0.316	10.06	0.012	144.20	10.71	6.68	0.168	4.83	11.79
2000.0	0.093	0.129	4.2	1.495	-3.894	0.286	3.90	0.068	144.33	5.80	17.23	0.174	1.69	3.76
3000.0	0.093	0.238	14.9	2.226	-1.366	0.363	1.41	0.390	145.18	6.13	47.57	0.172	0.78	1.[illegible]
3800.0	0.093	0.464	71.1	2.651	-0.185	0.541	0.57	0.898	147.79	9.06	117.50	0.162	0.47	1.12
3900.0	0.074	0.419	85.7	2.727	-0.036	0.490	0.49	0.882	145.63	7.78	108.73	0.162	0.46	1.07
4000.0	0.059	0.340	103.9	2.809	0.113	0.459	0.47	0.857	143.52	6.99	90.64	0.163	0.51	1.18
4100.0	0.093	0.419	112.8	2.857	0.228	0.542	0.58	0.892	147.73	8.64	114.30	0.162	0.48	1.15
4200.0	0.093	0.400	125.3	2.914	0.347	0.491	0.60	0.837	147.26	7.41	111.82	0.161	0.44	1.03
4300.0	0.093	0.356	137.5	2.993	0.486	0.445	0.65	0.766	146.77	6.34	102.03	0.162	0.44	1.00
3850.0	0.029	0.238	79.6	2.738	-0.061	0.334	0.34	0.750	136.47	4.44	61.05	0.165	0.56	1.17
3850.0	0.032	0.255	79.1	2.732	-0.067	0.350	0.35	0.766	137.57	4.77	65.42	0.165	0.54	1.16
3850.0	0.036	0.276	78.9	2.729	-0.071	0.362	0.36	0.778	138.65	5.04	70.91	0.165	0.52	1.12
3850.0	0.040	0.293	78.9	2.725	-0.075	0.383	0.39	0.799	139.78	5.51	75.11	0.164	0.52	1.14
3850.0	0.045	0.317	78.6	2.720	-0.080	0.396	0.40	0.810	140.86	5.80	81.42	0.164	0.49	1.10
3850.0	0.051	0.336	78.3	2.713	-0.086	0.419	0.42	0.829	142.00	6.30	86.24	0.164	0.49	1.12
3850.0	0.057	0.360	77.9	2.706	-0.094	0.438	0.44	0.844	143.11	6.72	92.41	0.163	0.48	1.10
3850.0	0.064	0.377	77.9	2.699	-0.100	0.470	0.48	0.866	144.29	7.41	96.77	0.163	0.49	1.15
3850.0	0.072	0.409	77.4	2.691	-0.108	0.485	0.49	0.875	145.37	7.76	104.89	0.162	0.47	1.10
3850.0	0.081	0.433	77.2	2.683	-0.116	0.514	0.52	0.891	146.53	8.38	111.10	0.162	0.47	1.11
3850.0	0.091	0.459	77.2	2.676	-0.123	0.544	0.55	0.907	147.69	9.05	117.69	0.161	0.47	1.12
3850.0	0.102	0.486	77.2	2.669	-0.131	0.577	0.59	0.921	148.85	9.76	124.66	0.161	0.47	1.14
3850.0	0.115	0.527	77.3	2.665	-0.134	0.597	0.61	0.929	149.96	10.21	135.12	0.161	0.45	1.09
3850.0	0.129	0.552	77.5	2.658	-0.142	0.640	0.65	0.945	151.17	11.16	141.49	0.160	0.46	1.13

RESONATOR CONFIGURATION NO.18

DEN	SONIC	VIS	CF	SIG	XL	T	D
0.0750	1129.0	0.12200E-04	0.686	0.0540	0.500	0.100	0.037

FREQ	PA1	PA2	PHASE	INERT	REACT	RESIS	IMPED	ABSOR	SPL	DNLD	UORF	LEFF	K2RES	DNLDK
2000.0	0.029	0.091	96.7	2.235	0.079	0.677	0.68	0.960	138.43	6.53	60.99	0.130	0.31	1.17
2000.0	0.045	0.116	96.9	2.258	0.101	0.842	0.84	0.989	143.15	9.03	77.67	0.131	0.31	1.23
2000.0	0.072	0.157	96.1	2.262	0.105	0.991	0.99	0.997	147.54	11.28	104.78	0.131	0.27	1.11
2000.0	0.115	0.200	94.5	2.253	0.097	1.236	1.24	0.986	151.05	15.00	133.44	0.131	0.26	1.14
2000.0	0.182	0.258	91.5	2.196	0.039	1.525	1.52	0.956	154.35	19.37	171.90	0.127	0.25	1.12
2000.0	0.290	0.317	90.2	2.163	0.006	1.966	1.96	0.893	157.55	26.03	211.48	0.125	0.26	1.21
2000.0	0.459	0.404	89.8	2.147	-0.008	2.447	2.44	0.823	160.95	33.30	269.33	0.125	0.26	1.21
2000.0	0.728	0.475	89.8	2.144	-0.011	3.301	3.30	0.713	164.27	46.21	316.43	0.124	0.29	1.42
2000.0	1.102	0.620	90.9	2.216	0.060	3.833	3.83	0.656	167.59	54.26	412.36	0.129	0.26	1.27

RESONATOR CONFIGURATION NO.19

DEN	SONIC	VIS	CF	SIG	XL	T	D
0.0750	1129.0	0.12200E-04	0.920	0.0540	0.500	0.100	0.094

FREQ	PA1	PA2	PHASE	INERT	REACT	RESIS	IMPED	ABSOR	SPL	DNLD	UORF	LEFF	K2RES	DNLDK
1800.0	0.029	0.116	102.1	2.520	0.124	0.581	0.59	0.924	137.88	7.20	69.90	0.163	0.42	1.06
1800.0	0.045	0.159	95.5	2.462	0.066	0.687	0.69	0.964	142.49	8.89	95.39	0.159	0.37	0.93
1800.0	0.072	0.196	91.9	2.425	0.029	0.889	0.89	0.996	147.49	12.11	117.36	0.156	0.39	1.01
1800.0	0.115	0.244	90.3	2.401	0.005	1.133	1.13	0.996	151.47	16.00	146.05	0.155	0.40	1.05
1800.0	0.182	0.303	89.7	2.388	-0.007	1.443	1.44	0.967	154.55	20.94	181.77	0.154	0.40	1.09
1800.0	0.290	0.373	89.3	2.373	-0.022	1.859	1.85	0.909	157.71	27.57	223.62	0.153	0.42	1.15
1800.0	0.459	0.475	90.4	2.411	0.016	2.314	2.31	0.842	161.09	34.82	284.79	0.156	0.41	1.13
1800.0	0.728	0.585	91.5	2.473	0.078	2.980	2.98	0.752	164.49	45.44	350.37	0.160	0.43	1.19
1800.0	1.040	0.672	93.9	2.648	0.252	3.702	3.71	0.667	167.14	56.94	402.28	0.171	0.47	1.30

II. DATA AT RESONANCE WITH INCREASING SOUND PRESSURE

DATA AT RESONANCE CONFIGURATION NO. 20

DEN	SONIC	VIS	CF	SIG	XL	T	D
0.0750	1130.0	0.12200F-04	0.780	0.0540	0.400	0.100	0.052

FREQ	PA1	PA2	PHASE	INERT	REACT	RESIS	IMPED	ABSOR	SPL	DNLD	UORF	LEFF	K2RES	DNLDK
2024.0	0.029	0.112	90.0	2.665	-0.000	0.685	0.68	0.965	138.51	7.38	60.64	0.153	0.41	1.32
2043.0	0.051	0.150	90.0	2.640	-0.000	0.905	0.90	0.997	144.57	10.63	81.62	0.150	0.41	1.37
2074.0	0.091	0.200	90.0	2.601	-0.000	1.189	1.18	0.992	149.28	14.74	110.50	0.146	0.39	1.38
2111.0	0.163	0.147	90.0	2.555	-0.000	2.834	2.83	0.771	151.60	38.83	82.42	0.141	1.27	4.73
2124.0	0.290	0.348	90.0	2.540	-0.000	2.112	2.11	0.872	157.34	28.10	196.66	0.139	0.39	1.45
2109.0	0.515	0.470	90.0	2.558	-0.000	2.805	2.80	0.774	161.62	38.41	263.42	0.141	0.39	1.46
2084.0	0.917	0.612	90.0	2.588	-0.000	3.873	3.87	0.652	165.97	54.50	339.21	0.144	0.42	1.59
2039.0	1.154	0.720	90.0	2.646	-0.000	4.242	4.24	0.617	167.81	60.66	389.93	0.151	0.40	1.52

DATA AT RESUNANCE CONFIGURATION NO. 21

DEN	SONIC	VIS	CF	SIG	XL	T	D
0.0750	1130.0	0.12200E-04	0.780	0.0540	0.600	0.100	0.052

FREQ	PA1	PA2	PHASE	INERT	REACT	RESIS	IMPED	ABSOR	SPL	DNLD	UORF	LEFF	K2RES	DNLDK
1675.0	0.029	0.093	90.0	2.147	-0.000	0.663	0.66	0.959	138.40	8.05	62.61	0.149	0.39	1.26
1683.0	0.051	0.129	90.0	2.137	-0.000	0.850	0.85	0.993	144.32	11.11	86.84	0.148	0.36	1.21
1685.0	0.091	0.168	90.0	2.134	-0.000	1.159	1.15	0.994	149.38	16.19	113.31	0.147	0.37	1.32
1688.0	0.163	0.230	90.0	2.130	-0.000	1.508	1.50	0.958	153.39	21.92	154.89	0.147	0.36	1.29
1692.0	0.290	0.296	90.0	2.125	-0.000	2.077	2.07	0.877	157.39	31.25	200.01	0.146	0.38	1.41
1688.0	0.515	0.409	90.0	2.130	-0.000	2.682	2.68	0.791	161.73	41.26	275.44	0.147	0.36	1.34
1678.0	0.917	0.527	90.0	2.143	-0.000	3.725	3.72	0.667	166.04	58.62	352.74	0.148	0.39	1.47
1620.0	1.154	0.598	90.0	2.220	-0.000	4.279	4.27	0.614	167.80	69.04	386.53	0.159	0.41	1.55

DATA AT RESONANCE CONFIGURATION NO. 22

DEN	SONIC	VIS	CF	SIG	XL	T	D
0.0750	1130.0	0.12200F-04	0.690	0.0800	0.400	0.100	0.056

FREQ	PA1	PA2	PHASE	INERT	REACT	RESIS	IMPE	ABSOR	SPL	DNLD	UORF	LEFF	K2RES	DNLDK
2351.0	0.029	0.019	90.0	2.294	-0.000	0.556	0.55	0.918	137.82	8.77	50.36	0.168	0.47	2.00
2372.0	0.051	0.166	90.0	2.274	-0.000	0.702	0.70	0.969	143.60	11.73	70.95	0.165	0.42	1.86
2386.0	0.091	0.219	90.0	2.261	-0.000	0.942	0.94	0.999	149.74	16.63	94.09	0.163	0.43	1.95
2396.0	0.163	0.296	90.0	2.251	-0.000	1.237	1.23	0.988	154.12	22.65	127.45	0.162	0.41	1.93
2474.0	0.290	0.400	90.0	2.180	-0.000	1.579	1.57	0.949	158.23	29.17	177.53	0.152	0.38	1.80
2487.0	0.515	0.470	90.0	2.169	-0.000	2.378	2.37	0.833	162.02	45.20	209.67	0.150	0.48	2.34

DATA AT RESONANCE CONFIGURATION NO. 23

DEN	SONIC	VIS	CF	SIG	XL	T	D
0.0750	1130.0	0.12200E-04	0.690	0.0800	0.600	0.100	0.056

FREQ	PA1	PA2	PHASE	INERT	REACT	RESIS	IMPED	ABSOR	SPL	DNLD	UORF	LEFF	K2RES	DNLDK
1927.0	0.029	0.105	90.0	1.866	-0.000	0.514	0.51	0.897	137.58	8.99	54.55	0.167	0.40	1.71
1938.0	0.051	0.142	90.0	1.855	-0.000	0.673	0.67	0.962	143.45	12.61	74.01	0.165	0.39	1.72
1940.0	0.091	0.187	90.0	1.854	-0.000	0.908	0.90	0.997	149.59	17.95	97.67	0.165	0.40	1.82
1947.0	0.163	0.258	90.0	1.847	-0.000	1.165	1.16	0.994	154.35	23.79	135.31	0.163	0.37	1.72
1954.0	0.290	0.336	90.0	1.840	-0.000	1.584	1.58	0.948	158.22	33.29	176.96	0.162	0.38	1.82
1951.0	0.515	0.444	90.0	1.843	-0.000	2.141	2.14	0.868	162.30	45.99	232.93	0.163	0.39	1.89
1947.0	0.917	0.572	90.0	1.847	-0.000	2.961	2.96	0.754	166.50	64.75	299.45	0.163	0.42	2.06

III. DATA FOR EVALUATION OF NEW DESIGN THEORY (SEE APPENDIX D)

EXPERIMENTAL DATA FOR COMPARISON WITH DESIGN THEORY

DEN	SONIC	VIS	CF	SIG	XL	T	D
0.0750	1130.0	0.12200E-04	0.780	0.0540	0.415	0.100	0.052

FREQ	PA1	PA2	PHASE	INERT	REACT	RESIS	IMPED	ABSOR	SPL	DNLD	UORF	LEFF	K2RES	DNLDK
645.0	0.258	0.258	6.6	0.053	-8.009	0.926	8.06	0.054	153.10	21.77	45.93	0.009	0.74	2.68
835.0	0.258	0.270	9.4	0.360	-5.867	0.971	5.94	0.101	153.20	19.82	62.26	0.050	0.57	2.05
995.0	0.258	0.293	12.3	0.727	-4.499	0.980	4.60	0.162	153.35	18.12	80.42	0.085	0.45	1.59
1135.0	0.258	0.317	19.8	1.077	-3.504	1.261	3.72	0.290	153.69	22.41	99.44	0.110	0.47	1.69
1260.0	0.258	0.332	24.1	1.202	-2.924	1.308	3.20	0.376	153.94	22.01	115.59	0.111	0.42	1.50
1401.0	0.258	0.352	36.6	1.528	-2.183	1.621	2.72	0.557	154.56	26.40	136.14	0.127	0.44	1.60
1561.0	0.258	0.356	45.1	1.627	-1.703	1.709	2.41	0.667	155.04	26.36	153.45	0.121	0.41	1.50
1651.0	0.258	0.356	54.6	1.827	-1.321	1.859	2.28	0.749	155.47	28.05	162.29	0.129	0.42	1.54
1850.0	0.258	0.348	69.3	2.074	-0.736	1.949	2.08	0.843	156.10	27.74	177.72	0.130	0.40	1.48
2000.0	0.258	0.332	85.7	2.448	-0.151	2.012	2.01	0.884	156.46	27.53	183.48	0.142	0.40	1.48
2104.0	0.258	0.317	90.0	2.471	-0.000	2.009	2.00	0.887	156.48	26.71	184.33	0.136	0.40	1.46
2409.0	0.258	0.270	112.1	2.934	0.775	1.910	2.06	0.842	156.09	23.41	179.63	0.142	0.39	1.42
2561.0	0.258	0.255	122.5	3.134	1.103	1.732	2.05	0.797	155.77	20.24	180.29	0.142	0.35	1.27
2856.0	0.258	0.200	139.2	3.596	1.775	1.532	2.34	0.640	154.92	16.48	157.87	0.146	0.36	1.26
3165.0	0.258	0.159	150.5	3.962	2.319	1.312	2.66	0.489	154.31	12.86	138.97	0.145	0.35	1.19
3525.0	0.258	0.126	160.4	4.312	2.837	1.010	3.01	0.334	153.81	8.59	122.94	0.142	0.30	0.98
4795.0	0.258	0.059	171.3	5.710	4.626	0.707	4.67	0.116	153.24	3.99	79.13	0.138	0.33	0.93

IV. STATIC (NO FLOW SIMULATOR DATA)

RESONATOR CONFIGURATION NO. 1

DEN	SONIC	VIS	CF	SIG	XL	T	D
0.0750	1129.0	0.12200E-04	0.825	0.0140	0.200	0.100	0.052

FREQ	PA1	PA2	PHASE	INERT	REACT	RESIS	IMPED	ABSOR	SPL	DNLD	UORF	LEFF	K2RES	DNLDK
1572.0	0.016	0.058	92.0	6.924	0.066	1.909	1.91	0.901	132.63	5.49	47.21	0.133	0.43	1.16
1572.0	0.029	0.079	88.7	6.801	-0.056	2.489	2.49	0.817	136.91	8.05	64.42	0.130	0.41	1.18
1572.0	0.051	0.105	87.6	6.717	-0.140	3.356	3.35	0.706	141.24	11.87	84.92	0.129	0.42	1.28
1572.0	0.091	0.140	87.2	6.639	-0.218	4.473	4.47	0.596	145.72	16.80	113.24	0.127	0.42	1.32
1572.0	0.163	0.187	87.5	6.597	-0.260	5.967	5.97	0.491	150.32	23.39	151.02	0.126	0.42	1.36
1572.0	0.290	0.252	86.8	6.418	-0.439	7.862	7.87	0.399	155.01	31.74	203.72	0.123	0.41	1.35

RESONATOR CONFIGURATION NO. 2

DEN	SONIC	VIS	CF	SIG	XL	T	D
0.0750	1129.0	0.12200E-04	0.780	0.0320	0.500	0.100	0.052

FREQ	PA1	PA2	PHASE	INERT	REACT	RESIS	IMPED	ABSOR	SPL	DNLD	UORF	LEFF	K2RES	DNLDK
1572.0	0.029	0.071	93.0	2.801	0.058	1.116	1.11	0.996	139.48	8.33	62.79	0.123	0.39	1.25
1572.0	0.032	0.074	92.3	2.791	0.048	1.196	1.19	0.991	140.23	9.14	65.75	0.122	0.39	1.30
1572.0	0.036	0.078	91.9	2.785	0.042	1.267	1.26	0.985	141.01	9.86	69.65	0.122	0.40	1.31
1572.0	0.040	0.083	91.6	2.780	0.037	1.343	1.34	0.978	141.80	10.62	73.78	0.122	0.40	1.33
1572.0	0.045	0.089	91.4	2.777	0.034	1.406	1.40	0.971	142.63	11.26	79.05	0.121	0.39	1.31
1572.0	0.051	0.093	91.1	2.772	0.028	1.507	1.50	0.958	143.39	12.28	82.78	0.121	0.40	1.35
1572.0	0.057	0.100	90.9	2.768	0.024	1.578	1.57	0.949	144.24	12.99	88.70	0.121	0.39	1.33
1572.0	0.064	0.106	90.7	2.763	0.020	1.672	1.67	0.936	145.05	13.94	93.96	0.121	0.39	1.34
1572.0	0.072	0.114	90.5	2.758	0.015	1.750	1.75	0.925	145.90	14.73	100.68	0.121	0.38	1.32
1572.0	0.081	0.119	90.5	2.759	0.016	1.876	1.87	0.907	146.69	16.00	105.42	0.121	0.39	1.36
1572.0	0.091	0.131	90.3	2.753	0.010	1.919	1.91	0.900	147.62	16.44	115.59	0.120	0.36	1.27
1572.0	0.102	0.137	90.7	2.768	0.025	2.057	2.05	0.880	148.42	17.82	121.04	0.121	0.37	1.31
1572.0	0.115	0.147	90.8	2.773	0.030	2.153	2.15	0.866	149.29	18.80	129.70	0.121	0.36	1.28
1572.0	0.129	0.157	90.6	2.766	0.023	2.255	2.25	0.851	150.16	19.82	138.98	0.121	0.35	1.26
1572.0	0.145	0.164	90.3	2.755	0.012	2.416	2.41	0.828	150.98	21.45	145.52	0.121	0.36	1.30
1572.0	0.163	0.174	90.1	2.747	0.004	2.560	2.56	0.807	151.84	22.90	154.15	0.120	0.36	1.30
1572.0	0.182	0.187	90.0	2.743	-0.000	2.680	2.68	0.791	152.73	24.11	165.17	0.120	0.35	1.28
1572.0	0.205	0.207	90.2	2.752	0.009	2.711	2.71	0.787	153.70	24.43	183.21	0.120	0.32	1.17
1572.0	0.230	0.212	90.0	2.743	-0.000	2.973	2.97	0.753	154.49	27.07	187.47	0.120	0.34	1.26
1572.0	0.258	0.225	90.0	2.743	-0.000	3.149	3.14	0.731	155.37	28.84	198.58	0.120	0.34	1.26
1572.0	0.290	0.235	88.9	2.678	-0.064	3.374	3.37	0.705	156.23	31.11	207.94	0.117	0.35	1.30
1572.0	0.325	0.255	88.3	2.639	-0.103	3.492	3.49	0.691	157.16	32.30	225.39	0.115	0.34	1.24
1572.0	0.365	0.276	88.1	2.623	-0.119	3.614	3.61	0.678	158.09	33.53	244.31	0.115	0.32	1.19
1572.0	0.409	0.293	88.3	2.629	-0.113	3.828	3.83	0.656	158.99	35.70	258.79	0.115	0.32	1.19
1572.0	0.459	0.314	88.9	2.666	-0.077	4.010	4.01	0.638	159.91	37.53	277.30	0.117	0.31	1.17

RESONATOR CONFIGURATION NO.3

DEN	SONIC	VIS	CF	SIG	XL	T	D
0.0750	1129.0	0.12200E-04	0.831	0.0470	0.600	0.100	0.052

FREQ	PA1	PA2	PHASE	INERT	REACT	RESIS	IMPED	ABSOR	SPL	DNLD	UORF	LEFF	K2RES	DNLDK
1540.0	0.029	0.099	53.9	1.932	-0.401	0.550	0.68	0.858	137.22	5.32	70.18	0.127	0.28	0.75
1540.0	0.032	0.104	54.7	1.912	-0.421	0.595	0.72	0.874	138.36	5.99	73.49	0.125	0.29	0.79
1540.0	0.036	0.110	56.0	1.901	-0.432	0.640	0.77	0.890	139.51	6.67	77.84	0.125	0.30	0.82
1540.0	0.040	0.118	58.0	1.904	-0.428	0.686	0.80	0.906	140.68	7.36	83.41	0.125	0.30	0.83
1540.0	0.045	0.126	59.2	1.899	-0.433	0.727	0.84	0.917	141.80	7.98	89.38	0.125	0.29	0.84
1540.0	0.051	0.132	60.8	1.890	-0.442	0.792	0.90	0.929	142.95	8.95	93.59	0.124	0.31	0.88
1540.0	0.057	0.143	62.2	1.895	-0.438	0.831	0.93	0.937	144.06	9.53	101.45	0.124	0.30	0.86
1540.0	0.064	0.155	63.8	1.904	-0.429	0.872	0.97	0.945	145.17	10.15	109.96	0.125	0.29	0.84
1540.0	0.072	0.164	64.9	1.896	-0.437	0.933	1.03	0.950	146.25	11.06	116.48	0.124	0.29	0.86
1540.0	0.081	0.176	66.1	1.896	-0.437	0.986	1.07	0.953	147.30	11.86	124.81	0.124	0.28	0.86
1540.0	0.091	0.187	67.3	1.892	-0.441	1.054	1.14	0.955	148.33	12.87	132.20	0.124	0.29	0.87
1540.0	0.102	0.198	68.5	1.889	-0.443	1.126	1.21	0.954	149.32	13.95	140.04	0.124	0.29	0.89
1540.0	0.115	0.210	69.7	1.888	-0.444	1.202	1.28	0.952	150.29	15.10	148.33	0.124	0.29	0.90
1540.0	0.129	0.225	70.9	1.894	-0.439	1.268	1.34	0.950	151.25	16.09	158.94	0.124	0.29	0.89
1540.0	0.145	0.235	72.0	1.888	-0.444	1.368	1.43	0.942	152.13	17.58	166.43	0.124	0.30	0.93
1540.0	0.163	0.249	72.9	1.885	-0.448	1.456	1.52	0.934	153.01	18.90	176.30	0.124	0.30	0.94
1540.0	0.182	0.264	74.2	1.894	-0.439	1.553	1.61	0.925	153.90	20.35	186.74	0.124	0.30	0.95
1540.0	0.205	0.283	75.1	1.898	-0.434	1.633	1.69	0.917	154.80	21.56	200.10	0.125	0.29	0.94
1540.0	0.230	0.296	76.1	1.898	-0.435	1.758	1.81	0.901	155.63	23.42	209.53	0.124	0.30	0.97
1540.0	0.258	0.317	77.2	1.913	-0.420	1.849	1.89	0.891	156.52	24.79	224.51	0.125	0.30	0.96
1540.0	0.290	0.336	78.0	1.915	-0.417	1.965	2.00	0.876	157.38	26.53	237.82	0.126	0.30	0.96
1540.0	0.325	0.356	78.7	1.916	-0.417	2.087	2.12	0.860	158.24	28.35	251.91	0.126	0.30	0.97
1540.0	0.365	0.373	80.2	1.945	-0.388	2.247	2.28	0.840	159.08	30.75	263.78	0.128	0.31	1.00
1540.0	0.409	0.400	82.5	2.021	-0.311	2.367	2.38	0.827	159.98	32.55	282.65	0.133	0.30	0.99

RESONATOR CONFIGURATION NO.4

DEN	SONIC	VIS	CF	SIG	XL	T	D
0.0750	1129.0	0.12200E-04	0.784	0.0700	0.500	0.100	0.052

FREQ	PA1	PA2	PHASE	INERT	REACT	RESIS	IMPED	ABSOR	SPL	DNLD	UORF	LEFF	K2RES	DNLDK
1572.0	0.029	0.067	13.7	1.593	-1.150	0.280	1.18	0.378	134.95	3.28	27.10	0.153	0.50	1.33
1572.0	0.051	0.114	19.7	1.576	-1.167	0.417	1.23	0.495	140.33	6.33	46.02	0.151	0.44	1.34
1572.0	0.091	0.180	28.5	1.521	-1.222	0.663	1.39	0.622	145.84	11.77	72.94	0.146	0.44	1.47
1572.0	0.163	0.283	37.2	1.485	-1.257	0.954	1.57	0.706	151.24	18.21	114.28	0.142	0.40	1.42
1572.0	0.290	0.419	46.5	1.436	-1.306	1.376	1.89	0.748	156.47	27.57	169.04	0.138	0.39	1.42

RESONATOR CONFIGURATION NO.5

DEN	SONIC	VIS	CF	SIG	XL	T	D
0.0750	1129.0	0.12200E-04	0.780	0.0940	0.600	0.100	0.052

FREQ	PA1	PA2	PHASE	INERT	REACT	RESIS	IMPED	ABSOR	SPL	DNLD	UORF	LEFF	K2RES	DNLDK
1572.0	0.029	0.059	9.4	1.194	-1.091	0.180	1.10	0.279	134.66	2.47	21.58	0.154	0.54	1.36
1572.0	0.040	0.083	11.7	1.189	-1.096	0.227	1.11	0.335	137.82	3.85	30.14	0.153	0.48	1.36
1572.0	0.051	0.102	13.6	1.172	-1.113	0.269	1.14	0.377	139.94	5.12	37.08	0.151	0.46	1.39
1572.0	0.064	0.129	16.2	1.185	-1.100	0.319	1.14	0.433	142.12	6.62	46.68	0.152	0.44	1.37
1572.0	0.091	0.174	20.7	1.163	-1.122	0.424	1.19	0.515	145.41	9.74	62.97	0.150	0.43	1.44
1572.0	0.129	0.230	26.6	1.136	-1.149	0.575	1.28	0.605	148.76	14.26	83.01	0.146	0.44	1.55
1572.0	0.163	0.273	28.4	1.088	-1.197	0.647	1.36	0.624	150.84	16.41	98.66	0.140	0.42	1.49
1572.0	0.205	0.365	27.2	1.142	-1.143	0.587	1.28	0.614	152.80	14.62	131.56	0.147	0.28	1.00
1572.0	0.290	0.481	34.5	1.150	-1.135	0.780	1.37	0.700	156.20	20.37	173.44	0.148	0.29	1.04
1572.0	0.409	0.627	43.9	1.210	-1.075	1.035	1.49	0.781	159.66	27.99	226.02	0.156	0.29	1.08

V. THROUGH FLOW EXPERIMENTS

DATA WITH VARIABLE VELOCITY AT CONSTANT SOUND LEVEL 145 DB

DEN	SONIC	VIS	CF	SIG	XL	T	D
0.0720	1150.0	0.12200E-04	0.864	0.0395	0.500	0.090	0.052

FREQ	PA1	PA2	PHASE	INERT	REACT	RESIS	IMPED	ABSOR	SPL	DNLD	UORF	LEFF	K2RES	VELTH
1750.0	0.051	0.110	76.9	2.243	-0.266	1.143	1.17	0.980	143.86	10.74	88.06	0.111	0.44	0.00
1750.0	0.051	0.088	74.5	2.119	-0.390	1.408	1.46	0.946	143.19	13.86	70.76	0.105	0.67	32.60
1750.0	0.051	0.061	72.6	1.878	-0.631	2.015	2.11	0.849	142.15	21.01	48.95	0.093	1.39	63.00
1750.0	0.051	0.040	74.5	1.655	-0.854	3.080	3.19	0.708	141.25	33.56	32.34	0.082	3.22	115.50
1750.0	0.051	0.031	76.5	1.537	-0.972	4.050	4.16	0.612	140.79	45.00	24.82	0.076	5.53	135.50
1750.0	0.051	0.025	78.3	1.470	-1.039	5.018	5.12	0.538	140.49	56.40	20.17	0.072	8.43	164.50
1750.0	0.051	0.021	80.0	1.452	-1.057	5.998	6.09	0.478	140.28	67.95	16.97	0.072	11.98	187.50
1750.0	0.051	0.018	81.2	1.427	-1.082	6.991	7.07	0.430	140.11	79.65	14.61	0.070	16.22	212.10
1750.0	0.051	0.016	82.4	1.448	-1.061	7.959	8.02	0.391	139.99	91.06	12.87	0.071	20.95	237.00
1750.0	0.051	0.014	83.6	1.517	-0.992	8.850	8.90	0.361	139.89	101.56	11.60	0.075	25.85	256.00
1750.0	0.051	0.013	84.5	1.563	-0.946	9.833	9.87	0.332	139.81	113.14	10.46	0.077	31.85	279.00
1750.0	0.051	0.011	85.6	1.649	-0.860	11.179	11.21	0.299	139.71	129.00	9.22	0.081	41.10	302.00
1750.0	0.051	0.010	86.5	1.785	-0.725	11.854	11.87	0.286	139.68	136.96	8.70	0.088	46.17	325.00

DATA WITH VARIABLE VELOCITY AT CONSTANT SOUND LEVEL 16. DB

DEN	SONIC	VIS	CF	SIG	XL	T	D
0.0720	1150.0	0.122000E-04	0.864	0.0395	0.500	0.090	0.052

FREQ	PA1	PA2	PHASE	INERT	REACT	RESIS	IMPED	ABSOR	SPL	DNLD	UORF	LEFF	K2RES	VELTH
1750.0	0.290	0.276	76.4	1.892	-0.618	2.554	2.62	0.784	156.69	27.37	221.21	0.093	0.39	0.00
1750.0	0.290	0.264	77.0	1.890	-0.619	2.681	2.75	0.769	156.59	28.87	211.25	0.093	0.43	32.60
1750.0	0.290	0.249	78.0	1.903	-0.606	2.851	2.91	0.750	156.47	30.87	199.43	0.094	0.48	63.00
1750.0	0.290	0.219	79.3	1.895	-0.614	3.251	3.30	0.704	156.23	35.58	175.71	0.094	0.62	115.50
1750.0	0.290	0.182	78.8	1.737	-0.772	3.902	3.97	0.633	155.88	43.25	146.15	0.086	0.90	135.50
1750.0	0.290	0.148	78.5	1.534	-0.975	4.796	4.89	0.555	155.56	53.78	118.79	0.076	1.36	164.50
1750.0	0.290	0.122	79.3	1.404	-1.105	5.848	5.95	0.486	155.30	66.19	97.68	0.069	2.03	187.50
1750.0	0.290	0.105	80.4	1.357	-1.152	6.816	6.91	0.436	155.13	77.59	84.10	0.067	2.74	212.10
1750.0	0.290	0.093	81.4	1.350	-1.159	7.669	7.75	0.400	155.02	87.65	74.95	0.066	3.46	237.00
1750.0	0.290	0.084	82.5	1.387	-1.123	8.530	8.60	0.370	154.92	97.79	67.57	0.068	4.28	256.00
1750.0	0.290	0.076	83.5	1.429	-1.080	9.481	9.54	0.341	154.83	109.00	60.92	0.070	5.27	279.00
1750.0	0.290	0.068	84.4	1.477	-1.032	10.534	10.58	0.314	154.75	121.41	54.93	0.073	6.50	302.00
1750.0	0.290	0.063	85.3	1.569	-0.940	11.434	11.47	0.294	154.70	132.02	50.67	0.077	7.65	325.00

DATA WITH VARIABLE FREQUENCY AT CONSTANT VELOCITY 136 ft/sec

DEN	SONIC	VIS	CF	SIG	XL	T	D
0.0720	1150.0	0.12200E-04	0.864	0.0395	0.500	0.090	0.052

FREQ	PA1	PA2	PHASE	INERT	REACT	RESIS	IMPED	ABSOR	SPL	DNLD	UORF	LEFF	K2RES	VELTH
500.0	0.290	0.233	26.3	-1.016	-9.801	4.844	10.93	0.148	154.32	104.06	53.17	-0.176	3.08	136.00
1000.0	0.290	0.222	45.1	0.351	-4.040	4.054	5.72	0.387	154.97	60.48	101.57	0.030	1.35	136.00
1500.0	0.290	0.202	63.4	1.054	-1.873	3.741	4.18	0.575	155.64	44.89	138.95	0.061	0.91	136.00
1600.0	0.290	0.196	70.0	1.356	-1.388	3.815	4.06	0.607	155.77	44.29	143.18	0.073	0.90	136.00
1700.0	0.290	0.193	80.0	1.912	-0.671	3.807	3.86	0.646	155.94	42.79	150.39	0.097	0.85	136.00
1750.0	0.290	0.180	78.6	1.714	-0.795	3.944	4.02	0.629	155.86	43.75	144.48	0.085	0.92	136.00
1800.0	0.290	0.189	79.3	1.746	-0.693	3.671	3.73	0.658	156.00	39.92	155.61	0.084	0.80	136.00
1900.0	0.290	0.172	86.0	2.041	-0.270	3.871	3.88	0.650	155.96	41.05	149.80	0.093	0.87	136.00
2000.0	0.290	0.168	90.8	2.249	0.052	3.772	3.77	0.662	156.02	38.85	154.10	0.097	0.83	136.00
2200.0	0.290	0.172	100.5	2.607	0.610	3.295	3.35	0.700	156.20	31.90	173.45	0.102	0.64	136.00
2500.0	0.290	0.123	104.3	2.774	1.017	3.991	4.11	0.615	155.80	36.62	141.16	0.096	0.95	136.00
2800.0	0.290	0.105	108.2	2.918	1.349	4.104	4.32	0.588	155.69	35.51	134.56	0.090	1.03	136.00
3000.0	0.290	0.104	112.7	3.038	1.574	3.763	4.07	0.598	155.73	31.14	142.52	0.087	0.89	136.00
3600.0	0.290	0.093	120.4	3.128	1.908	3.252	3.77	0.598	155.73	23.99	154.19	0.075	0.71	136.00
3900.0	0.290	0.072	124.9	3.691	2.565	3.677	4.48	0.516	155.41	26.29	129.66	0.082	0.96	136.00
4250.0	0.290	0.072	133.9	3.886	2.853	2.964	4.11	0.497	155.34	19.68	141.30	0.079	0.71	136.00

DATA WITH VARIABLE FREQUENCY AT CONSTANT VELOCITY 237 ft/sec

DEN	SONIC	VIS	CF	SIG	XL	T	D
0.0720	1150.0	0.12200E-04	0.864	0.0395	0.500	0.090	0.052

FREQ	PA1	PA2	PHASE	INERT	REACT	RESIS	IMPED	ABSOR	SPL	DNLD	UORF	LEFF	K2RES	VELTH
500.0	0.290	0.174	38.5	-2.625	-11.410	9.076	14.58	0.156	154.34	197.37	39.87	-0.455	7.71	237.00
1000.0	0.290	0.134	58.7	-0.542	-4.935	8.117	9.50	0.302	154.72	123.81	61.20	-0.047	4.49	237.00
1500.0	0.290	0.105	71.2	0.329	-2.599	7.635	8.06	0.375	154.94	94.45	72.08	0.019	3.59	237.00
1600.0	0.290	0.104	72.6	0.458	-2.287	7.299	7.64	0.393	154.99	87.22	76.01	0.024	3.25	237.00
1700.0	0.290	0.100	82.4	1.598	-0.985	7.386	7.45	0.414	155.06	85.58	78.02	0.081	3.21	237.00
1750.0	0.290	0.093	81.5	1.363	-1.146	7.671	7.75	0.401	155.02	87.67	74.95	0.067	3.47	237.00
1800.0	0.290	0.094	82.7	1.493	-0.947	7.397	7.45	0.414	155.06	83.19	77.99	0.071	3.21	237.00
1900.0	0.290	0.090	84.2	1.564	-0.747	7.357	7.39	0.417	155.07	80.48	78.61	0.071	3.17	237.00
2000.0	0.290	0.089	85.5	1.638	-0.557	7.085	7.10	0.431	155.11	75.37	81.60	0.071	2.93	237.00
2200.0	0.290	0.100	97.1	2.708	0.711	5.714	5.75	0.501	155.35	57.32	100.97	0.106	1.91	237.00
2500.0	0.290	0.067	97.2	2.707	0.950	7.522	7.58	0.409	155.04	71.43	76.68	0.093	3.32	237.00
2800.0	0.290	0.059	95.5	2.305	0.736	7.648	7.68	0.406	155.03	68.52	75.67	0.071	3.42	237.00
3000.0	0.290	0.059	100.2	2.734	1.269	7.058	7.17	0.424	155.09	60.79	81.07	0.079	2.95	237.00
3600.0	0.290	0.059	103.5	2.615	1.395	5.811	5.97	0.480	155.28	45.01	97.29	0.063	2.02	237.00
3900.0	0.290	0.045	108.5	3.381	2.254	6.739	7.10	0.414	155.06	50.46	81.81	0.075	2.79	237.00
4250.0	0.290	0.050	114.1	3.434	2.400	5.367	5.87	0.463	155.22	37.85	98.89	0.070	1.84	237.00

DATA WITH VARIABLE FREQUENCY AT CONSTANT VELOCITY 302 ft/sec

DEN	SONIC	VIS	CF	SIG	XL	T	D
0.0720	1150.0	0.12200E-04	0.864	0.0395	0.500	0.090	0.052

FREQ	PA1	PA2	PHASE	INERT	REACT	RESIS	IMPED	ABSOR	SPL	DNLD	UORF	LEFF	K2RES	VELTH
500.0	0.290	0.145	44.5	-3.717	-12.502	12.286	17.52	0.147	154.31	268.13	33.16	-0.645	12.56	302.00
1000.0	0.290	0.104	63.9	-0.991	-5.384	10.990	12.23	0.254	154.59	168.60	47.50	-0.086	7.84	302.00
1500.0	0.290	0.077	74.3	-0.049	-2.978	10.565	11.00	0.295	154.70	132.13	52.82	-0.002	6.80	302.00
1600.0	0.290	0.077	74.3	-0.046	-2.792	9.933	10.31	0.312	154.75	119.69	56.35	-0.002	5.97	302.00
1700.0	0.290	0.072	85.5	1.776	-0.807	10.255	10.28	0.322	154.78	119.88	56.52	0.090	6.15	302.00
1750.0	0.290	0.069	84.4	1.488	-1.021	10.413	10.46	0.317	154.76	119.99	55.56	0.073	6.35	302.00
1800.0	0.290	0.069	85.4	1.624	-0.815	10.140	10.17	0.325	154.79	115.09	57.15	0.078	6.01	302.00
1900.0	0.290	0.065	85.3	1.475	-0.836	10.174	10.20	0.324	154.78	112.33	56.95	0.067	6.05	302.00
2000.0	0.290	0.065	85.9	1.502	-0.693	9.673	9.69	0.338	154.82	103.90	59.95	0.065	5.47	302.00
2200.0	0.290	0.077	99.1	3.183	1.186	7.409	7.50	0.410	155.05	75.14	77.48	0.125	3.24	302.00
2500.0	0.290	0.048	98.1	3.248	1.491	10.481	10.58	0.312	154.75	100.61	54.91	0.112	6.47	302.00
2800.0	0.290	0.043	93.5	2.208	0.640	10.465	10.48	0.317	154.76	94.76	55.45	0.068	6.39	302.00
3000.0	0.290	0.045	98.2	2.781	1.317	9.144	9.23	0.349	154.86	79.57	62.93	0.080	4.92	302.00
3600.0	0.290	0.045	99.5	2.490	1.270	7.593	7.69	0.402	155.02	59.65	75.52	0.060	3.40	302.00
3900.0	0.290	0.034	105.6	3.674	2.548	9.127	9.47	0.334	154.81	69.32	61.35	0.081	5.04	302.00
4250.0	0.290	0.038	107.3	3.365	2.331	7.485	7.84	0.386	154.97	53.87	74.15	0.068	3.42	302.00

DATA WITH VARIABLE VELOCITY AT CONSTANT SOUND LEVEL 145 DB

DEN	SONIC	VIS	CF	SIG	XL	T	D
0.0720	1150.0	0.12200E-04	0.916	0.1080	0.500	0.100	0.052

FREQ	PA1	PA2	PHASE	INERT	REACT	RESIS	IMPED	ABSOR	SPL	DNLD	UORF	LEFF	K2RES	VELTH
2350.0	0.051	0.200	86.3	1.838	-0.031	0.479	0.48	0.875	142.37	10.54	78.70	0.185	0.63	0.00
2350.0	0.051	0.205	83.9	1.819	-0.049	0.466	0.46	0.866	142.29	10.19	80.54	0.183	0.60	5.00
2350.0	0.051	0.172	81.4	1.785	-0.083	0.551	0.55	0.913	142.76	12.57	67.76	0.180	0.84	38.00
2350.0	0.051	0.143	80.1	1.753	-0.115	0.660	0.67	0.953	143.30	15.64	56.36	0.177	1.22	55.50
2350.0	0.051	0.101	80.3	1.709	-0.159	0.934	0.94	0.992	144.25	23.31	39.90	0.172	2.43	81.70
2350.0	0.051	0.082	82.4	1.715	-0.154	1.155	1.16	0.989	144.16	29.53	32.43	0.173	3.71	108.00
2350.0	0.051	0.072	83.2	1.712	-0.156	1.314	1.32	0.977	143.77	33.98	28.57	0.172	4.79	129.00
2350.0	0.051	0.063	84.4	1.720	-0.148	1.512	1.51	0.955	143.33	39.55	24.88	0.173	6.33	147.00
2350.0	0.051	0.057	85.7	1.744	-0.124	1.661	1.66	0.936	143.04	43.73	22.69	0.176	7.62	169.00
2350.0	0.051	0.053	86.4	1.755	-0.113	1.802	1.80	0.916	142.79	47.69	20.94	0.177	8.96	188.00
2350.0	0.051	0.050	87.0	1.769	-0.100	1.910	1.91	0.901	142.62	50.73	19.77	0.178	10.06	206.00
2350.0	0.051	0.045	87.2	1.766	-0.102	2.094	2.09	0.873	142.36	55.91	18.03	0.178	12.10	223.00
2350.0	0.051	0.044	88.0	1.793	-0.075	2.169	2.17	0.863	142.26	58.02	17.41	0.181	12.98	241.00
2350.0	0.051	0.041	88.3	1.800	-0.069	2.325	2.32	0.840	142.08	62.39	16.25	0.181	14.90	258.00

DATA WITH VARIABLE VELOCITY AT CONSTANT SOUND LEVEL 160 DB

DEN	SONIC	VIS	CF	SIG	XL	T	D
0.0720	1150.0	0.12200E-04	0.916	0.1080	0.500	0.100	0.052

FREQ	PA1	PA2	PHASE	INERT	REACT	RESIS	IMPED	ABSOR	SPL	DNLD	UORF	LEFF	K2RES	VELTH
2350.0	0.290	0.546	85.4	1.789	-0.079	0.989	0.99	0.998	159.65	24.86	214.29	0.180	0.48	0.00
2350.0	0.290	0.527	84.8	1.776	-0.093	1.022	1.02	0.997	159.59	25.81	207.02	0.179	0.51	5.00
2350.0	0.290	0.527	84.0	1.761	-0.107	1.021	1.02	0.997	159.54	25.77	207.02	0.177	0.51	38.00
2350.0	0.290	0.515	83.8	1.755	-0.113	1.044	1.05	0.996	159.49	26.42	202.30	0.177	0.53	55.50
2350.0	0.290	0.503	83.5	1.747	-0.121	1.068	1.07	0.995	159.43	27.09	197.70	0.176	0.56	81.70
2350.0	0.290	0.449	83.8	1.738	-0.130	1.199	1.20	0.988	159.10	30.77	176.20	0.175	0.70	108.00
2350.0	0.290	0.404	85.2	1.757	-0.112	1.333	1.33	0.977	158.78	34.54	158.86	0.177	0.87	129.00
2350.0	0.290	0.373	86.7	1.785	-0.083	1.448	1.45	0.965	158.51	37.76	146.55	0.180	1.03	147.00
2350.0	0.290	0.325	87.9	1.808	-0.061	1.664	1.66	0.937	158.05	43.84	127.64	0.182	1.35	169.00
2350.0	0.290	0.296	89.0	1.817	-0.031	1.826	1.82	0.914	157.77	48.37	116.41	0.185	1.63	188.00
2350.0	0.290	0.270	90.3	1.879	0.010	2.002	2.00	0.888	157.49	53.33	106.17	0.189	1.96	206.00
2350.0	0.290	0.252	91.0	1.906	0.037	2.145	2.14	0.867	157.30	57.35	99.08	0.192	2.25	223.00
2350.0	0.290	0.233	91.9	1.946	0.077	2.325	2.32	0.840	157.08	62.38	91.41	0.196	2.65	241.00
2350.0	0.290	0.222	92.2	1.962	0.093	2.434	2.43	0.824	156.96	65.44	87.30	0.198	2.90	258.00

DATA WITH VARIABLE VELOCITY AT CONSTANT SOUND LEVEL 150 DB

DEN	SONIC	VIS	CF	SIG	XL	T	D
0.0780	1151.0	0.12900E-04	0.670	0.0212	0.510	0.300	0.051

FREQ	PA1	PA2	PHASE	INERT	REACT	RESIS	IMPED	ABSOR	SPL	DNLD	UORF	LEFF	K2RES	VELPT
1200.0	0.091	0.044	142.0	9.437	5.845	4.567	7.41	0.280	144.66	28.41	42.58	0.366	1.17	0.00
1200.0	0.091	0.072	113.6	5.402	1.810	4.143	4.52	0.557	145.57	25.14	69.87	0.209	0.64	82.90
1200.0	0.091	0.066	112.1	5.457	1.865	4.593	4.95	0.528	145.45	28.62	63.72	0.212	0.78	106.50
1200.0	0.091	0.061	111.9	5.596	2.004	4.986	5.37	0.500	145.35	31.65	58.78	0.217	0.92	124.50
1200.0	0.091	0.059	111.2	5.580	1.988	5.127	5.49	0.494	145.33	32.74	57.45	0.216	0.97	141.10
1200.0	0.091	0.058	110.6	5.571	1.980	5.267	5.62	0.487	145.31	33.83	56.14	0.216	1.02	155.00
1200.0	0.091	0.057	110.0	5.561	1.969	5.411	5.75	0.481	145.28	34.94	54.86	0.216	1.08	167.60
1200.0	0.091	0.056	109.6	5.546	1.954	5.487	5.82	0.478	145.27	35.53	54.23	0.215	1.10	178.80
1200.0	0.091	0.056	108.8	5.480	1.888	5.546	5.85	0.477	145.27	35.98	53.92	0.212	1.12	188.80
1200.0	0.091	0.056	107.8	5.382	1.791	5.578	5.85	0.480	145.28	36.23	53.92	0.209	1.13	198.50
1200.0	0.091	0.053	107.0	5.396	1.804	5.900	6.17	0.463	145.22	38.72	51.20	0.209	1.26	207.50
1200.0	0.091	0.052	106.7	5.406	1.814	6.048	6.31	0.456	145.20	39.86	50.03	0.210	1.32	215.90
1200.0	0.091	0.050	105.9	5.362	1.770	6.214	6.46	0.450	145.18	41.14	48.89	0.208	1.39	223.30
1200.0	0.091	0.050	104.2	5.195	1.603	6.336	6.53	0.449	145.17	42.09	48.33	0.201	1.43	230.30
1200.0	0.091	0.048	104.0	5.228	1.636	6.564	6.76	0.438	145.14	43.85	46.69	0.203	1.53	237.20
1200.0	0.091	0.048	103.4	5.178	1.586	6.657	6.84	0.435	145.13	44.57	46.16	0.201	1.57	243.90
1200.0	0.091	0.046	103.0	5.185	1.593	6.903	7.08	0.424	145.09	46.47	44.59	0.201	1.69	250.10
1200.0	0.091	0.045	102.7	5.167	1.575	6.991	7.16	0.421	145.08	47.15	44.08	0.200	1.73	256.20
1200.0	0.091	0.045	102.0	5.099	1.507	7.091	7.24	0.418	145.07	47.92	43.58	0.198	1.78	262.10
1200.0	0.091	0.044	101.8	5.108	1.517	7.261	7.41	0.411	145.05	49.24	42.58	0.198	1.86	267.50
1200.0	0.091	0.043	100.8	5.014	1.422	7.457	7.59	0.405	145.03	50.75	41.61	0.194	1.96	272.80
1200.0	0.091	0.041	100.9	5.077	1.485	7.716	7.85	0.394	145.00	52.75	40.20	0.197	2.10	278.10
1200.0	0.091	0.040	100.2	5.015	1.423	7.914	8.04	0.388	144.98	54.28	39.29	0.194	2.20	285.20

DATA WITH VARIABLE VELOCITY AT CONSTANT SOUND LEVEL 160 DB

DEN	SONIC	VIS	CF	SIG	XL	T	D
0.0845	1155.0	0.13000E-04	0.670	0.0212	0.510	0.300	0.051

FREQ	PA1	PA2	PHASE	INERT	REACT	RESIS	IMPED	ABSOR	SPL	DNLD	UORF	LEFF	K2RES	VELPT
1200.0	0.290	0.122	127.7	8.831	5.226	6.762	8.54	0.308	154.74	47.50	107.52	0.344	0.69	0.00
1200.0	0.290	0.108	104.0	5.924	2.320	9.305	9.59	0.333	154.81	67.94	95.83	0.230	1.06	145.30
1200.0	0.290	0.107	104.0	5.951	2.346	9.413	9.70	0.330	154.80	68.81	94.73	0.232	1.09	155.00
1200.0	0.290	0.105	103.9	5.989	2.384	9.636	9.92	0.324	154.78	70.61	92.58	0.233	1.14	167.50
1200.0	0.290	0.105	103.9	5.989	2.384	9.636	9.92	0.324	154.78	70.61	92.58	0.233	1.14	178.80
1200.0	0.290	0.105	103.9	5.989	2.384	9.636	9.92	0.324	154.78	70.61	92.58	0.233	1.14	189.10
1200.0	0.290	0.105	103.9	5.989	2.384	9.636	9.92	0.324	154.78	70.61	92.58	0.233	1.14	198.70
1200.0	0.290	0.105	103.9	5.989	2.384	9.636	9.92	0.324	154.78	70.61	92.58	0.233	1.14	207.70
1200.0	0.290	0.105	103.8	5.972	2.367	9.640	9.92	0.324	154.78	70.64	92.58	0.232	1.14	216.10
1200.0	0.290	0.105	103.7	5.955	2.351	9.644	9.92	0.324	154.78	70.67	92.58	0.232	1.14	224.00
1200.0	0.290	0.105	103.5	5.921	2.317	9.653	9.92	0.324	154.79	70.74	92.58	0.230	1.14	231.50
1200.0	0.290	0.105	103.2	5.871	2.266	9.665	9.92	0.325	154.79	70.84	92.58	0.228	1.14	238.60
1200.0	0.290	0.105	103.0	5.837	2.233	9.672	9.92	0.325	154.79	70.90	92.58	0.227	1.14	245.40
1200.0	0.290	0.105	102.8	5.803	2.199	9.680	9.92	0.325	154.79	70.96	92.58	0.226	1.14	251.80
1200.0	0.290	0.105	102.6	5.769	2.165	9.688	9.92	0.325	154.79	71.02	92.58	0.224	1.15	257.20
1200.0	0.290	0.105	102.1	5.685	2.080	9.706	9.92	0.326	154.79	71.17	92.58	0.221	1.15	263.00
1200.0	0.290	0.105	101.8	5.634	2.030	9.717	9.92	0.326	154.79	71.26	92.58	0.219	1.15	269.40
1200.0	0.290	0.105	101.4	5.566	1.962	9.731	9.92	0.327	154.79	71.37	92.58	0.217	1.15	274.90
1200.0	0.290	0.105	101.2	5.532	1.928	9.738	9.92	0.327	154.79	71.42	92.58	0.215	1.15	279.30
1200.0	0.290	0.104	101.0	5.520	1.916	9.857	10.04	0.324	154.78	72.39	91.52	0.215	1.18	284.20

DATA WITH VARIABLE VELOCITY AT CONSTANT SOUND LEVEL 150 DB

DEN	SONIC	VIS	CF	SIG	XL	T	D
0.0861	1130.0	0.12450E-04	0.670	0.0272	0.510	0.300	0.099

FREQ	PA1	PA2	PHASE	INERT	REACT	RESIS	IMPED	ABSOR	SPL	DNLD	UORF	LEFF	K2RES	VELPT
1100.0	0.091	0.066	140.0	7.914	4.067	3.413	5.31	0.378	144.95	33.11	42.79	0.422	1.10	0.00
1100.0	0.091	0.067	117.8	6.295	2.448	4.643	5.24	0.490	145.32	46.49	43.28	0.336	1.48	82.10
1100.0	0.091	0.072	117.9	6.139	2.292	4.329	4.89	0.514	145.40	43.08	46.38	0.327	1.28	105.20
1100.0	0.091	0.074	117.7	6.046	2.199	4.190	4.73	0.527	145.45	41.56	48.01	0.322	1.20	123.70
1100.0	0.091	0.076	116.0	5.874	2.027	4.156	4.62	0.541	145.50	41.20	49.13	0.313	1.16	139.30
1100.0	0.091	0.078	113.0	5.592	1.745	4.112	4.46	0.563	145.59	40.72	50.85	0.298	1.11	153.20
1100.0	0.091	0.080	111.1	5.418	1.571	4.073	4.36	0.577	145.65	40.29	52.04	0.289	1.07	166.00
1100.0	0.091	0.081	108.7	5.230	1.383	4.088	4.31	0.588	145.69	40.46	52.64	0.279	1.07	177.20
1100.0	0.091	0.082	106.5	5.058	1.211	4.091	4.26	0.597	145.73	40.49	53.25	0.270	1.05	187.50
1100.0	0.091	0.084	104.7	4.905	1.058	4.033	4.16	0.609	145.78	39.86	54.49	0.261	1.02	197.00
1100.0	0.091	0.085	102.8	4.760	0.913	4.019	4.12	0.617	145.81	39.71	55.12	0.254	1.00	206.50
1100.0	0.091	0.083	100.5	4.615	0.768	4.147	4.21	0.612	145.79	41.10	53.87	0.246	1.06	114.20
1100.0	0.091	0.083	98.5	4.470	0.623	4.171	4.21	0.614	145.80	41.36	53.87	0.238	1.06	222.00
1100.0	0.091	0.083	96.6	4.331	0.484	4.190	4.21	0.616	145.81	41.56	53.87	0.231	1.07	229.40
1100.0	0.091	0.083	94.6	4.185	0.338	4.204	4.21	0.618	145.82	41.72	53.87	0.223	1.07	236.50
1100.0	0.091	0.081	93.5	4.110	0.263	4.308	4.31	0.610	145.78	42.85	52.64	0.219	1.12	243.10
1100.0	0.091	0.081	92.8	4.057	0.210	4.311	4.31	0.610	145.78	42.88	52.64	0.216	1.12	249.40
1100.0	0.091	0.079	91.5	3.962	0.115	4.415	4.41	0.601	145.75	44.01	51.44	0.211	1.18	255.50
1100.0	0.091	0.078	90.5	3.885	0.038	4.467	4.46	0.597	145.73	44.58	50.85	0.207	1.21	261.80
1100.0	0.091	0.078	90.1	3.854	0.007	4.519	4.51	0.593	145.71	45.15	50.27	0.205	1.24	267.30
1100.0	0.091	0.076	89.9	3.838	-0.008	4.625	4.62	0.584	145.67	46.29	49.13	0.204	1.29	272.50
1100.0	0.091	0.075	89.9	3.838	-0.008	4.678	4.67	0.580	145.66	46.87	48.56	0.204	1.32	277.50
1100.0	0.091	0.074	89.9	3.838	-0.008	4.732	4.73	0.576	145.64	47.46	48.01	0.204	1.36	282.40

DATA WITH VARIABLE VELOCITY AT CONSTANT SOUND LEVEL 160 DB

DEN	SONIC	VIS	CF	SIG	XL	T	D
0.0861	1130.0	0.12450E-04	0.670	0.0272	0.510	0.300	0.099

FREQ	PA1	PA2	PHASE	INERT	REACT	RESIS	IMPED	ABSOR	SPL	DNLD	UORF	LEFF	K2RES	VELPT
1100.0	0.290	0.207	125.5	6.966	3.119	4.373	5.37	0.453	155.19	43.55	133.77	0.371	0.45	0.00
1100.0	0.290	0.210	119.9	6.494	2.647	4.603	5.31	0.479	155.28	46.06	135.32	0.346	0.46	103.86
1100.0	0.290	0.202	114.3	6.108	2.262	5.009	5.49	0.485	155.30	50.48	130.72	0.326	0.52	127.70
1100.0	0.290	0.196	113.5	6.115	2.268	5.218	5.69	0.476	155.27	52.74	126.28	0.326	0.57	138.70
1100.0	0.290	0.196	111.9	5.969	2.122	5.279	5.69	0.480	155.28	53.41	126.28	0.318	0.57	152.10
1100.0	0.290	0.196	111.3	5.913	2.066	5.301	5.69	0.482	155.29	53.65	126.28	0.315	0.57	164.20
1100.0	0.290	0.196	110.2	5.811	1.964	5.340	5.69	0.484	155.30	54.07	126.28	0.310	0.58	175.20
1100.0	0.290	0.196	109.6	5.755	1.908	5.360	5.69	0.486	155.30	54.29	126.28	0.307	0.58	185.20
1100.0	0.290	0.196	108.8	5.680	1.833	5.386	5.69	0.488	155.31	54.58	126.28	0.303	0.58	194.90
1100.0	0.290	0.196	107.8	5.586	1.739	5.417	5.69	0.490	155.31	54.91	126.28	0.298	0.59	203.20
1100.0	0.290	0.196	106.8	5.491	1.644	5.447	5.69	0.492	155.32	55.24	126.28	0.293	0.59	211.10
1100.0	0.290	0.196	106.3	5.443	1.597	5.461	5.69	0.493	155.33	55.39	126.28	0.290	0.59	218.40
1100.0	0.290	0.196	105.9	5.405	1.558	5.472	5.69	0.493	155.33	55.51	126.28	0.288	0.59	225.60
1100.0	0.290	0.196	105.4	5.357	1.511	5.485	5.69	0.494	155.33	55.66	126.28	0.286	0.59	232.20
1100.0	0.290	0.196	104.9	5.310	1.463	5.498	5.69	0.495	155.33	55.80	126.28	0.283	0.60	238.60
1100.0	0.290	0.193	104.7	5.307	1.460	5.567	5.75	0.491	155.32	56.54	124.84	0.283	0.61	244.70
1100.0	0.290	0.193	104.6	5.297	1.450	5.570	5.75	0.492	155.32	56.57	124.84	0.282	0.61	250.60
1100.0	0.290	0.193	104.4	5.278	1.431	5.575	5.75	0.492	155.32	56.63	124.84	0.281	0.61	256.50
1100.0	0.290	0.193	104.2	5.258	1.411	5.580	5.75	0.492	155.32	56.68	124.84	0.280	0.61	261.40
1100.0	0.290	0.193	103.9	5.229	1.382	5.587	5.75	0.493	155.33	56.76	124.84	0.279	0.61	266.50
1100.0	0.290	0.193	103.0	5.141	1.294	5.608	5.75	0.494	155.33	56.99	124.84	0.274	0.61	290.60

APPENDIX E

DISTRIBUTION LIST*

Copies	Recipient
	NASA Headquarters Washington D. C., 20546
2	Attn: Dr. R. S. Levine, RPL
1	Attn: Mr. Ward Wilcox
1	Attn: Mr. A. O. Tischler, RP
1	Attn: Director Advanced Manned Missions, MT Office of Manned Space Flight
6	NASA Marshall Space Flight Center Huntsville, Alabama, 35812 Attn: Purchasing Office, A&TS-PR-MA
1	Attn: Scientific and Technical Information Branch, A&TS-MS-IP
1	Attn: Patent Office, A&TS-PAT
1	Attn: Technology Utilization Office, A&TS-MS-T
1	Attn: Mr. Robert Richmond, S&E-ASTN-PA
1	Attn: Mr. Rex Bailey, S&E-ASTN-PA
2	Attn: Mr. Richard Counts, S&E-ASTN-PPB
1	Mr. Dale Burrows, S&E-ASTN-PJ
	NASA Ames Research Center Moffett Field, California 94035
1	Attn: Technical Librarian for Dr. H. J. Allen, Director

*The report is to be sent directly to the "recipient" except where the technical librarian for the recipient is designated. In these cases the report is to be sent to the librarian and a copy of the transmittal letter to the recipient.

Copies	Recipient
1	NASA Goddard Space Flight Center Greenbelt, Maryland, 20771 Attn: Technical Librarian for Merland L. Moseson, Code 620
	NASA Lewis Research Center 21000 Brookpark Road Cleveland, Ohio, 44135
1	Attn: Dr. Richard Priem
2	Attn: Mr. Irvin Johnsen
1	Attn: Technical Librarian for Dr. Abe Silverstein, Director
	NASA Jet Propulsion Laboratory California Institute of Technology 4800 Oak Grove Drive Pasadena, California, 91103
1	Attn: Technical Librarian for Robert F. Rose, Propulsion Division, 38
1	Attn: Mr. Jack H. Rupe
	NASA Langley Research Center Langley Station Hampton, Virginia, 23365
1	Attn: Technical Librarian for Floyd L. Thompson, Director
	NASA Manned Spacecraft Center Houston, Texas, 77058
1	Attn: Technical Librarian for Robert R. Gilruth, Director
1	Attn: Mr. Cecil Gibson, Code EP2
	NASA John F. Kennedy Space Center Cocoa Beach, Florida, 32931
1	Attn: Technical Librarian for Dr. Kurt H. Debus, Director
24	Scientific and Technical Information Facility P. O. Box 5700 Bethesda, Maryland, 40014 Attn: NASA Representative, Code CRT

Copies	Recipient
	Advanced Research Projects Agency Washington 25, D. C.
1	Attn: Technical Librarian for Dr. D. E. Mock
	Defense Documentation Center Headquarters Cameron Station, Bldg. 5 5010 Duke Street Alexandria, Virginia 22314
1	Attn: Technical Librarian for TISIA
	Picatinny Arsenal Dover, New Jersey, 07801
1	Attn: Technical Librarian for Mr. I. Forsten, Chief, Liquid Propulsion Laboratory, SMUPA-DL
	Rocket Research Laboratories Edwards Air Force Base Edwards, California, 93253
1	Attn: Technical Librarian
1	Attn: Lt. Wayne Pritz, RPRRG
	U. S. Army Missile Command Redstone Arsenal, Alabama, 35809
1	Attn: Technical Librarian for Gen. Zierdt
1	Attn: Dr. Walter W. Wharton, AMSMI-RRK
	U. S. Naval Ordnance Test Station China Lake, California, 93557
1	Attn: Technical Librarian for Chief, Missile Propulsion Division, Code 4562
1	Attn: Mr. Edward W. Price, Code 5008
	Chemical Propulsion Information Agency Johns Hopkins University Applied Physics Laboratory 8621 Georgia Avenue Silver Spring, Maryland, 20910
1	Attn: Tech. Librarian for Tom Reedy
1	Attn: Mr. T. W. Christian

Copies	Recipient
	ARL Wright-Patterson AFB Dayton, Ohio, 45433
1	Attn: Mr. K. Scheller, Bldg. 450
	Headquarters Air Force Office of Scientific Research Propulsion Division Washington, D. C.
1	Attn: Dr. Bernard T. Wolfson
	Department of the Navy Office of Naval Research Washinton, D. C., 20360
1	Attn: Mr. R. O. Jackel
	RTNT Bolling Field Washington, D. C. 20332
1	Attn: Dr. L. Green, Jr.
	Aerojet-General Corporation P. O. Box 1947 Sacramento, California, 95809
1	Attn: Technical Librarian for Mr. R. Stiff
	Aerospace Corporation P. O. Box 95085 Los Angeles, California, 90045
1	Attn: Technical Librarian for Mr. J. C. Wilder
1	Attn: Mr. O. W. Dykema
1	Attn: Dr. W. G. Strahle
	Arthur D. Little, Inc. Acorn Park Cambridge, Massachusetts, 02140
1	Attn: Technical Librarian for Dr. E. K. Bastress
	Bell Aerosystems Company P. O. Box 1 Buffalo 5, New York
1	Attn: Technical Librarian for Mr. W. M. Smith
1	Attn: Dr. Theodor G. Rossmann
	Boeing Company P. O. Box 3707 Seattle, Washington, 98124
1	Attn: Technical Librarian for Mr. J. D. Alexander

Copies	Recipient
	Curtiss-Wright Corporation Wright Aeronautical Division Wood-ridge, New Jersey, 07075
1	Attn: Technical Librarian for Mr. G. Kelly
	General Electric Company Cincinnati, Ohio, 45215
1	Attn: Technical Librarian for Mr. D. Suichu
	The Marquardt Corporation 16555 Saticoy Street Van Nuys, California, 91409
1	Attn: Technical Librarian for Mr. Warren P. Broardman, Jr.
	North American Aviation, Inc. Space and Information Systems Division 12214 Lakewood Boulevard Downey, California
1	Attn: Technical Librarian for Mr. Bergen
	Reaction Motors Division Thiokol Chemical Corporation Denville, New Jersey, 07832
1	Attn: Technical Librarian for Mr. O. Mann
	Space Technology Laboratories TRW Incorporated One Space Park Redondo Beach, California, 90278
1	Attn: Mr. G. W. Elverum
	Stanford Research Institute 333 Ravenswood Avenue Menlo Park, California, 94025
1	Attn: Technical Librarian for Dr. Lionel Dickinson
	TAPCO Division TRW, Incorporated 23555 Euclid Avenue Cleveland, Ohio, 44117
1	Attn: Technical Librarian for Mr. P. T. Angell

Copies	Recipient
	Thiokol Chemical Corporation Redstone Division Huntsville, Alabama
1	Attn: Technical Librarian for Mr. John Goodloe
	United Aircraft Corporation Research Laboratories 400 Main Street East Hartford, Connecticut, 06108
1	Attn: Technical Librarian for Mr. Erle Martin
1	Attn: Dr. D. H. Utvik
	United Technology Center 587 Mathilda Avenue P. O. Box 358 Sunnyvale, California, 94088
1	Attn: Technical Librarian for Mr. B. Adelman
1	Attn: Mr. R. H. Osborn
	Rocketdyne Division of North American Aviation 6633 Canoga Avenue Canoga Park, California, 91304
1	Attn: Technical Librarian for Mr. S. Hoffman
1	Attn: Dr. Robert B. Lawhead
1	Attn: Mr. Eugene Clinger
	Warner-Swasey Company Control Instrument Division 32-16 Downing Street Flushing, New York, 11354
1	Attn: Mr. R. H. Tourin
	Rocket Research Corporation 520 South Portland Street Seattle, Washington, 98109
1	Attn: Technical Librarian for Mr. Robert Bridgeforth
	Defense Research Corporation P. O. Box 3587 Santa Barbara, California
1	Attn: Mr. B. Gray

Copies	Recipient
	Geophysics Corporation of America Technical Division Bedford, Massachusetts
1	Attn: Mr. A. C. Tobey
	Applied Physics Laboratory The Johns Hopkins University 8621 Georgia Avenue Silver Spring, Maryland 20910
1	Attn: Dr. W. G. Berl
	Ohio State University Rocket Research Laboratory Department of Aeronautical & Astronautical Engineering Columbus 10, Ohio, 43201
1	Attn: Dr. R. Edse
	Princeton University Forrestal Research Center Princeton, New Jersey
1	Attn Dr. I. Glassman
1	Attn: Mr. D. T. Harrje
	University of Wisconsin Dept. Mechanical Engineering 1513 University Avenue Madison, Wisconsin, 53705
1	Attn: Dr. P. S. Myers
	Dartmouth University Hanover, New Hampshire
1	Attn: Dr. P. D. McCormack
	University of Michigan Aeronautical & Astronautical Engineering Laboratories Aircraft Propulsion Lab. North Campus Ann Arbor, Michigan
1	Attn: Dr. J. A. Nicholls
	Institute of Engineering Research University of California Berkley, California
1	Attn: Dr. A. K. Oppenheim

Copies	Recipient
	Purdue University School of Mechanical Engineering Lafayette, Indiana
1	Attn: Dr. J. R. Osborn
	Massachusetts Institute of Technology Department of Mechanical Engineering Cambridge 39, Massachusetts
1	Attn: Dr. T. Y. Toong
	Illinois Institute of Technology 10W. 35th Street Chicago, Illinois
1	Attn: Dr. P. T. Torda
1	Georgia Institute of Technology Aerospace School Atlanta, Georgia Attn: Dr. Ben T. Zinn
	The Pennsylvania State University Mechanical Engineering Department 207 Mechanical Eng. Boulevard University Park, Pennsylvania, 16502
1	Attn: G. M. Faeth